SYNTHESIS OF POLYANILINE MODIFIED WITH PALM OIL-BASED ALKYD AS COUNTER ELECTRODE IN SOLAR CELL APPLICATION

MARIAM FADZLINA BINTI RAMLI

FACULTY OF SCIENCE
UNIVERSITI MALAYA
KUALA LUMPUR

2020

SYNTHESIS OF POLYANILINE MODIFIED WITH PALM OIL-BASED ALKYD AS COUNTER ELECTRODE IN SOLAR CELL APPLICATION

MARIAM FADZLINA BINTI RAMLI

DISSERTATION SUBMITTED IN FULFILMENT OF THE REQUIREMENTS FOR THE DEGREE OF MASTER IN RESEARCH

DEPARTMENT OF CHEMISTRY
FACULTY OF SCIENCE
UNIVERSITI MALAYA
KUALA LUMPUR

2020

UNIVERSITI MALAYA

ORIGINAL LITERARY WORK DECLARATION

Name of Candidate: **MARIAM FADZLINA BINTI RAMLI**

Matric No: **SGR150044**

Name of Degree: **MASTER OF SCIENCE**

Title of Project Paper/Research Report/Dissertation/Thesis (“This Work”):

SYNTHESIS ~~OF POLYANILINE M~~ODIFIED ~~WITH P~~ALM OIL-BASED ALKYD AS COUNTER ELECTRODE IN SOLAR CELL APPLICATION

Field of Study: **POLYMER CHEMISTRY**

I do solemnly and sincerely declare that:

(1) I am the sole author/writer of this Work;
(2) This Work is original;
(3) Any use of any work in which copyright exists was done by way of fair dealing and for permitted purposes and any excerpt or extract from, or reference to or reproduction of any copyright work has been disclosed expressly and sufficiently and the title of the Work and its authorship have been acknowledged in this Work;
(4) I do not have any actual knowledge nor do I ought reasonably to know that the making of this work constitutes an infringement of any copyright work;
(5) I hereby assign all and every rights in the copyright to this Work to the University of Malaya (“UM”), who henceforth shall be owner of the copyright in this Work and that any reproduction or use in any form or by any means whatsoever is prohibited without the written consent of UM having been first had and obtained;
(6) I am fully aware that if in the course of making this Work I have infringed any copyright whether intentionally or otherwise, I may be subject to legal action or any other action as may be determined by UM.

Candidate’s Signature Date:

Subscribed and solemnly declared before,

Witness’s Signature Date:

Name:

Designation:

SYNTHESIS OF POLYANILINE MODIFIED WITH PALM OIL-BASED ALKYD AS COUNTER ELECTRODE IN SOLAR CELL APPLICATION

ABSTRACT

Presently, shortage of sustainable and environmental friendly energy resources has become an important global concern. Dye-sensitized solar cell (DSSC) has widely been used as a clean energy conversion device that can solve this problem. Platinum (Pt) has commonly been used as counter electrode (CE) in DSSC due to its good redox property. However, Pt is expensive and could be easily corroded in tri-iodide solution. Recently, polyaniline (PAni) has shown promising performance in DSSC, but PAni exhibit poor adhesion on fluorine-doped tin oxide (FTO) substrate. In this study, an environmental friendly CE was developed by modifying PAni using titanium dioxide (TiO_2) and a palm oil-based (POB) alkyd to improve both the electrocatalytic activity and adhesion on FTO without using any toxic organic solvent like m-Cresol. A series of PAni and PAni-TiO_2 with different TiO_2 content (10%, 20% and 40%) were synthesized via chemical oxidative polymerization. POB alkyd was synthesized through alcoholysis and esterification reactions. Chemical structures of PAni, PAni-TiO_2 and POB alkyd were confirmed by FTIR, UV-Vis, XRD and ^{1}H NMR analyses. Result obtained showed that PAni exist as emeraldine salt phase with electrical conductivity of 1.23×10^3 to 1.31×10^3 Scm^{-1}. The preparation of PAni modified with POB alkyd (PAni/Alkyd) films were investigated by different PAni:Alkyd ratios (1:0.5, 1:0.75 and 1:1), different acid number (AN) of POB alkyd (5.66, 14.74 and 17.60 mgKOH/g) and different reactive diluents such as methyl acrylate (MA), methyl methacrylate (MMA) and cyclohexyl methacrylate (CMA) under UV curing method. Among all PAni/Alkyd films, PAni/Alkyd using ratio 1:0.5 with alkyd having AN of 5.66 mgKOH/g and CMA as diluent give the lowest curing time of 5 min to give adhesion of 5B. Besides, PAni-TiO_2 modified with POB alkyd (PAni-TiO_2/Alkyd) films were prepared using similar ratio as discussed earlier. The results showed that all PAni/Alkyd and PAni-TiO_2/Alkyd films exhibit high conductivity range of 6.11×10^2 to 6.49×10^2 Scm^{-1} with good adhesion on FTO substrate. The adhesion of PAni on FTO is significantly contributed by the reactive C=C of the POB alkyd that undergo crosslinking in the PAni/Alkyd coating during UV curing. Conductivity and adhesion are two main crucial factors that will contribute to high power conversion efficiency (PCE) of DSSC. In this research, the fabrications of DSSC were prepared using TiO_2 photoanode, ruthenium dye, PAni/Alkyd and PAni-TiO_2/Alkyd as CE and iodolyte AN50 electrolyte. The highest PCE was shown by PAni/Alkyd with 0.60% while PAni-TiO_2/Alkyd showed lower PCE range of 0.20% to 0.30%. This is because PAni/Alkyd possessed higher conductivity of 6.49×10^2 Scm^{-1} compared with PAni-TiO_2/Alkyd (6.11×10^2 to 6.32×10^2 Scm^{-1}). As a result, an environmentally POB alkyd modified PAni as CE with high electrical conductivity of 6.11×10^2 to 6.49×10^2 Scm^{-1}, excellent adhesion of 5B and moderate PCE of 0.20% to 0.60% in DSSC were successfully obtained. This research results confirmed that PAni modified with POB alkyd can be potentially applied as cost-effective and environmental friendly materials used for DSSC study.

Keywords: Polyaniline, Conductivity, Adhesion, Dye-Sensitized Solar Cell

SINTESIS POLIANILINA YANG DIUBAH SUAI DENGAN ALKID BERASASKAN-MINYAK KELAPA SAWIT SEBAGAI ELEKTROD LAWAN DALAM APLIKASI SEL SURIA

ABSTRAK

Kini, kekurangan sumber tenaga yang kekal dan mesra alam telah menarik perhatian global. Sel suria terpeka-pewarna (DSSC) digunakan secara meluas sebagai alat penukaran tenaga yang bersih di mana ia dapat menyelesaikan masalah ini. Platinum (Pt) biasanya digunakan sebagai elektrod lawan (CE) dalam DSSC disebabkan oleh ciri redoks yang baik. Walau bagaimanapun, Pt adalah mahal dan akan mudah terhakis dalam larutan tri-iodida. Baru-baru ini, polianilina (PAni) telah menunjukkan prestasi yang memberangsangkan dalam DSSC tetapi PAni menunjukkan sifat perlekatan yang lemah pada substrat timah oksida terdop florin (FTO). Dalam kajian ini, CE mesra alam telah dibangunkan dengan pengubahsuaian menggunakan titania dioksida (TiO_2) dan alkid berasaskan-minyak kelapa sawit (POB) untuk penambah baikan kedua-dua aktiviti elektrokatalitik dan perlekatan pada FTO tanpa menggunakan sebarang pelarut organik yang toksik seperti m-Kresol. Suatu siri PAni dan PAni-TiO_2 dengan pelbagai kandungan TiO_2 (10%, 20% and 40%) telah disintesis melalui pempolimeran oksidatif kimia. Alkid POB telah disintesis melalui tindak balas alkoholisis dan esterifikasi. Struktur kimia bagi PAni, PAni-TiO_2 dan alkid POB telah disahkan dengan analisis FTIR, UV-Vis, XRD dan ^{1}H NMR. Keputusan yang telah diperolehi menunjukkan bahawa PAni wujud sebagai fasa garam emeraldina dengan kekonduksian sebanyak 1.23×10^3 hingga 1.31×10^3 Scm^{-1}. Penyediaan filem PAni yang diubah suai dengan alkid POB (PAni/Alkid) telah dikaji menggunakan pelbagai nisbah PAni:Alkid (1:0.5, 1:0.75, 1:1), pelbagai nilai asid (AN) alkid POB (5.66, 14.74 dan 17.60 mgKOH/g) dan pelbagai diluen reaktif seperti metil akrilat (MA), metil metakrilat (MMA) dan sikloheksil metakrilat (CMA) melalui proses pengawetan UV. Di antara kesemua filem

PAni/Alkid, PAni/Alkid dengan nisbah 1:0.5, AN 5.66 mgKOH/g dan diluen CMA telah mencatatkan masa bagi pengawetan UV yang paling rendah iaitu 5 min bagi menunjukkan perlekatan yang terbaik iaitu 5B. Di samping itu, filem PAni-TiO_2 yang diubah suai dengan alkid POB (PAni-TiO_2/Alkid) telah disediakan dengan menggunakan nisbah yang sama seperti dibincangkan sebelum ini. Keputusan yang diperolehi menunjukkan kesemua filem PAni/Alkid dan PAni-TiO_2/Alkid mempunyai kekonduksian yang tinggi dalam julat 6.11×10^2 hingga 6.49×10^2 Scm^{-1} dengan perlekatan yang baik pada substrat FTO iaitu 5B. Perlekatan PAni pada FTO adalah disumbangkan oleh C=C reaktif daripada alkid POB yang telah mengalami taut-silang dalam salutan PAni/Alkid semasa proses pengawetan UV. Kekonduksian dan perlekatan adalah dua faktor utama bagi menghasilkan kecekapan penukaran tenaga (PCE) yang tinggi dalam DSSC. Dalam kajian ini, fabrikasi DSSC telah disediakan dengan menggunakan fotoanod TiO_2, pewarna rutenium, PAni/Alkid dan PAni-TiO_2/Alkid sebagai CE dan elektrolit iodolit AN50. PAni/Alkid telah menunjukkan PCE yang paling tinggi iaitu 0.60% manakala PAni-TiO_2/Alkid telah menunjukkan PCE yang lebih rendah dalam julat 0.20% hingga 0.30%. Hal ini kerana PAni/Alkid mempunyai kekonduksian yang lebih tinggi iaitu 6.49×10^2 Scm^{-1} berbanding dengan PAni-TiO_2/Alkid (6.11×10^2 hingga 6.32×10^2 Scm^{-1}). Kesimpulannya, PAni terubah suai alkid POB yang mesra alam sebagai CE dengan kekonduksian elekrik yang tinggi iaitu 6.11×10^2 hingga 6.49×10^2 Scm^{-1}, perlekatan yang baik iaitu 5B dan PCE yang sederhana iaitu 0.20% hingga 0.60% dalam DSSC telah berjaya diperolehi. Keputusan kajian ini telah mengesahkan bahawa PAni terubah-suai POB alkid berpotensi diaplikasi sebagai bahan kos-efektif dan mesra alam untuk kajian DSSC.

Kata kunci: Polianilina, Kekonduksian, Perlekatan, Sel Suria Terpeka-Pewarna

ACKNOWLEDGEMENTS

In the name of Allah, the most beneficent, the most merciful, I would like to express my very profound gratitude to all people that always help and being with me throughout my master's journey.

Foremost, I would especially like to thank my supervisors, Prof. Dr. Gan Seng Neon, Assoc. Prof. Dr. Phang Sook Wai, Assoc. Prof. Dr. Sharifah Mohamad and Dr. Lim Wen Huei for providing me an extensive professional guidance from the start of the research to the final phase. I would like to extend my sincere gratitude to Dr. Mohd Sukor Su'ait and his student, Mr. Izwan from Universiti Kebangsaan Malaysia for the guidance and opportunity to use the DSSC device. I would also like to acknowledge Malaysian Palm Oil Board (MPOB) for the financial support of this research study under MPOB Graduate Students Assistantship Scheme (GSAS). Special thanks also dedicated to University of Malaya (UM) for the Postgraduate Research Grant, PPP (PG198-2016A).

Nevertheless, my sincere thanks also goes to all my dearest lab mates and friends from UM, kak Hazira, Yka, Ziera, Fiqa, kak Shafiza, kak Ani, Pedram, Pejvak, Abbas, Nadia, Nadila and Ama for all their help and memories here. Not forgetting, many thanks to my lovely housemates, Ezah, Zeehan, Diba, Dila, Lina and kak ekin. Last but not the least important, I owe a deep sense of gratitude to my parent (Mr. Ramli Ismail and Mrs. Che Fatimah Abdul Rahman) and siblings (Abe, Angah, Lan and Fatihah) for all the support and continuous encouragement throughout my years of study. I am very grateful having all of you in my life.

Thank You!

TABLE OF CONTENTS

LIST OF FIGURES

LIST OF TABLES

LIST OF SYMBOLS AND ABBREVIATIONS

cm : Centimeter

˚C : Degree celcius

eV : Electronvolt

Fg^{-1} : Specific capacitance

fM : Frequency modulation

g : Gram

gmol^{-1} : Gram per mol

GU : Gloss unit

h : Hour

µm : Micrometer

mAcm^{-2} : Milliampere per square centimeter

mAhg^{-1} : Milliampere hour per gram

mg : Milligram

MHz : Megahertz

Min : Minute

ml : Milliliter

mVs^{-1} : Millivolt per second

mWcm^{-2} : Milliwatt per square centimeter

Nm : Nanometer

Ω : Ohm

Ωcm : Ohm centimeter

Ωcm^{-1} : Ohm per centimeter

Ωm : Ohm meter

% : Percentage

%T : Percentage of transmission
π : Pi
η : Power conversion efficiency
Rpm : Revolutions per minute
Scm^{-1} : Siemens per centimeter
2°min^{-1} : Two degrees per minute
V : Volt
V^{-1}s^{-1} : Volt per second
Whkg^{-1} : Watt-hour per kilogram
Wkg^{-1} : Watt per kilogram
Wt% : Weight percentage
Ag : Silver
AN : Acid number
Ani : Aniline
AOAC : Official methods of analysis
AOT : Dioctyl sodium sulfosuccinate
APS : Ammonium persulphate
ASTM : American society for testing and materials
ATR : Attenuated total reflectance
ATSDR : Agency for toxic substances and disease registry
Au : Gold
CB/PAniNT : Carbon black/polyaniline nanotube
CdCl$_3$: Deuterated chloroform
CdTe : Cadmium telluride
Co : Cobalt
CE : Counter electrode

CPs : Conducting polymers
CMA : Cyclohexyl methacrylate
Cu : Copper
CV : Cyclic voltammogram
DC : Direct current
DRIFTS : Diffuse reflectance
DSSC : Dye-sensitized solar cell
e^- : Electron
EB : Emeraldine base
ES : Emeraldine salt
FA : Fumaric acid
ff : Fill factor
FTIR : Fourier transform infrared
FTO : Fluorine-doped tin oxide
HCl : Hydrochloric acid
H_2PtCl_6 : Chloroplatinic acid
^{13}C NMR : Carbon-13 nuclear magnetic resonance
^{1}H NMR : Proton nuclear magnetic resonance
I^-/I_3^- : Iodide/triiodide
Ir : Iridium
ITO : Indium tin oxide
I-V : Current voltage
J_{max} : Current density
J_{sc} : Short circuit current density
KHP : Potassium hydrogen phthalate
KOH : Potassium hydroxide

l : Liquid

MA : Methyl acrylate

MgO : Magnesium oxide

MMA : Methyl methacrylate

MWCNT : Multiwalled carbon nanotubes

NaCl : Sodium chloride

NC : Nanocup

Ni : Nickel

NIL : Nanoimprint lithography

NPs : Platinum nanoparticles

PA : Pthalic anhydride

PAc : Polyacetylene

PAMAM : Polyamidoamine

PAni : Polyaniline

PCE : Power conversion efficiency

Pd : Palladium

PEDOT : Poly(3,4-ethylenedioxithiophene)

P_{in} : Incident light power density

POB : Palm oil based

PNTs : Platinum nanotubes

Pt : Platinum

PTh : Polythiophene

PPV : Polyphenylene vinylene

PV : Photovoltaic

QDSC : Quantum dot solar cell

R_{CT} : Charge transfer resistance

Ru : Ruthenium

S : Solid

SILAR : Successive ionic layer adsorption and reaction

SWCNT : Single wall carbon nanotube

TCO : Transparent conducting oxide

T_{cure} : Curing time

TiO_2 : Titanium dioxide

TMS : Tetramethylsilane

T_{room} : Room temperature

UV-Vis : Ultraviolet-Visible

V_{max} : Voltage

V_{oc} : Open circuit voltage

WE : Working electrode

XRD : X-ray diffractometer

ZnO : Zinc oxide

LIST OF APPENDICES

CHAPTER 1: INTRODUCTION

1.1 Dye-Sensitized Solar Cell (DSSC)

Nowadays, solar cell technology has gained popularity to the researchers because of its diverse advantages such as it generates clean energy which is without noise, toxicity and emissions of greenhouse gases (Chung et al., 2012). In general, there are three generations of solar cell. The generation on bases of crystalline or non-crystalline silicon materials that are usually known as conventional, traditional and wafer-based cell is classified as the first solar cell's generation. This generation was firstly proposed by Chapin and co-workers through silicon crystalline cell. Previous research study based on this solar cell produced power conversion efficiency (PCE) from 12.00% to 16.00%. Unfortunately, this solar cell's generation has a complicated manufacturing method and high cost (Chapin et al., 1954).

The second solar cell's generation is built upon technology of thin-film coating beginning with the invention of cadmium telluride (CdTe) solar cell by Cusano. This generation of solar cell provides lower manufacturing cost because it has an ability to operate with low temperature and high automation in serial production. However it has a difficult module technology and poor stability (Cusano et al., 1963). The third generation is known as emerging photovoltaic (PV) cell for example DSSC, perovskite cell, quantum dot solar cell (QDSC) and organic polymer solar cell. DSSC gets the most attraction from researchers over the others PV technology due to its high PCE, environmental friendly, inexpensive and uncomplicated fabrication procedures (Bagher et al., 2015).

DSSC was firstly introduced in 1991 by Gratzel and O' Regan with 7.10% efficiency. Although the efficiency of silicon cell remain higher than DSSC, the advantages of DSSC such as easy preparation as well as low production cost have accelerates the research and development of DSSC. The basic concept of DSSC is correlated to the nature of photosynthesis reaction where light energy is converted into electricity. In general, DSSC consist of four primary parts which include redox electrolyte, dye, working electrode (WE) comprising of nanocrystalline semiconductor oxide and counter electrode (CE) (Saranya et al., 2015).

Firstly, dye will harvest light and electrons are excited into the conduction band of the WE. Redox electrolyte having iodide/triiodide (I^-/I_3^-) ions then will donates electrons to the oxidized dye molecules and regenerates it. After that, the oxidized dye is reduced by I^- ions and electron-acceptor species (I_3^-) are transported to the CE. The cycle is completed by electron migration between WE and CE (Theerthagiri et al., 2014). CE with high conductivity and electrocatalytic activity properties is crucial for the effectiveness of I^-/I_3^- redox reaction (Park et al., 2015). **Figure 1.1** showed the completed cycle of DSSC.

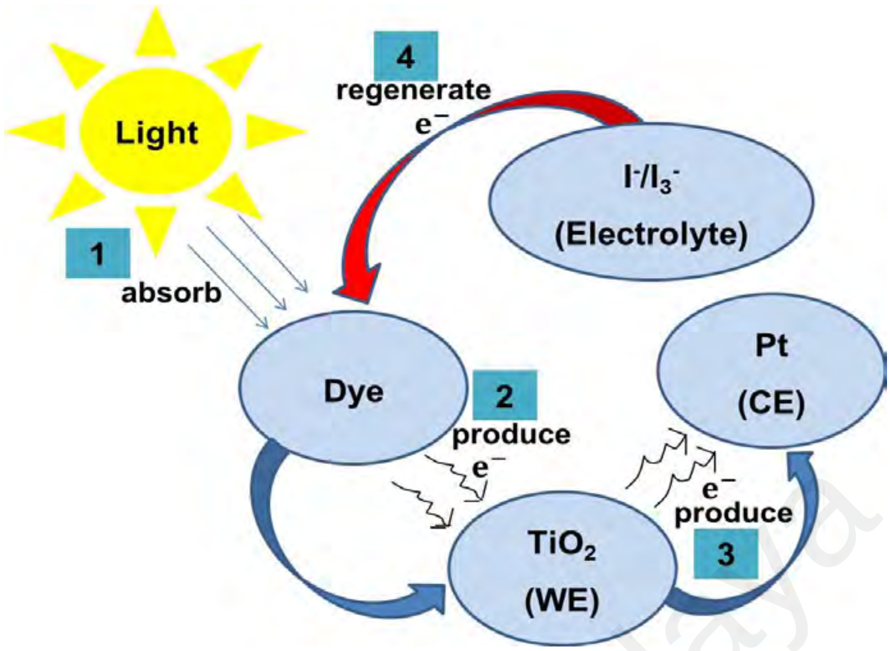

Figure 1.1: Complete cycle of DSSC.

1.2 Counter Electrode (CE)

CE is a vital part of DSSC as it undertakes two important roles in the working principle of DSSC. Firstly, CE functions as a catalyst where it reduces the I_3^- ions into I^- ions in the redox electrolyte and finally complete the process. Secondly, CE is the positive electrode of the cells where electrons from the external circuit are collected through CE and then are transmitted into the cell (Wu et al., 2014; Yang et al., 2015). Thus, CE should possess high conductivity, great electrocatalytic activity, good reflectivity, larger surface area, good adhesion towards transparent conducting oxide (TCO) substrate, high corrosion resistance, high chemical, electrochemical and mechanical stability (Theerthagiri et al., 2015).

Metals like platinum (Pt), palladium (Pd), iridium (Ir), ruthenium (Ru), titanium (Ti), gold (Au) and silver (Ag) as well as an alloy are the commonly traditional materials used as CE in DSSC. Among these traditional materials, Pt is tremendously selected because it has superior electrical conductivity, high electrocatalytic activity towards the reduction of I_3^- ions and good reflecting characteristics. Nazeerudin and co-workers reported DSSC with PCE of 10.00% by using Pt as CE while Dao and co-workers recorded the PCE of 9.30% using Pt nanoparticles as CE.

However, Pt is costly, has a complex fabrication and encounter slow dissolution in I^-/I_3^- electrolyte. These disadvantages minimized the applications of Pt as CE in DSSC. Thus, others elements that can replace Pt for example carbonaceous materials and polymer are the good solutions for DSSC application. Carbon is abundantly materials on earth with great properties such as high conductivity, high surface area, high thermal stability, good corrosion resistance towards iodine and high reactivity for triiodide reduction (Wu et al., 2017).

Despite of all its advantages, carbonaceous materials showed lower PCE compare to Pt as CE. Thus, a huge amount of carbonaceous materials are required to achieve enough catalytic activity and producing high PCE in DSSC. Besides, these materials also possess poor adhesion towards the substrate (Wu et al., 2017). Recently, many research attempts are conducted based on the conducting polymers (CPs) as CE to reduce the cost of DSSC while maintain its high efficiency.

1.3 Conducting Polymers (CPs)

The discovery of CPs by Alan J. Heeger, Alan MacDiarmid and Hideki Shirakawa has attracted a great attention among researchers due to its high electrical conductivity (Shirakawa et al., 1977). CPs composed of the organic materials that capable to conduct electricity owing to the existence of π-conjugation bonds along the polymer skeleton. Electrical conductivity of CPs can be increased through a doping or dedoping process.

Besides being electrically conductive, CPs also exhibit electronic, mechanical, magnetic, optical, microwave-absorbing and wetting properties (K. Saranya et al., 2015).

In recent years, CPs are the favorable materials used as CE in DSSC as CPs show excellent conductivity and high catalytic activity for reduction of I_3^- species (Bhadraa et al., 2009). **Figure 1.2** shows the most common example of CPs including polypyrrole (Ppy), poly(3,4-ethylenedioxythiophene) (PEDOT), polyacetylene (PA), polyaniline (PAni) and polythiophene (PTh) that have been applied as CE for DSSC. Among the CPs, PAni has extensively studied because it is easy to synthesize, low synthetic cost, electrical conductive and encounter special redox property (AbdulAlmohsin et al., 2012).

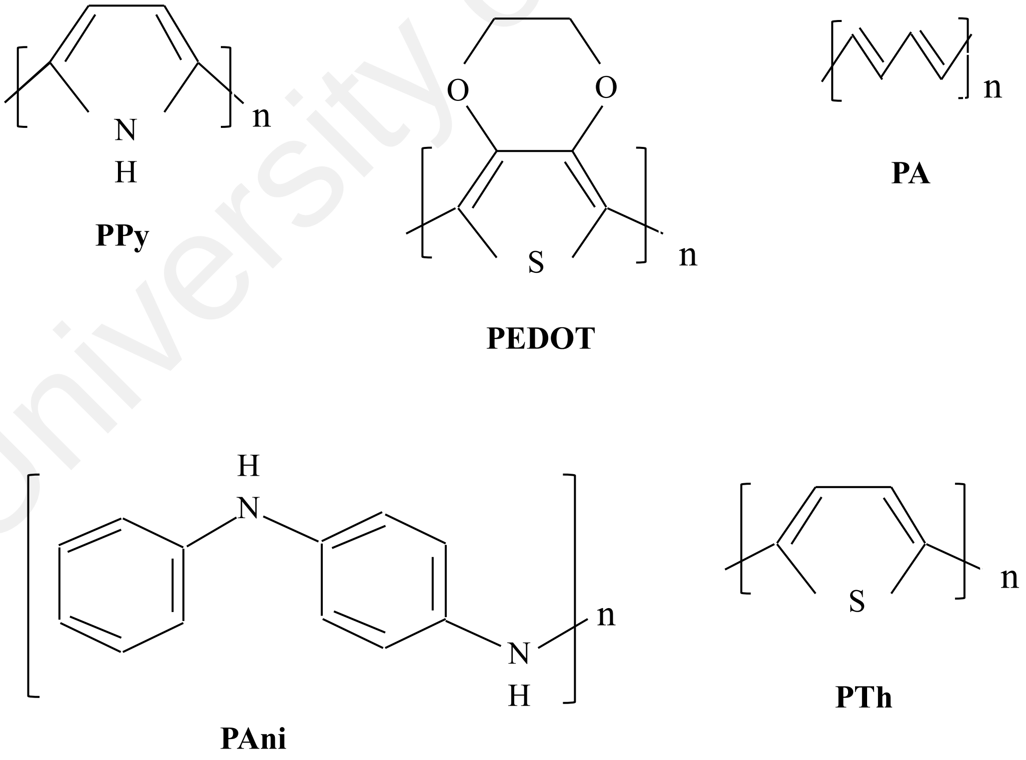

Figure 1.2: Example of CPs (Li et al., 2009).

Based on recent study, Cu-doped PAni that synthesized by Tas and co-workers in acetonitrile possessed PCE of 6.37% (Tas et al., 2016). Besides, another research study by Yu and co-workers on PAni-doped Pt alloy as CE produced PCE of 8.08 % in DSSC (Yu et al., 2016). Based on our knowledge, PAni exhibits high brittleness and poor adhesion towards the substrate during its application in DSSC. These disadvantages of PAni as CE are shown in the previous research study by Li and co-workers. They reported that PCE of PAni (7.15%) is higher than Pt (6.90%) under the same condition. However, PAni exhibits poor adhesion on the glass substrate and possessed instability in catalytic activity (Li et al., 2008).

Adhesion of material with the substrate is correlated to its surface energy. PAni can be classified as a high surface energy material. Thus, when PAni is coated onto a solid surface, it exhibits higher surface energy than the attractive forces toward the surface, which result in lower bond strength. PAni molecules are prone to remain associated among themselves and will not spread uniformly causing low adhesion with the substrate to be bonded (Baldan et al., 2012).This disadvantage of PAni will reduce its catalytic activity as CE and significantly affect the overall PCE of DSSC. Thus, poor adhesion property of PAni has restricted its application in DSSC (Saad et al., 2019).

1.4 Problem Statement

Environmental contamination and energy depletion turn into a predominant world issues at the present time. One of the solutions for these problems is through the utilization of sustainable energy sources. Energy sources from the sun such as solar cells are expected to be capable of supplying energy for mankind (Asim et al., 2012; Su’ait et al., 2015). Among all conventional solar cells, DSSC has great attention to the researchers due to its advantages for example cost-efficient, clean energy technology and simple fabrication procedures.

Pt is the greatest conventional materials that applied as a CE component in a typical DSSC device because it has an excellent redox property and stability against iodine ions in the electrolyte. Nevertheless, Pt being a noble metal is costly and shows low corrosive resistance in tri-iodide solution. Thus, the modification of DSSC using others functional materials as a CE component have extremely studied in recent time. Based on our knowledge, CPs have the most encouraging outlook because CPs are easier to process, easier to be put into mass production and more environmental friendly (Zohski et al., 2017). The most common examples of CPs are PA, PAni, PTh, PPy, PEDOT and polyphenylene vinylene (K. Saranya et al., 2015).

Among all CPs obtainable in the market, PAni is the most encouraging due to its high conductivity, great electrocatalytic activity, noncorrosive property and high stability compared to other CPs (Stejskal et al., 2010). However, PAni thin film is highly brittle, so it will not adhere strongly onto the fluoride-doped tin oxide (FTO) substrate during DSSC application. Initial study by Kawata and co-workers specified that adhesion of PAni on FTO substrate was increased through the incorporation of palm oil-based (POB) alkyd (PAni/m-Cresol/TiO_2/Alkyd) with conductivity range of (9.03 to 72.90 Scm^{-1}) and PCE of 3.00% (Kawata et al., 2013). However, an exposure to the toxic m-Cresol lead to serious health issues (Agency for Toxic Substances and Disease Registry, ATSDR, 2008).

Since there are no others work besides Kawata and co-workers have been recorded with the accomplishment of PAni/Alkyd on high performance of DSSC, an improvement in the utilization of environmental friendly and cost-effective for CE materials in DSSC still open a space to be explored. Therefore, application of

PAni/Alkyd as CE in the absence of noxious chemicals in detailed study can be further investigated in order to produce CE with good adhesion on FTO substrate, possess high conductivity and exhibits high PCE in DSSC.

1.5 Research Objectives

The objectives of this research study are listed below:

i. To synthesize PAni and PAni-TiO_2, then characterize its chemical structures by fourier transform infrared (FTIR) and ultraviolet-visible (UV-Vis) spectrometers.

ii. To synthesize POB alkyd, then characterize its chemical structures by FTIR and proton nuclear magnetic resonance (^{1}H NMR) spectrometers.

iii. To prepare PAni/Alkyd and PAni-TiO_2/Alkyd films then characterized its chemical structures by FTIR, UV-Vis and XRD spectrometers.

iv. To apply PAni/Alkyd and PAni-TiO_2/Alkyd films in DSSC application (adhesion, conductivity and PCE analyses).

1.6 Scope of Thesis

Primarily, this study attempts to produce PAni/Alkyd films with short curing time, good adhesion on FTO substrate and high conductivity properties that can be apply in solar cell application. The aim of this study is to apply PAni composite as a conducting material together with an incorporation of POB alkyd as a non-conductive and non-toxic binder in DSSC application. Based on the previous research study, implementation of PAni/Alkyd as CE in DSSC in the absence of noxious chemicals is still new and reserves a space to be explored.

1.7 Thesis Outline

Chapter 1 describes background of the study with the introduction of solar cell technology and focusing on DSSC device. A basic components and working principles of DSSC is described here. Besides, this chapter also summarized the problem statements arising from the DSSC application, thus bring the aim and objectives of the study.

In Chapter 2, the literature review regarding CPs, POB alkyd and DSSC are discussed. The techniques used and findings from their research are reported in this part. Various applications of using CPs, PAni and POB alkyd are briefly described to observe its advantages and disadvantages. Then, many examples of DSSC application based on different CE materials are also reported.

In Chapter 3, all the chemicals and methods used for synthesis of PAni and POB alkyd are explained. A flow chart for the whole preparation of PAni/Alkyd films are also shown to explain the detail work of this study. The techniques and instrument used for sample characterizations are described. Besides, fabrication of PAni and PAni/Alkyd as CE in DSSC application is discussed.

In Chapter 4, all the results from the conducted experiment are presented. All the data and the outcomes of the research are discussed with scientific explanation. Finally, Chapter 5 concluded the overall findings of the study and suggestions for future research study are also included in this part.

CHAPTER 2: LITERATURE REVIEW

2.1 Conducting Polymers (CPs)

The discovery of CPs in 1977 through the research work based on polyacetylene (PA) has received much attention among researchers up to now. PA was the first CPs found to behave as semiconductor that capable of conducting electricity. Shirakawa et al., reported that the conductivity of the *trans*-PA films significantly increased many orders of magnitude when doped with halogens such as chlorine, bromine and iodine vapour. The conductivity of the *trans*-PA films were measured by four probe of direct current (DC) technique at room temperature. The *trans*-PA doped with iodine vapor has recorded the highest conductivity of 38.00 $\Omega^{-1}cm^{-1}$ where it has rapidly increased over seven orders of magnitude compared to pristine *trans*-PA with initial conductivity of 4.40×10^{-5} $\Omega^{-1}cm^{-1}$ (Shirakawa et al., 1977).

CPs are conjugated polymers containing alternating single and double bonds at polymer backbone as well as exhibiting a semiconducting behavior. Principally, CPs became an electrically conductive after the doping process. This process has converted an organic polymers either insulator or semiconductor with low conductivity range of 10^{-10} to 10^{1} Scm^{-1} to metallic behavior with high conductivity range of 1.00 to 10^{4} Scm^{-1} (Mishra., 2018). Furthermore, CPs have uncomplicated synthesis procedures either via chemical oxidation or electrochemical methods and its molecular structure can be easily adjusted through structural derivations or copolymerization process (Bai & Shi, 2007).

Besides PA, CPs such as Polypyrrole (PPy), polythiophene (PTh) and polyaniline (PAni) also have gained attraction to the researchers. Ppy is extensively applied in biosensors, tissue engineering and anti-corrosion application (Balint et al., 2014). In year 2015, PPy has been used in the fabrication of DNA biosensor by Miodek and co-workers. In this biosensor, Ppy and polyamidoamine (PAMAM) dendrimers were applied as a coating layer on multiwalled carbon nanotubes (MWCNTs) as a molecular transducer that amplifies the electrochemical signal for DNA detection. PPy was coated on carboxylated MWCNTs through electropolymerization reaction followed by electrochemical oxidation of PAMAM. The real samples of DNA from *Mycobacterium tuberculosis* were tested using MWCNTs-PPy-PAMAM biosensor and recorded a detection limit of 0.3 fM. In brief, this biosensor has highlighted a significant sensitivity and selectivity results (Miodek et al., 2015).

On the other hand, PTh is being extensively used in display devices, photovoltaic applications and electrochemical capacitors. In year 2012, PTh thin films were synthesized by Patil et al., through simple successive ionic layer adsorption and reaction (SILAR) method at room temperature for supercapacitor application. The electrochemical performances of the PTh were investigated using cyclic voltammetry (CV) and galvanostatic methods. The PTh supercapacitor showed maximum specific capacitance of 252.00 Fg^{-1} at the scan rate 5.00 mVs^{-1} with specific energy of 4.86 $Whkg^{-1}$ and specific power of 363.36 Wkg^{-1}. As a result, they reported that the PTh thin film electrode is suitable for the energy storage application such as electrochemical capacitor due to its high supercapacitive performance and good stability (Patil et al., 2012).

Presently, research interests are most focusing on PAni due to its great chemical stability, conductive and good stability in term of intrinsic redox property as compared to other CPs. Furthermore, PAni has potential approach in diverse fields inclusive of sensors, battery electrodes, microwave absorption and solar cells (Asim et al., 2012; Kouhnavard et al., 2014).

2.2 Polyaniline (PAni)

Principally, PAni is a phenylene based polymer containing hundreds to thousands of Ani constitutional units. Based on the chemical structure of PAni as shown in **Figure 2.1**, the –NH groups are presented in the PAni backbone which promote a stable intrinsic redox reaction (Palaniappan et al., 2008).

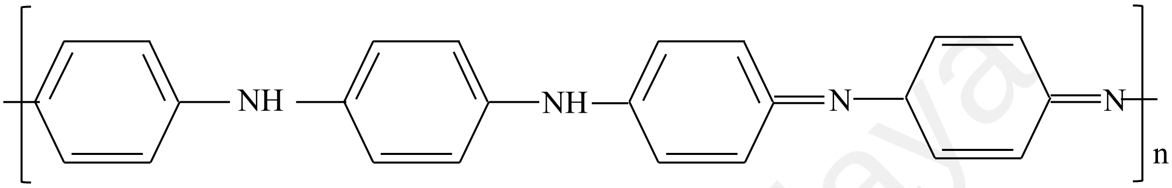

Figure 2.1: The chemical structure of PAni (Saleh et al., 2019).

Apart from that, PAni exists in various oxidation states with different colours which are fully oxidized pernigraniline (blue-violet), fully reduced leucoemeraldine (transparent yellow), and half oxidized/half reduced emeraldine base (EB, blue) as shown in **Figure 2.2**. Each oxidation state of PAni has different physical characteristics and can be converted from one to another state through redox reaction. The redox reactions for these conversions are reversible (Albuquerque et al., 2004; Zohshki et al., 2017).

Among these oxidation states, EB is the most effective form of PAni because it is highly stable at room temperature and becomes conductive through acid protonation or doping process. PAni in EB state can be easily switched from insulating form to conductive form known as emeraldine salt (ES, green) while pernigraniline and leucoemeraldine are poor conductors even doped with acid (Afzal et al., 2009; Karaoglan & Bindal, 2018).

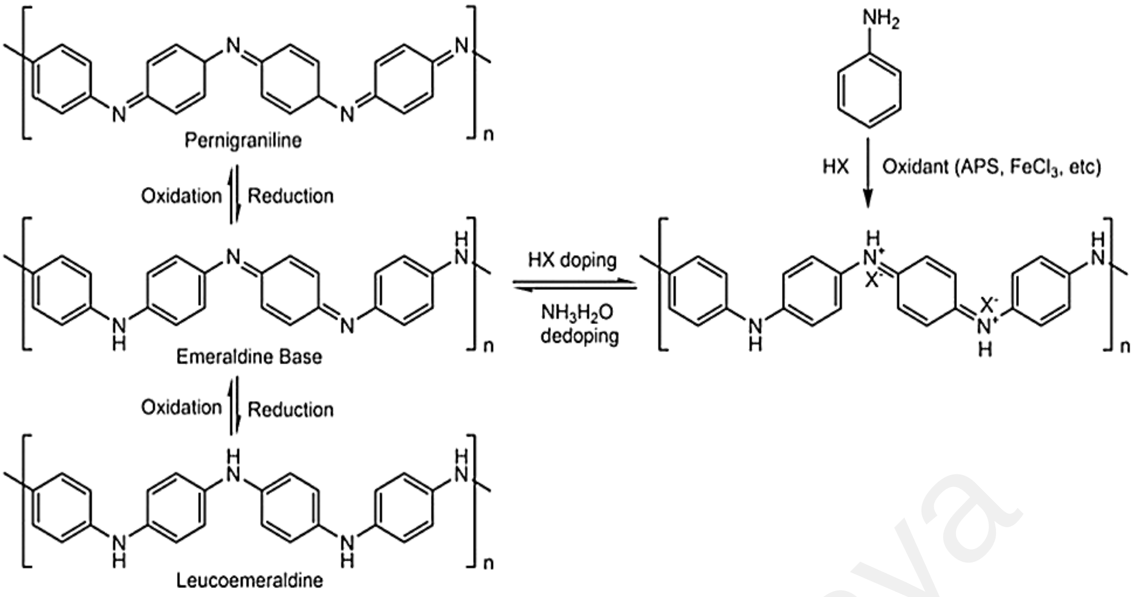

Figure 2.2: Chemical structures for different oxidation states of PAni (Li et al., 2009).

PAni is broadly applied in many industrial uses due to its excellent characteristics for example easy synthesis route, low cost, easy availability and good environmental stability. Besides, the different colors for different forms of PAni, doping/dedoping response, and the multiple oxidation/reduction states of PAni has broaden its application in various fields for example as an electrochromic devices, supercapacitors, flexible electrodes, catalysis, sensing platforms, conductive adhesive, corrosion inhibitor, solar cells and others (Stejskal et al., 2010).

Despite of the instability for PAni in pernigraniline salt form, some researchers have worked on the stabilization of pernigraniline salt. In year 2013, Jeon and co-workers were firstly reported the pernigraniline salt form of PAni (PAni:Polyacid) electrode for electrochemical energy storage system. Poly(2-acrylamido-2-methyl-1-propanesulfonic acid) was used as polyacid to stabilize the fully oxidized pernigraniline salt which is normally unstable as a homopolymer. As a result, they reported that PAni:polyacid electrode was capable to store charge under extremely oxidizing potentials of 4.50 V with storage capacity of 243.00 mAhg^{-1} (Jeon et al., 2013).

Boddula and Srinivasan utilized PAni EB nanofibers as catalyst in the preparation of aldoximes. Aldoximes are normally used to synthesize oximes that are effective in the purification and characterization of carbonyl compounds. In this research work, PAni EB nanofibers were synthesized using Ani as monomer and sodium persulfate as oxidant in the hydrochloric acid (HCl) medium. The resulted PANI-HCl salts were then dedoped to PAni EB. After that, the synthesized PAni EB nanofibers were used as novel polymer base catalyst to prepare aldoximes from different kind of aldehydes at room temperature. Finally, they reported that, PAni EB gave an excellent yield of aldoximes range of 75.00 to 98.60% in short reaction time of 10 min (Boddula & Srinivisan, 2014).

In year 2003, the investigation on the application of conductive adhesive using PAni ES were done by Sancaktar and Liu. Thus, a non-conductive nitrocellulose solution based adhesive was mixed with PAni ES (30%, 40%, and 50% by volume) and were used to produce an electrically conductive composite adhesive films. The composite films were cured at room temperature for 24 h. The best result showed by the composite films with 30% of PAni ES as the conductive adhesive with resistivity of 2700.00 Ωcm (Sancaktar & Liu, 2003). Besides being a conductive adhesive material, PAni ES also effective in inhibiting corrosion on steel (Ramlan et al., 2017).

Apart from that, PAni in ES state can be potentially applied as solar cell materials because of its electrically conductive property. In year 2012, AbdulAlmohsin and co-workers reported on the preparation aluminum-doped zinc oxide (ZnO)/PAni hybrid solar cell. In this study, PAni was synthesized on indium tin oxide (ITO) substrate via electropolymerization while aluminum-doped ZnO (AZO) nanoparticles were coated on

ITO substrate through sputtering technique. The prepared AZO/PAni cells were tested and recorded acceptable photovoltaic parameters including open circuit voltage (V_{oc}) of 195.00 V, short circuit current density (J_{sc}) of 0.08 $mAcm^{-2}$, fill factor (*ff*) of 0.41 and final PCE of 0.01% (AbdulAlmohsin et al., 2012).

In year 2014, nano PAni film was electrochemically deposited on organic solar cell by Han and co-workers. This solar cell device resulted good photovoltaic performance with overall efficiency of 2.76% (Han et al., 2014). Based on the reported previous research study, PAni offers wide benefits in many applications. However, the brittleness of PAni has affected its adhesion onto the substrate and unfortunately has minimized its application in various specializations (Li et al., 2009; Kawata et al., 2013). Thus, it is important to find others options to enhance the adhesion of PAni for example by finding the suitable adhesive materials that can overcome these drawbacks.

Polyisobutylene, polyisoprene, polyurethane, silicone, polyolefin and polyacrylate are the commonly used adhesive materials. However, an environmental issue should be considered when handling these materials for industrial application (Dinte & Sylvester, 2017). Thus, the utilization of environmental friendly adhesive material such as POB alkyd can overcome all the drawbacks of the available commercial adhesive materials.

2.3 Palm Oil-Based (POB) Alkyd

In recent years, POB alkyd resins have mostly gained popularity in coating industry because it is highly resistant to moisture, flexible and good in preventing surface corrosion (Uzoh et al., 2015). Generally, the term ‘alkyd’ is derived from alcohol and acid. Alkyd is commonly synthesized from vegetable oils that react with polyol via alcoholysis reaction with the addition of acid or base catalyst to form monoglycerides.

Then, the reaction was further continued with addition of dibasic acids through esterification reaction (Islam et al., 2015).

There are many vegetable oils such as linseed, sunflower, castor, soybean, rapeseed and palm oils that are used for the synthesis of alkyd resins. These vegetable oils are comprises mainly of triglyceride, consisting three elements that are carbon, hydrogen and oxygen. Triglyceride consists of carboxylic acids molecules from three fatty acids and one glycerol molecule as shown in **Figure 2.3**. The presence of fatty acids group improves the physical properties of alkyd in terms of flexibility, adhesion as well as the resistance to water and chemicals (Güner et al., 2006; Liang et al., 2014).

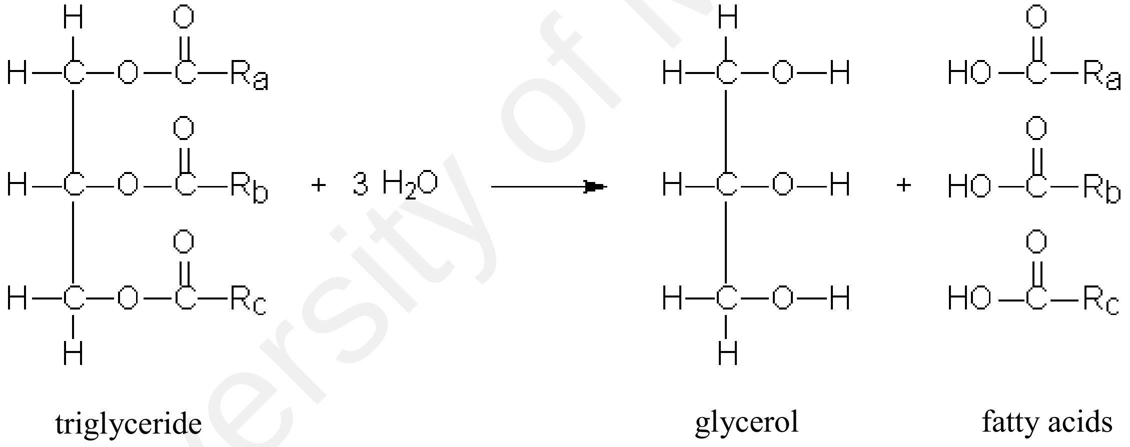

Ra, Rb, Rc represents the hydrocarbon chain in a fatty acid molecule

Figure 2.3: Components of triglyceride (Díaz et al., 2014).

In year 2008, alkyd resin was prepared from crude castor oil by Hlaing and Oo. Castor oil is useful in protective coating that act as a plasticizer in alkyd system. There are three important stages before further synthesized to alkyd resin including neutralization of crude castor oil, bleaching of neutralized oil and dehydration of castor oil. The dehydrated castor oil can be classified as drying oils that able to polymerize or ‘dry’ immediately on the substrate to form a tough, adherent and abrasion resistance film. In their study, alkyd resin with acid value of 6.60 and iodine value of 80.24 was prepared from the dehydrated castor oil through alcoholysis reaction in excess glycerol using 0.30% (wt%) of sodium hydroxide as catalyst. The resulted alkyd resin was significantly useful for surface coating application due to its high chemical resistance, scratch hardness of F grade and gouge hardness of HB grade (Hlaing & Oo, 2008).

On the other hand, soybean is one of the popular vegetable oils that have been used to synthesize alkyd resin for paints and inks manufacturing. In year 2018, alkyd resin based on soybean oil and glycerin was prepared by Elba et al., using zirconium octoate as catalyst. The function of zirconium octoate in alcoholysis reaction is to prevent oxidation of oil and useful for the light colour of final product of alkyd resin. As a result, alkyd resin with good impact resistance of 125.00 cm as well as good chemical resistance where the films were completely unaffected when immersed in distilled water, aqueous sodium chloride (10%) and potassium hydroxide (KOH) solution at room temperature. Besides, the synthesized alkyd resin also has light colour with high yellowing resistance and high flexibility where no cracking or peeling was observed during the test (Elba et al., 2018).

Besides, Zheng and co-workers reported on the preparation of alkyd resin with soy-based polyols. In their study, soybean oil was firstly epoxidized through solution polymerization to get the soy-based alkyd. The final alkyd resins with light yellowish in colour indicated its good transparency appearance and low acid value range of 24.42–26.82 were produced (Zheng et al., 2011). Therefore, the previous research works regarding the preparation of soy-based alkyds were significantly applied as additive binder in coating and paint industry. Among all vegetable oils, palm oil is the most abundantly oil in Malaysia as Malaysia can be classified among the world's biggest palm oil production.

Thus, preparation of the alkyd resin from non-drying palm oil has expands the application of the oil in various areas as environmental friendly material because of its abundance and renewability (Uzoh et al., 2013). In year 2014, Islam et al., reported the synthesized of alkyd based resin from palm oil through alcoholysis and esterification reactions using pthalic and maleic anhydrides. Overall results from this research study indicated that POB alkyd resins with high gloss (62.00 to 77.00 GU), good hardness (2B), sufficient molecular weight (2283.00 to 2803.00 g mol^{-1}) and good resistivity. These POB alkyd resins are potentially applied in paint and coating industries (Islam et al., 2014).

In year 2013, Nanvaee and co-workers utilised the less valuable by product of palm oil known as palm stearin for alkyd synthesis. The objective of this study is to replace others valuable vegetable oils like linseed and dehydrated castor oil for the preparation of alkyd. They reported on alkyd resin with good adhesion property with crosshatch adhesion of 98% to 100% and good chemical resistance towards water as well as acid. Finally, the alkyd paint that prepared from the resulted alkyd resin from palm stearin (POB alkyd) showed drying time with set-to-touch time of 50 − 55 min and tack free time of 180 − 205 min that produce a smooth and homogeneous films, indicating excellent coating performance (Nanvaee et al., 2013).

As such, POB alkyd significantly has a good adhesive property that is actively applied in coating and paint industry. Thus, POB alkyd could be a great match for improving the adhesion property of PAni and consequently will broaden its application in various fields especially as a good counter electrode (CE) in dye-sensitized solar cell (DSSC) device. Implementation of PAni as CE in DSSC set up by improving its adhesion on FTO substrate using POB alkyd still new and reserves a space to be explored.

2.4 Dye-Sensitized Solar Cell (DSSC)

Solar cells are generally divided into three generations up to recent years. The first generation was invented by Chapin and co-workers in 1954 through a silicon *p-n* junction photocell that has converted light energy into electricity. PCE of 6.00% is achieved but this type of solar cell has complicated manufacturing method and high cost (Chapin et al., 1954). In year 1963, second generation of solar cell was continued by Cusano and co-workers through cadmium telluride (CdTe) solar cell with PCE of 6.00%. The manufacturing cost for second generation was significantly reduced but it has difficult module technology and limited stability (Cusano et al., 1963).

In order to overcome the drawbacks of first and second generations of solar cells, many research studies were implemented and finally bring to the next generation of solar cells. The primary purpose of this generation is to reduce the cost as well as to increase its efficiency, beginning with the DSSC prototype (Saranya et al., 2015). DSSC or Gratzel cell was firstly invented by O'Regan and Gratzel in 1991 with PCE of 7.10% to 7.90%. They applied the mesoporous film of titanium dioxide (TiO_2) nanocrystalline particles with 10.00 μm thick and high surface area as a semiconductor electrode in DSSC set up. In order to absorb higher light harvesting efficiency, a monolayer of a charge transfer dye was coated on the TiO_2 electrode.

As a result, 46.00% and 80.00% efficiencies of the incident solar energy flux were successfully harvested. Finally, large J_{sc} value with >12 $mAcm^{-2}$ was obtained, thus, significantly increased the performance for PCE of the system during DSSC measurement (O'Regan & Gratzel, 1991). Principally, DSSC device consist of four main components including photoanode of metal oxide semiconductor, sensitized dye, redox couple electrolyte and CE. **Figure 2.4** illustrated the diagrammatic scheme of DSSC. Generally, TiO_2 is used as photoanode due to its larger energy bandgap (3.2 eV) for high PCE of DSSC.

Then, the most frequent high performing dye are ruthenium (Ru)-centered polypyridyl complexes such as di-tetrabutylammonium cis-bis(isothiocyanato)bis(2,2'-bipyridyl-4,4'-dicarboxylato) ruthenium (ii) (N719), cis-Bis(isothiocyanato)bis(2,2'-bipyridyl-4,4'-dicarboxylato) ruthenium (ii) (N3) and cis-Bis(isothiocyanato) (2,2'-bipyridyl-4,4'-dicarboxylato) (4,4'-di-nonyl-2'-bipyridyl) ruthenium (ii) (Z907). Other components of DSSC such as liquid electrolyte of iodide/triiodide (I^-/I_3^-) is usually apply as the redox couple electrolyte that is sandwiched between the photoanode and CE (Theerthagiri et al., 2015).

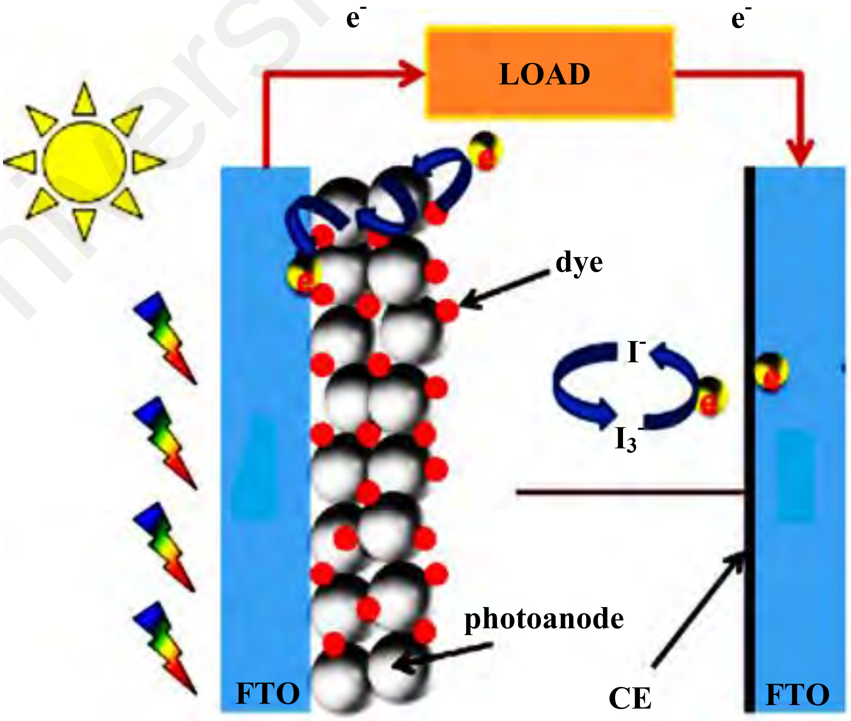

Figure 2.4: Diagrammatic scheme of DSSC (Bella et al., 2015).

Metals like gold (Au), silver (Ag), Ru, titanium (Ti), palladium (Pd), iridium (Ir), and Pt as well as an alloy are the commonly traditional materials used as CE in DSSC because these materials exhibit high conductivity and good electrocatalytic activity (Wu et al., 2017). Au has been used as CE material as it possessed high electrocatalytic activity and good corrosion resistance property. In year 2015, Sun and co-workers have prepared a transparent conductive CE of Au/amorphous indium zinc oxide bilayer. They reported CE with conductivity of 1.20×10^{5} Scm^{-1}. As a result, solar cell parameters with V_{oc}: 0.64 V, Jsc: 9.83 $mAcm^{-2}$, *ff* : 0.59 and good PCE of 3.73% were recorded (Sun et al., 2015).

Besides, Ag has widely applied as CE because it shows high electrical and thermal conductivity with an excellent corrosion resistance. Therefore, Snaith and co-workers have replaced Au with Ag electrodes. They reported PCE of 5.10% under irradiation of high-intensity simulated sunlight (Snaith et al., 2007). In year 2016, An and co-workers have fabricated Ru nanofibers as CE in DSSC device through a sequential process of electrospinning, post-calcination and hydrogen reduction. They manage to attain excellent photovoltaic performance consisting of resistance (R_{CT}) value of 12.5 Ωcm^{-1}, J_{sc} value of 14.77 $mAcm^{-2}$ and PCE of 6.23% (An et al., 2016).

Apart from that, Noh and Song have successfully used Ti metal as a CE material in DSSC device by coating the Ti/Ru bilayer with 50.00 nm-Ti/50.00 nm-Ru on FTO substrate using RF sputtering technique. The prepared Ti/Ru bilayer has reduced the interface resistance on substrate and consequently increased its catalytic activity in the system during DSSC measurement. Thus, high performance of DSSC wih PCE of 2.40% was significantly recorded (Noh and Song, 2014). Pd also is a noble metal that shows an excellent heat conductivity, low resistivity and chemically stable metal that was applied as CE in DSSC. In year 2013, Noh and co-workers have coated Pd on FTO glass using atomic layer deposition (ALD) and obtained good PCE of 4.32% in DSSC device (Noh & Song, 2013).

Metal like Ir has attracted wide attention to many researchers due to its lower resistivity of 4.70×10^{-8} Ωm and lower cost with nearly same electrocatalytic activity with Pt. Mokurala and co-workers have achieved PCE of 7.20% with the application of Ir as CE in DSSC. Ir metal was coated on FTO glass at room temperature via radio-frequency (RF) sputtering technique. Alloy has also gained popularity as CE materials among researchers for the cost reduction of CE while increase the PCE during DSSC measurement (Mokurala et al., 2015). In year 2014, Pt-free alloy as CE has been investigated by Chen and co-workers through the preparation of a binary Cobalt-Nickel (Co-Ni) alloy through hydrothermal treatment. They reported that the prepared Co-Ni alloy as exhibits ideal charge-transfer ability and good electrocatalytic activity with high PCE of 8.39% in DSSC device (Chen et al., 2014).

Furthermore, Pt-alloy as CE also has been extremely studied to improve the DSSC performance. In year 2016, Yang and Tang reported the synthesized of NiCuPt alloy as CE. Ni was firstly electrodeposited on zinc oxide (ZnO) microrod templates followed by galvanic displacement of outward Ni and copper (Cu). This NiCuPt alloy exhibits superior electrocatalytic activity and charge-transfer ability, producing an enhancement of PCE up to 9.66% in DSSC device (Yang and Tang, 2016). Up to now, Pt is the best favored CE material for DSSC device with PCE over 12.00% (Wu et al., 2017). It is because Pt is highly conductive, highly reflective and great electrocatalytic properties as well as excellent physical and chemical properties.

In year 1993, Nazeerudin and co-workers have achieved high performance of PCE (10.00%) during DSSC measurement. The DSSC was fabricated by coating Pt with thickness of 2.00 mm on TCO substrate using sputtering technique. They reported the improvement of light harvesting efficiency through the thicker Pt film that was deposited on TCO substrate, resulting to higher PCE of DSSC device (Nazeerudin et al., 1993). In year 2012, Jeong and co-workers introduced a Pt nanocup (NC) array with a diameter of 300.00 nm as CE using UV-based nanoimprint lithography (NIL). The Pt NC array produced in their research finding showed low R_{CT} and PCE of 9.75% (Jeong et al., 2012).

In year 2014, Wu et al., have developed Pt nanotubes (PNTs) using facile polycarbonate template method. The DSSC fabrication composed of PNTs as CE and magnesium oxide (MgO) block layer on TiO_2 photoanode, leading to good performance of PCE with 9.05% (Wu et al., 2014). In year 2013, Dao and co-workers were deposited Pt nanoparticles (NPs) on FTO substrate. According to their research study, the heating rate would affect the catalytic activity and overall efficiency of DSSC. The DSSC using Pt-NPs as CE gave PCE of 9.30% (Dao et al., 2013). Although application of Pt as CE produces high PCE in DSSC device but Pt is expensive where it cost over 40% of the whole photovoltaic cell. Therefore, CPs have been extensively studied in order to overcome this drawback of Pt.

2.5 Application of CPs in DSSC

Over the last decade, research efforts have been directed towards CPs due to the potential uses as conducting substrates, holes conductors and CE materials for DSSC device. Among various CPs in the market, PAni is one of the most intensively studied CPs for DSSC because PAni possess high conductivity, good environmental stability and interesting redox properties. Thus, different varieties of PAni with carbonaceous materials and various metals have been synthesized by many researchers and used as CE materials to improve the performance of PCE during DSSC measurement. The development of PAni as CE in DSSC device from previous research works were outlined in **Table 2.1, Table 2.2 and Table 2.3.** It can be observed that pristine PAni as CE showed PCE range of 0.42% to 7.15% while PAni-carbonaceous material recorded PCE range of 1.00% to 7.91% and PAni-metal obtained PCE range of 2.72% to 8.55%.

In year 2008, pristine PAni was prepared by Li and co-workers as CE in DSSC. PAni was synthesized through aqueous oxidative polymerization with perchloric acid as dopant and APS as oxidant. They produced PAni nanoparticles with diameter of 100.00 nm that able to improve its catalytic activity as it exhibits high surface area and microporous structure. As a result, overall PCE of 7.15% was obtained with PAni as CE that is higher than Pt as CE (6.90%) under the same condition. Although better PCE has been achieved, PAni exhibits brittleness and poor adhesion towards the substrate during its application in DSSC. Thus, the poor adhesion property of PAni restricted its application in DSSC (Li et al., 2008).

Besides, PAni-carbonaceous material as CE also showed high PCE in DSSC device. Bora et al., have fabricated a carbon black/PAni nanotube (CB/PAniNT) nanocomposite as a potential CE material to replace Pt in DSSC. CB is used due to its mesoporous structure which generates a large active surface area that can increases the interface between the CE and electrolyte for excellent performance of DSSC. CB/PAniNT was synthesized through in-situ chemical oxidation polymerization technique. The DSSC was assembled using 0.75 wt% CB/PAniNT nanocomposite film with a 10.58 μm thick as CE resulting to J_{SC}, V_{0C} and R_{CT} values of 12.52 mAcm^{-2}, 0.74 V and 0.99 Ω. Overall PCE of 6.62% was obtained compare to PAniNT with PCE of 3.49% (Bora et al., 2017). However, PAni and CB encounter shortage of self-adhesion causing low surface contact with the substrate, subsequently reduced its application in DSSC (Chen et al., 2011).

Apart from that, PAni-metal like Cu-doped PAni was prepared as CE in DSSC by Tas and co-workers in various solvents including water, dioxane, dimethyl formamide, tetrahydrofuran, acetonitrile and acetone. They found that Cu-doped PAni synthesized in acetonitrile possessed the highest PCE of 6.37% and by comparison, PCE of pristine PAni was 2.44% (Tas et al., 2017). Besides, application of PAni-metal as CE was also reported by Yu and co-workers as they used PAni-Pt alloy in their study and the phothovoltaic performances were investigated by electrochemical deposition method. The PCE of 8.08%, 7.26% and 6.83% were obtained from employing PAni/CoPt, PAni/PdPt and PAni/MoPt as CE, yielding 42%, 25% and 20% improvement in comparison with 5.69% on PAni as CE in DSSC (Yu et al., 2016).

Although application of PAni as CE in DSSC showed quite high PCE in DSSC compare to Pt CE, PAni has a drawback in term of adhesion towards the substrate. The introduction of POB alkyd into PAni and PAni/m-Cresol/TiO_2 by Kawata and co-workers has significantly enhanced the adhesion of PAni on FTO substrate. The films exhibited conductivity range of 9.03×10^0 to 7.29×10^1 Scm^{-1} and PCE range of 3.00% to 5.50% (Kawata et al., 2013). m-Cresol is used as a solvent to dissolve the TiO_2 paste and would reduce the blockage of TiO_2 along PAni chain. Then, m-Cresol can also act as a secondary dopant and significantly increased the electrical conductivity of PAni/m-Cresol/TiO_2/Alkyd composite, producing high PCE in the system during DSSC measurement.

However, the presence of toxic substance like m-Cresol produced non-environmental friendly material as CE for DSSC and exposure to m-Cresol over a long period time will causes adverse health issues (Agency for Toxic Substances and Disease Registry, ATSDR, 2008). Therefore, different type of PAni and POB alkyd can be further studied in order to produce an environmental friendly of PAni/Alkyd as CE with good adhesion on the FTO substrate, possess high conductivity and high PCE in DSSC device. Besides, this research study opens new perspectives for the use of conducting PAni composite that has modified with POB alkyd as a non-conductive binder without any toxic substances in solar panel application.

Table 2.1: A list of DSSC components based on pristine PAni as CE with conductivity and PCE results.

CE	Photoanode	Dye	Conductivity (Scm^{-1})	PCE (%)	References
PAni	TiO_2	N3	-	0.42	Saad et al., 2014
PAni	TiO_2-methyl cellulose	N719	1.25×10^{-2}	1.91	Amalina et al., 2019
PAni	TiO_2	N719	1.51×10^{-4}	2.96	Tas et al., 2017
PAni	TiO_2	N719	-	3.1	Duan et al., 2015
PAni	TiO_2	N3	1.01×10^{2}	3.70	Kawata et al., 2013
Porous PAni nanotubes	TiO_2	N719	-	5.57	Park et al., 2015
PAni	TiO_2	N719	-	5.65	Yang et al., 2015
PAni	TiO_2	N719	-	5.69	Yu et al., 2016
PAni	TiO_2	N719	-	7.15	Li et al., 2008

Table 2.2: A list of DSSC components based on PAni-carbonaceous material as CE with conductivity and PCE results.

CE	Photoanode	Dye	Conductivity (Scm^{-1})	PCE (%)	References
PAni-single wall carbon nanotube (SWCNT)	TiO_2	N3	-	1.00	Saad et al., 2014
PAni-SWCNT/ graphite	TiO_2	N3	-	1.80	Saad et al., 2014
Water-soluble PAni/graphene	TiO_2	N719	-	4.46	Wan et al., 2014
$NiCo_2O_4$/ reduced graphene oxide/PANI	TiO_2	N719	-	4.67	Manikandan et al., 2019
CB/PAniNT	TiO_2	N719	4.06	6.62	Bora et al., 2017
PAni nanofiber/carbon	TiO_2	N719	-	6.85	Chen et al., 2011
PAni-multiwalled carbon nanotube (MWCNT)	TiO_2	N719	-	9.24	Zhang et al., 2015

Table 2.3: A list of DSSC components based on PAni-metal as CE with conductivity and PCE results.

CE	Photoanode	Dye	Conductivity (Scm^{-1})	PCE (%)	References
Tungsten trioxide/ PAni/ Polyacrylonitrile	electrospun nanofibrous mats	-	8.33×10^{-7}	2.72	Eslah & Nouri., 2019
PAni/m-Cresol/ TiO_2/ POB Alkyd	TiO_2	N3	7.29×10^{1}	3.0	Kawata et al., 2013
PAni/m-Cresol/ TiO_2	TiO_2	N3	1.01×10^{2}	5.50	Kawata et al., 2013
Al-doped PAni	TiO_2	N719	1.30×10^{-2}	5.97	Tas et al., 2017
Cu-doped PAni	TiO_2	N719	2.92×10^{-2}	6.37	Tas et al., 2016
Ni sulfide/ PAni/ Ti	TiO_2	Z907	-	7.35	Yue et al., 2014
PAni/CoPt	TiO_2	N719	-	8.08	Yu et al., 2016
PAni/Co sulfide	TiO_2	N719	-	8.55	Yang et al., 2015

CHAPTER 3: METHODOLOGY

3.1 Chemicals

All chemicals used in the synthesis of polyaniline (PAni) and PAni-titanium dioxide (TiO_2) such as aniline (Ani, 99.50%) monomer, dioctyl sodium sulfosuccinate (AOT, 96.00%) and ammonium persulphate (APS, 98.00%) were purchased from Sigma-Aldrich, USA while hydrochloric acid (HCl, 37.00%) was acquired from RCI Labscan Limited, Thailand. TiO_2 nanoparticles (99.50%) with particle size of ~21.00 nm that used for the synthesis of PAni-TiO_2 were obtained from Merck, Germany.

Chemicals that used in the synthesis of palm oil-based (POB) alkyd such as glycerine (99.50%) was received from Emery Oleochemicals Malaysia Sdn. Bhd and potassium hydroxide (KOH, 85.00%) was purchased from Systerm, Malaysia. Refined, bleached and deodorised palm stearin with iodine value, IV of 38.82 was acquired from Southern Edible Oil Industries Malaysia Sdn. Bhd. Phthalic anhydride (PA) was purchased from DC Chemical, Korea while fumaric acid (FA, 99.00%) was obtained from Merck, Germany.

Other chemicals used for the preparation of PAni-Alkyd and PAni-TiO_2/Alkyd films are benzophenone (99.00%, Sigma-Aldrich, USA), methyl acrylate (MA, 99.50%, Fluka Chemika, Switzerland), methyl methacrylate (MMA, 99.00%, Merck, Germany) and cyclohexyl methacrylate (CMA, Degussa-Huls Gruppe, Germany). Fluoride-doped tin oxide (FTO) glass that used for the film's substrate was acquired from Kumpulan Abex Sdn. Bhd, Malaysia. Chemicals used in the solar cell application such as TiO_2, ruthenium dye and iodolyte AN50 were purchased from Solaronix, Switzerland. Besides, acetone (99.50%) that obtained from Sigma-Aldrich, USA and distilled water were used to clean laboratory glass wares. All chemicals and solvent were used as received without further purification.

3.2 Apparatus

In this study, apparatus such as measuring cylinder, beaker, dropper, spatula, pipette, magnetic stirrer, separating funnel, retord stand and ice box were used for PAni and PAni-TiO_2 synthesis. Another important apparatus that were used during POB alkyd synthesis including digital thermometer, overhead stirrer, straight stainless steel stirrer, condenser, reaction flask, volumetric flask and measuring cylinder. Besides, conical flask and burrete were used to determine acid number (AN) of the POB alkyd resin produced at the last stage of POB alkyd synthesis. For dye-sensitized solar cell (DSSC) application, syringe was used to inject electrolyte between the TiO_2 photoanode and counter electrode (CE).

3.3 Synthesis of PAni and PAni-TiO_2

PAni and PAni-TiO_2 were synthesized through chemical oxidation method by using Ani as monomer, AOT as dopant and APS as oxidant at 0 ˚C. For the synthesis of PAni, AOT dopant (6.67 g, molar ratio: 5) was firstly dissolved in 1.00 M of HCl solution, then Ani monomer (1.40 g, molar ratio: 5) was slowly added into the AOT solution to obtain a homogenized Ani/AOT mixture. The mixture was stirred for 2 h. Then, APS (3.42 g, molar ratio: 5) solution was slowly dropped into the mixture to initiate the polymerization. The reaction was left for 24 h. Meanwhile, for the synthesis of PAni-TiO_2, TiO_2 were added into the Ani/AOT mixture under ultrasonic action for around 4 h before addition of APS solution. PAni-TiO_2 was prepared with different quantity of

TiO_2 content (10%, 20% and 40%) labelled as PAni-Ti10, PAni-Ti20 and PAni-Ti40, respectively.

The polymerization reaction for PAni-TiO_2 was continued for 24 h. After that, excess amount of toluene was added into the mixture to terminate the polymerization process of PAni and PAni-TiO_2. PAni and PAni-TiO_2 were then extracted into toluene layer by using separating funnel to remove the unreacted Ani monomer, excess AOT and APS in the aqueous phase. The organic phase was washed with distilled water to remove others water soluble impurities. In this study, the concentration of PAni and PAni-TiO_2 solution (~ 2.50 %) were coated on FTO glass by using SPS Spin 150 spin coater using three-step process. Firstly, acceleration steps for 10 s at 1000 RPM. Secondly, steady-state coating steps for 10 s at 5000 RPM. Thirdly, deceleration steps for 10 s at 1000 RPM. The concentration of PAni and PAni-TiO_2 solution were determined by calculating its percentage in toluene based on **Equation 3.1**.

$$\text{Percentage of PAni in toluene (\%)} = \frac{(y-x)}{(z-x)} \times 100\ \% \qquad \textbf{Equation 3.1}$$

where,

x = weight of empty petri dish
y = weight of dry PAni (after dried in oven)
z = weight of PAni solution

3.3.1 Characterizations of PAni and PAni-TiO_2

3.3.1.1 Fourier Transform Infrared (FTIR) Spectrometer

FTIR spectrometer is used to obtain the specific information on molecular and chemical structure of the chemical compounds. It is widely used for analysis of organic compound, polymer synthesis, petrochemical engineering, pharmaceutical and food industry. There are four types of FTIR analysis techniques which are transmission, Attenuated Total Reflectance (ATR), Diffuse Reflectance (DRIFTS) and specular reflectance. Among all FTIR analysis techniques, FTIR-ATR is mainly conducted by most of the researchers due to its ability to measure all types of samples such as solids, liquids, powders, pastes, pellets, slurries and fibers. Besides, FTIR-ATR only requires simple analysis technique, able to analyze the samples within a few seconds and produces data with high accuracy (Nancy and Qian, 2018).

In this study, FTIR-ATR spectrometer (Perkin Elmer RX1 model) was used to characterize the chemical structure of PAni and PAni-TiO_2 films. PAni and PAni-TiO_2 that coated on the glass substrate were analysed using FTIR-ATR spectrometer from wavenumber 400 cm^{-1} to 4000 cm^{-1} at resolution of 4 cm^{-1}.

3.3.1.2 Ultraviolet-Visible (UV-Vis) Spectrometer

UV-Vis spectrometer is one of the most popular analytical instruments over the last three decades as it offers simplicity, versatility, fast detection and low cost. Principally, it analyzed samples with electromagnetic radiations between 190 nm to 800 nm. This electromagnetic radiations are referring to the ultraviolet (UV, 190-400 nm) and visible (Vis, 400-800 nm) regions. UV-Vis spectrometer provides information about π-electron system, conjugated unsaturation, aromatic compound and conjugated non-bonding electron system (Kumar, 2006).

In this study, the conducting behavior of PAni and PAni-TiO_2 were determined by using UV-Vis spectrometer (UV-1650 PC, Shimadzu). During UV-Vis analysis, PAni and PAni-TiO_2 films that coated on the glass substrates were placed at the sample position while non-coated glass substrates were placed at the reference position. UV-Vis measurements were done in the wavelength range of 300 nm to 900 nm with intervals scan rate of 1.00 nm.

3.3.1.3 Conductivity Measurement

Four-point probe method is the most convenience way to measure the resistivity and electrical conductivity of semiconductor materials. Principally, conductivity measurement of a material is carried out by contact the surface of the material using four equally spaced probes that connected to the resistivity meter.

In this study, electrical conductivity of PAni and PAni-TiO_2 thin films with different TiO_2 content were measured by using a standard four-point probe resistivity meter (Loresta GP, MCP-T610) at room temperature. This four-point probe resistivity meter is able to measure the sample within the conductivity range of 10^{-7} to 10^{7} Scm^{-1}. PSP probe with interspin distance of 1.50 mm was used for conductivity measurement of PAni and PAni-TiO_2 films in this study. The recorded conductivity given by this resistivity meter is in the unit of siemens per centimeter (Scm^{-1}). The conductivity measurement was conducted on several different places of the films and the final conductivity of PAni and PAni-TiO_2 was tabulated from the average conductivity at different positions.

3.3.1.4 Adhesion Test

It is very important to check how well the materials adhere to the substrate when involving coating substances. There are many test methods of adhesion that can be used such as knife test, tape test, pull-off test and others. In this study, a cross cut tape test technique referring to the American Society for Testing and Materials (ASTM) D3359 was carried out to determine the adhesion of PAni and PAni-TiO_2 films on the FTO substrate. The cross cut tape test method has applied for adhesion measurement of this study as this technique is suitable for use in the laboratory on coatings less than 125.00 microns thick.

The dried PAni and PAni-TiO_2 films were firstly cut in the form of lattice pattern consist of 11 intersecting vertical and horizontal lines with 1.00 mm apart by using blade. Any detached flakes or ribbons of the coating were gently brush off using brush. A 3M Scotch 530 tape was firmly placed on the lattice pattern for 90 s, then was removed quickly by pulling off the tape from the test area to observe the flaking of cross-cut area (if any). After that, the test area was examined with an illuminated magnifier and rated according to the classification of adhesion test results from 0B to 5B based on the percentage of film removed as shown in **Table 3.1.**

Table 3.1: Classification of adhesion test results.

Classification	Percentage of film removed (%)	The flaking of cross-cut area (if any)
5B	0	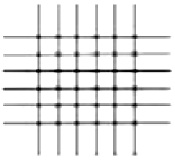
4B	< 5	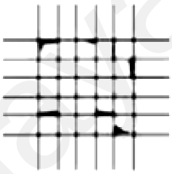
3B	5 - 15	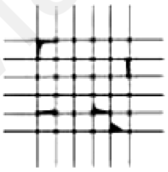 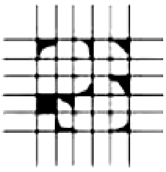
2B	15 - 35	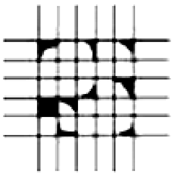 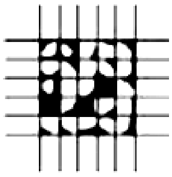
1B	35 - 65	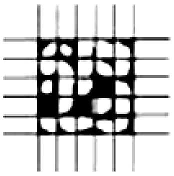 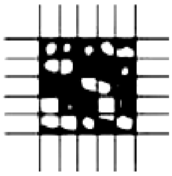
0B	> 65	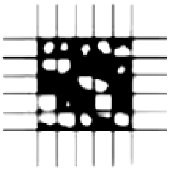

3.4 Synthesis of POB Alkyd

POB alkyd was synthesized as long oil alkyd with 59.92% oil length by alcoholysis and esterification reactions. The first stage is alcoholysis of palm stearin (592.24 g) with glycerine (167.11 g, 1.81 mol) using KOH (0.78 g, 0.01 mol) as catalyst. The reaction was carried out in a four neck round bottom 2000 ml flask equipped with digital overhead stirrer, condenser and digital thermometer. The reaction mixture was slowly heated up to 230 ˚C and held constant for 2 h. The completion for alcoholysis reaction to form monoglycerides was determined by solubility test of the product withdrawn from reaction mixture in anhydrous ethanol at a ratio of 1:3.

The second stage of synthesis is an esterification reaction between monoglycerides with diacids (PA and FA). The reaction mixture was cooled to 100 ˚C. After that, PA (169.00 g, 1.10 ml) and FA (60.02 g, 0.52 mol) were added into the mixture. The temperature of reaction mixture was slowly raised up and maintained at 230 ˚C to 240 ˚C for nearly 8 h. In this synthesis, the progress of the reaction was examined based on the AN of the POB alkyd using titration method according to the procedure adapted from Official Methods of Analysis (AOAC, standard 969.17, 1997).

AN can defined as number of milligrams (mg) of KOH necessary to neutralize the free acidic groups in 1.00 g of sample. There are two stages required based on this method which are standardization of the ethanolic KOH solution, then titration of the sample and blank with ethanolic KOH solution. In this study, POB alkyd with three different AN (5.66, 14.74, and 17.60 mgKOH/g) were isolated from these reactions and were calculated based on **Equation 3.2 and Equation 3.3**.

$$\text{Normality of KOH (N)} = \frac{1000 \text{ x } W_{KHP}}{204.23 \text{ x } V_{KOH}}$$ **Equation 3.2**

$$AN = \frac{56.1 \text{ x N x } (V - V_b)}{W}$$ **Equation 3.3**

where,

V = Volume of KOH solution required for titration of sample, mL

V_b= Volume of KOH solution required for titration of blank, mL

W= Weight of sample, g

W_{KHP}= Weight of potassium hydrogen phthalate (KHP), g

V_{KOH}= Volume of titrant (KOH), mL

(204.23 gmol^{-1} is molar mass of KHP)

3.4.1 Characterization of POB Alkyd

3.4.1.1 FTIR Spectrometer

The chemical structure of POB alkyd was characterized by using FTIR-ATR spectrometer (Perkin-Elmer FTIR RX1) at room temperature. POB alkyd in solid form was placed on the sodium chloride (NaCl) cell and scanned from wavenumber 400 cm^{-1} to 4000 cm^{-1} with resolution of 4 cm^{-1}.

3.4.1.2 Proton Nuclear Magnetic Resonance (^{1}H NMR) Spectrometer

NMR spectroscopy is one of the most favor analytical techniques over the past fifty years that use by researchers to obtain the molecular structural information especially for the organic structure determination. There are two common types of NMR spectroscopy which are ^{1}H NMR and ^{13}C NMR. ^{1}H NMR provides information about the type and number of H atoms in the molecules. However, ^{13}C NMR identifies the type and number of C atoms in the molecules. Principally, a ^{1}H NMR spectrum is ~64,000 times more sensitive than a ^{13}C NMR spectrum (Xiaohua et al., 2008).

In this study, 0.02 g of POB alkyd was dissolved in 0.06 ml of deuterated chloroform containing 99.80% $CDCl_3$ and 0.03% of tetramethylsilane (TMS) for ^{1}H NMR characterization. TMS functions as the internal standard to lock the signal at 0 ppm. The chemical structure of POB alkyd was characterized at room temperature using JEOL JMM-GSX 270 NMR with 16 scans at 270 MHz.

3.4.1.3 Adhesion Test

The adhesion property of the POB alkyd film on FTO substrate was examined following cross cut tape test technique of ASTM D3359. The grade of adhesion test for POB alkyd film on FTO glass was classified into six different levels which are from 0B to 5B as shown in **Table 3.1**.

3.5 Preparations of PAni/Alkyd and PAni-TiO_2/Alkyd Films

As shown in **Figure 3.1**, PAni/Alkyd films were prepared by mixing PAni solution (1.00 g) together with a POB alkyd (0.50 g) using weight ratio of 1:0.5. Then, 6.00% of benzophenone that acts as a UV-photoiniator (0.09 g) was added into PAni/Alkyd mixture and stirred for 6 h at room temperature. Similar procedure was repeated for the preparation of PAni/Alkyd films with different ratio of PAni and POB alkyd (1:0.75 and

1:1). After that, all the prepared films were coated on FTO glass by using SPS Spin 150 spin coater.

A DYMAX Ultraviolet Light Source with 400 W lamp and UV light intensity with 225 mWcm^{-2} was used to cure the films. The curing process of PAni/Alkyd films was initiated by the free radicals that generated from benzophenone with the C=C functional group of POB alkyd. As refer to **Figure 3.2**, the ratio of PAni/Alkyd films (1:0.5) that shows the shortest curing time (10 min) was chosen to prepare PAni/Alkyd films with different types of reactive diluents (MA, MMA and CMA) using weight ratio of 1:0.5:0.4 following similar procedures as discussed earlier.

In this part, PAni/Alkyd with CMA diluent showed the shortest curing time (5 min). After that, PAni/Alkyd films with different TiO_2 content (10%, 20% and 40%) were synthesized through same preparation methods using CMA diluent due to its shortest curing time. **Figure 3.3** showed the flow chart for the preparation of PAni-TiO_2/Alkyd films with different TiO_2 content. Next, the thickness of the prepared PAni/Alkyd and PAni-TiO_2/Alkyd films were measured using micrometer gauge (Mitsutoyo, Japan) for further characterizations.

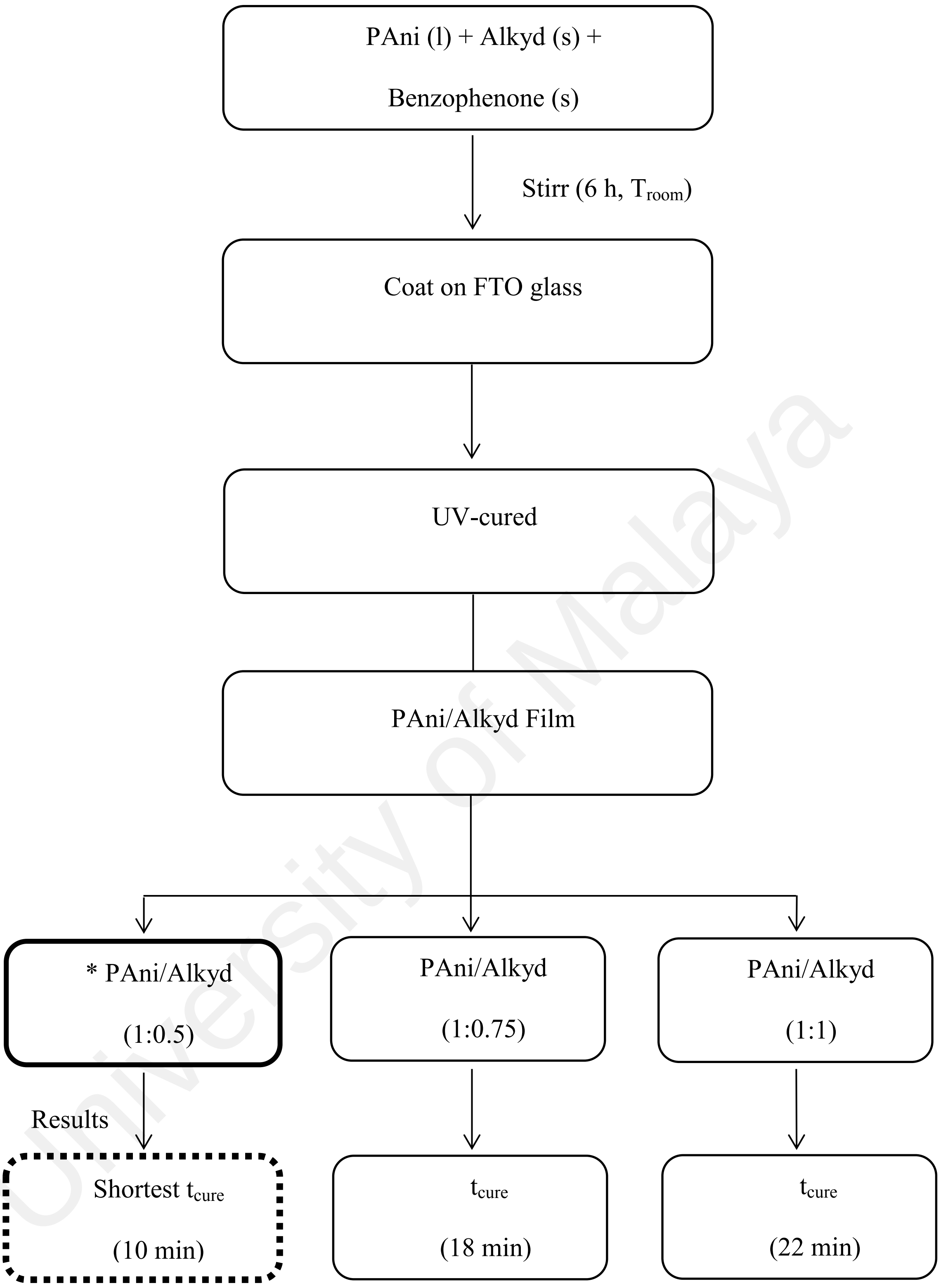

Figure 3.1: Flow chart for the preparation of PAni/Alkyd films with different ratios of PAni and palm oil-based alkyd.

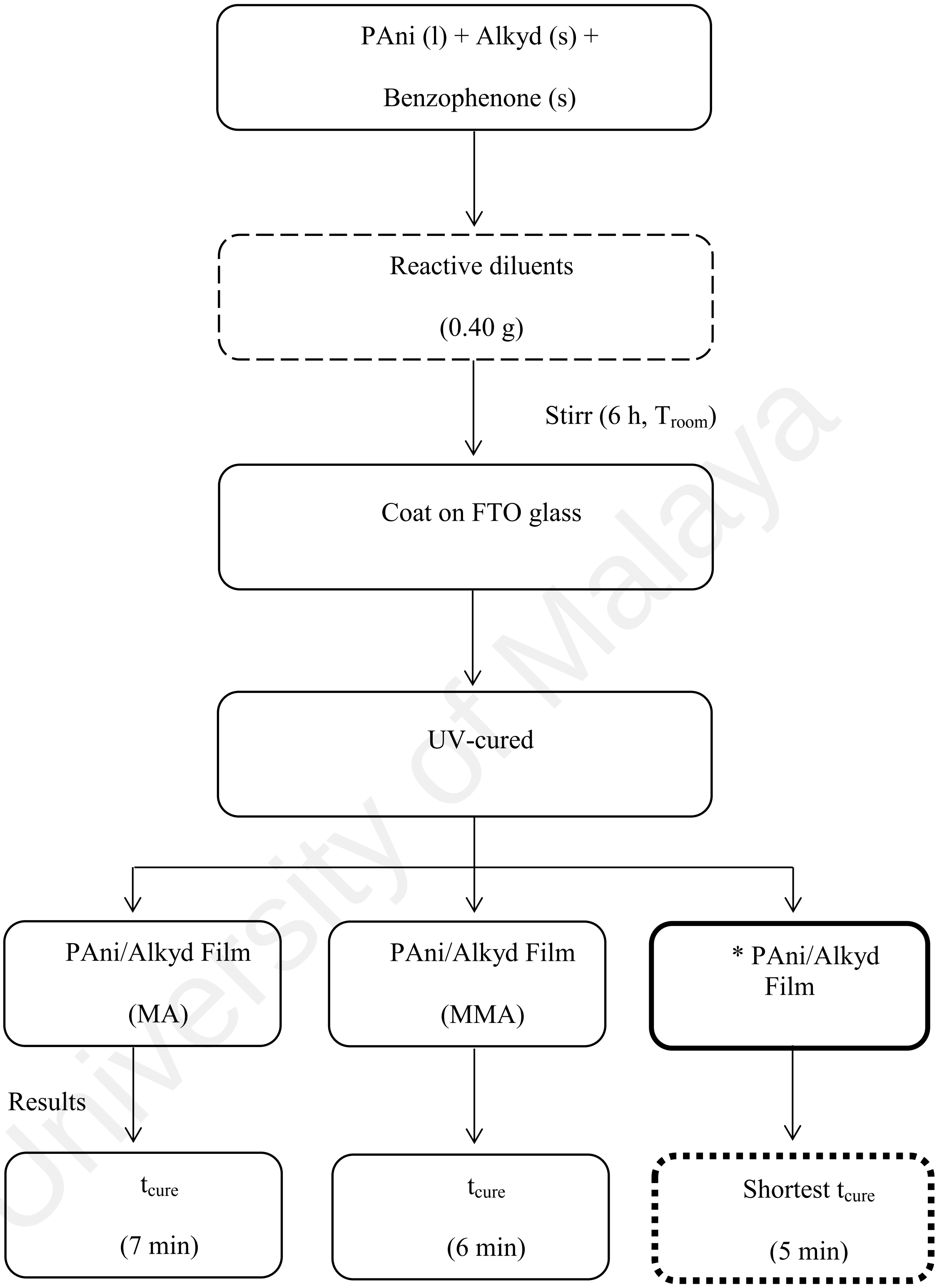

Figure 3.2: Flow chart for the preparation of PAni/Alkyd films using different type of reactive diluents.

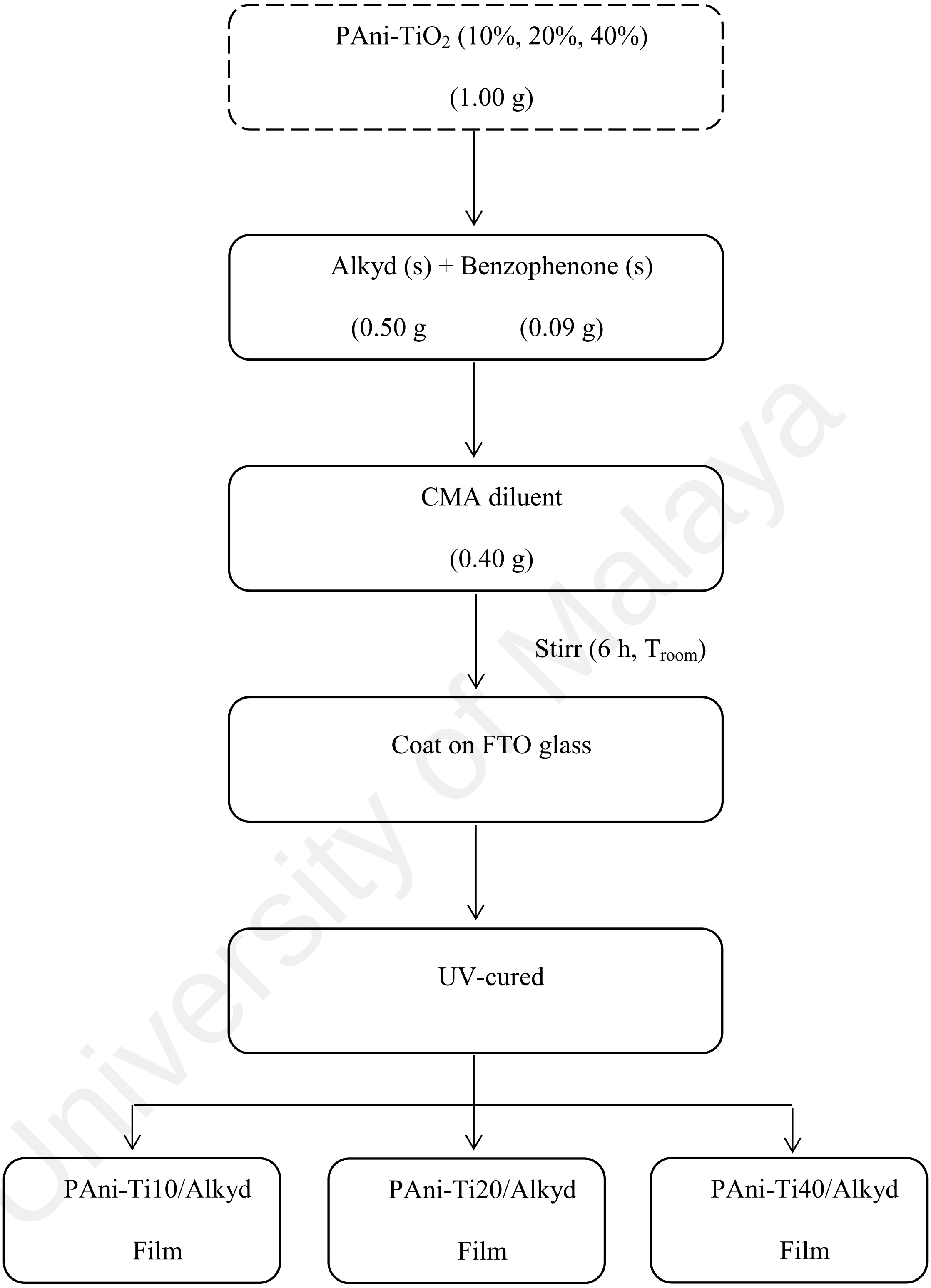

Figure 3.3: Flow chart for the preparation of PAni-TiO_2/Alkyd films with different TiO_2 content.

3.5.1 Characterizations of PAni/Alkyd and PAni-TiO_2/Alkyd Films

3.5.1.1 FTIR Spectrometer

For PAni/Alkyd and PAni-TiO_2/Alkyd (different TiO_2 content) films that coated on FTO glass were directly placed on the sample holder of FTIR-ATR spectrometer and analyzed in wavenumber range of 400 cm^{-1} to 4000 cm^{-1} at room temperature. The objective to run this analysis is to determine the chemical structure of the resulted PAni/Alkyd and PAni-TiO_2 alkyd films.

3.5.1.2 UV-Vis Spectrometer

Similar preparation method as discussed earlier in part **3.3.1.2** was repeated for UV-Vis measurement for PAni/Alkyd and PAni-TiO_2/Alkyd films that coated on FTO glass. The films were analyzed in the wavelength range of 300 nm to 900 nm with intervals scan rate of 1.00 nm at room temperature.

3.5.1.3 X-ray Diffractometer (XRD) Spectrometer

XRD spectrometer is a non-destructive structural analysis for crystalline or amorphous materials. It provides structures, textures and structural parameters of the characterized materials. This X-ray diffraction technique is principally based on constructive interference of monochromatic X-rays and a crystalline sample. In this study, the existence of inorganic substance such as TiO_2 was confirmed by XRD analysis. XRD analysis was examined for PAni-TiO_2/Alkyd films with different TiO_2 content (10%, 20% and 40%) that coated on FTO glass that was investigated using Empyrean X-ray diffractometer, equipped with a Cu target at 40.00 kV and 40.00 mA. All films were performed within 2θ range of $5 - 80^\circ$ at scan speed of 2°/min.

3.5.1.4 Conductivity Measurement

Electrical conductivity measurement of PAni/Alkyd and PAni-TiO_2/Alkyd films that coated on FTO glass were conducted using PSP probe (Loresta GP, MCP-T610) at room temperature. Similar measurement procedures were repeated as refer to part **3.3.1.4** for comparison study.

3.5.1.5 Adhesion Test

The adhesion property of PAni/Alkyd and PAni-TiO_2/Alkyd films on FTO glass were performed by cross cut tape test method following ASTM D3359 using similar procedures as discussed earlier in part **3.3.1.5**. Based on the data obtained, PAni/Alkyd and PAni-TiO_2/Alkyd films that possessed the highest electrical conductivity with the best adhesion property will proceeded to the following part for DSSC analysis.

3.6 Application of PAni/Alkyd and PAni-TiO_2/Alkyd in DSSC

3.6.1 Fabrication of PAni as CE in DSSC

As discussed earlier, there are four important components of DSSC including semiconductor oxide photoanode as working electrode (WE), CE, dye and redox electrolyte. The fabrication procedures for the standard cells of DSSC device were prepared based on the standard method from Solaronix Company. Firstly, the TiO_2 photoanodes were spin coated on FTO glass as WE and were sintered in a furnace for 20 min at 450 ˚C. Then, TiO_2 films were immersed in 5.00 mM solution of ruthenium dye (N-719) for 24 h at room temperature. PAni, PAni/Alkyd and PAni-TiO_2/Alkyd coated on FTO glass that prepared earlier were functioned as a CE in DSSC system.

In this fabrication, the prepared WE films were assembled with CE films into sandwich-type cells as shown in **Figure 3.4**. After that, iodolyte AN50 that act as an electrolyte was injected in between WE and CE films. The completed standard cells were used to determine the PCE value in DSSC device.

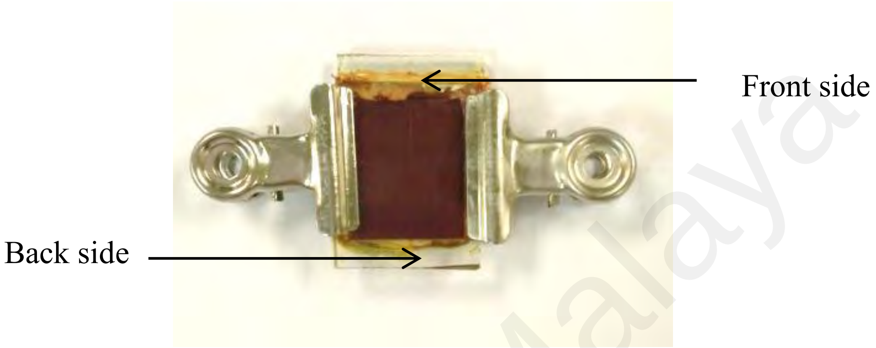

Figure 3.4: Standard cells for DSSC measurement.

3.6.2 Power Conversion Efficiency (PCE) of PAni as CE

During DSSC measurement (Keithley high voltage source model 237), the prepared standard cell was placed at the sample holder by facing WE film to the light source using tungsten light source with light intensity of 100 mWcm^2. The illuminated standard cell area of WE and CE was set to 0.10 cm^2. All analyses were conducted at room temperature and PCE (η) of the cells (PAni, PAni/Alkyd and PAni-TiO$_2$/Alkyd) were calculated according to the **Equation 3.4 and Equation 3.5**.

$$\eta\ (\%) = \frac{\mathrm{V_{oc}} \times \mathrm{J_{sc}} \times ff \times 100}{\mathrm{P_{in}}}$$ **Equation 3.4**

$$ff = \frac{\mathrm{V_{max}} \times \mathrm{J_{max}}}{\mathrm{V_{oc}} \times \mathrm{J_{sc}}}$$ **Equation 3.5**

where,

ff = fill factor, %

$\mathrm{V_{max}}$ = voltage, V (in the J-V curve)

$\mathrm{J_{max}}$ = current density, mAcm^{-2} (in the J-V curve)

$\mathrm{V_{oc}}$ = open-circuit voltage, V

$\mathrm{J_{sc}}$ = short-circuit current density, mAcm^{-2}

$\mathrm{P_{in}}$ = incident light power density, mWcm^{-2}

CHAPTER 4: RESULTS AND DISCUSSION

4.1 Characterizations of polyaniline (PAni) and PAni-Titanium dioxide (TiO_2)

4.1.1 FTIR Analysis

Figure 4.1 shows the FTIR spectra of pristine PAni and PAni-TiO_2 composites with different TiO_2 content (10%, 20% and 40%) while the peaks present in the spectra were summarized in **Table 4.1**. In general, PAni, PAni-Ti10, PAni-Ti20 and PAni-Ti40 showed similar pattern of FTIR spectra. The peaks at 1465 – 1500 cm^{-1} and 1210 – 1280 cm^{-1} are characteristic peaks of pristine PAni associated with C=N and C=C stretching vibration modes for the benzenoid and quinoid units, respectively. Peaks at 2854 – 2895 cm^{-1} indicate the C-H stretching of CH_3 and CH_2 while the broad peak range at 3243 – 3250 cm^{-1} corresponds to the N-H stretching vibration. FTIR spectra as shown in **Figure 4.1** confirmed the characteristic peaks of PAni and PAni-TiO_2 composites with different TiO_2 content.

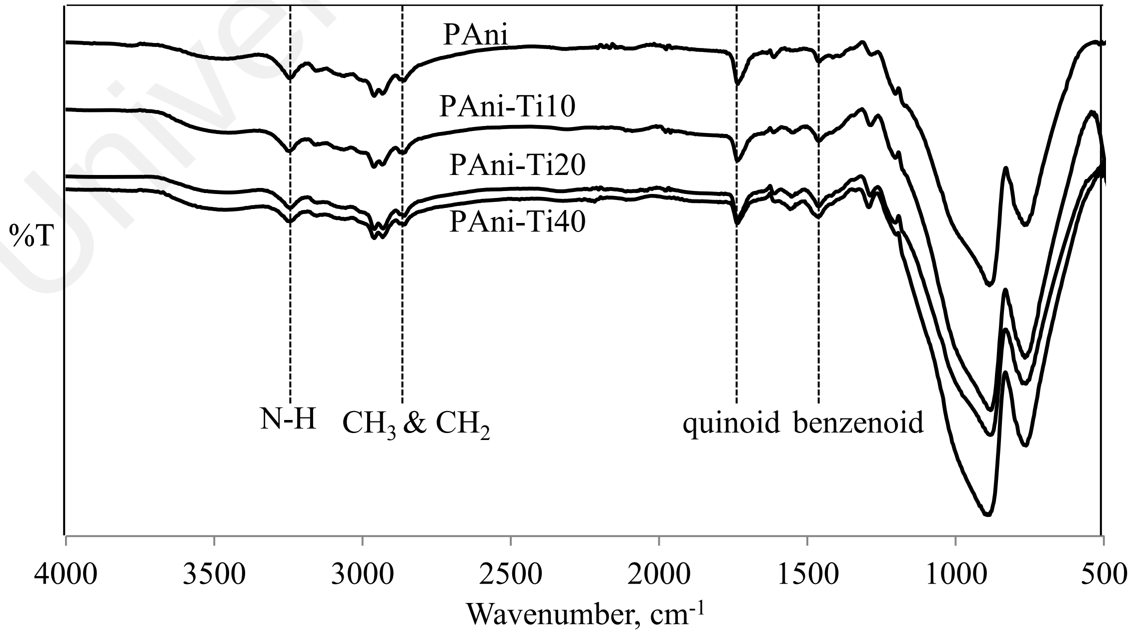

Figure 4.1: FTIR spectra of PAni and PAni/TiO_2 with different TiO_2 content.

Table 4.1: Peak assignments for FTIR spectra of PAni and PAni-TiO_2 composites with different TiO_2 content.

Wavenumber (cm^{-1})	Functional groups
888 – 937	C-H bend
1178 – 1207	C=O stretch
1286 – 1292	C-N stretch
1458 – 1466	benzenoid
1738	quinoid
2931– 2934	aromatic C-H stretch
3243 – 3250	N-H stretch

4.1.2 UV-Vis Analysis

UV-Vis spectra of PAni and PAni-TiO_2 composites with different TiO_2 content are in **Figure 4.2** while the peaks present in the spectra were summarized in **Table 4.2**. PAni-Ti10, PAni-Ti20 and PAni-Ti40 spectra possessed similar UV-Vis patterns as the spectrum of pristine PAni. In general, all samples showed peak around 340 – 350 nm, 433 – 440 nm and 730 nm – 750 nm, attributed to the π–π*, polaron–π* and π–polaron transitions, respectively. These peaks are corresponding to the characteristic peaks of typical conducting forms of PAni.

From the UV-Vis spectra, addition of TiO_2 into PAni has slightly shifts the π–polaron peaks from 750 nm to 730 – 740 nm. This condition is referred to as solvatochromic shift known as the blue shift involving movement of the polaron peak to lower wavelength (Budzak et al., 2016). These wavelength shifts, indicates a redistribution of polaron density in the band gap of the doped PAni due to the effective incorporation of TiO_2 nanoparticles (Huyen et al., 2011; Li et al., 2004). It is also observed that the absorption intensity of all PAni-TiO_2 spectra are lower compared to PAni due to the effective hydrogen bonding in the form of NH•••O−Ti (Yavuz & Gök, 2007).

UV-Vis spectra as shown in **Figure 4.2** confirmed that PAni and PAni-TiO_2 composites with different TiO_2 content are in the conducting form of emeraldine salt (ES) state that exhibit electrical and electrochemical properties. PAni and PAni-TiO_2 became electrically conductive where this property depends on the degree of protonation involving acid doping process using HCl dopant during synthesis reactions (Bhadra et al., 2020; Stejskal et al., 2015).

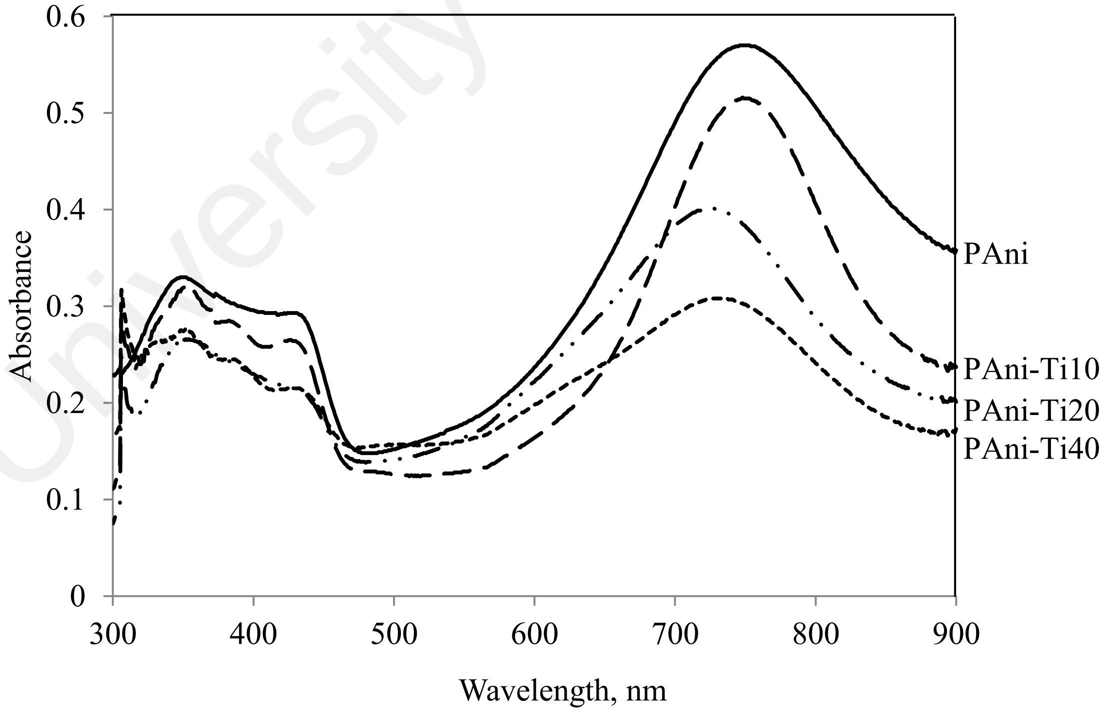

Figure 4.2: UV-Vis spectra of PAni and PAni/TiO_2 composites with different TiO_2 content.

Table 4.2: Peak assignments for UV-Vis spectra of PAni and PAni-TiO_2 composites with different TiO_2 content.

Polymer	π–π* (nm)	polaron–π* (nm)	π–polaron (nm)
PAni	350	440	750
PAni-Ti10	348	433	740
PAni-Ti20	340	438	730
PAni-Ti40	345	435	734

4.1.3 Conductivity Property

Figure 4.3 shows the electrical conductivities of PAni and PAni-TiO_2 composites with different TiO_2 content that were performed on an ordinary glass slides (3.53×10^{-3} Scm^{-1} to 6.59×10^{-2} Scm^{-1}). It can be observed that the conductivity of PAni significantly improved from 3.53×10^{-3} Scm^{-1} (pristine PAni) to 8.16×10^{-3} Scm^{-1} – 6.59×10^{-2} Scm^{-1}(with TiO_2). The conductivity of the PAni-TiO_2 films increased with increasing TiO_2 content at 10% (8.16×10^{-3} Scm^{-1}) and reached a maximum at 20% (6.59×10^{-2} Scm^{-1}) but dropped to $1.55x10^{-2}$ Scm^{-1} at 40% of TiO_2.

The conductivity of PAni-TiO_2 (10% and 20%) increased due to the adsorption of anilinium ions on the surface of TiO_2 grains (O^- anions) during the oxidative polymerization of PAni. The interaction between anilinium ions and O^- anions caused the decreasing of the potential barrier between PAni and TiO_2 nanoparticles. As a result, the charge carrier mobility become higher and eventually increased the conductivity of PAni-TiO_2 (10% and 20%) (Nasirian & Moghaddam, 2014). However, the addition of

40% TiO_2 could cause the charge blockage along the conductive pathway of PAni and lowering its conductivity (Jumat et al., 2017; Lia et al., 2004).

Based on **Figure 4.3**, the highest conductivity is shown by PAni-Ti20 because of the strong interfacial interaction between PAni and TiO_2 nanoparticles. The oxidative polymerization of the aniline monomer on the surface of TiO_2 also has led to the uniform distribution of TiO_2 nanoparticles during PAni synthesis. Therefore, the interfacial interaction has improved the orientation of TiO_2 within PAni and enhanced the electrical conductivity of PAni-Ti20 (Ramesan et al., 2014; Sampreeth et al., 2017).

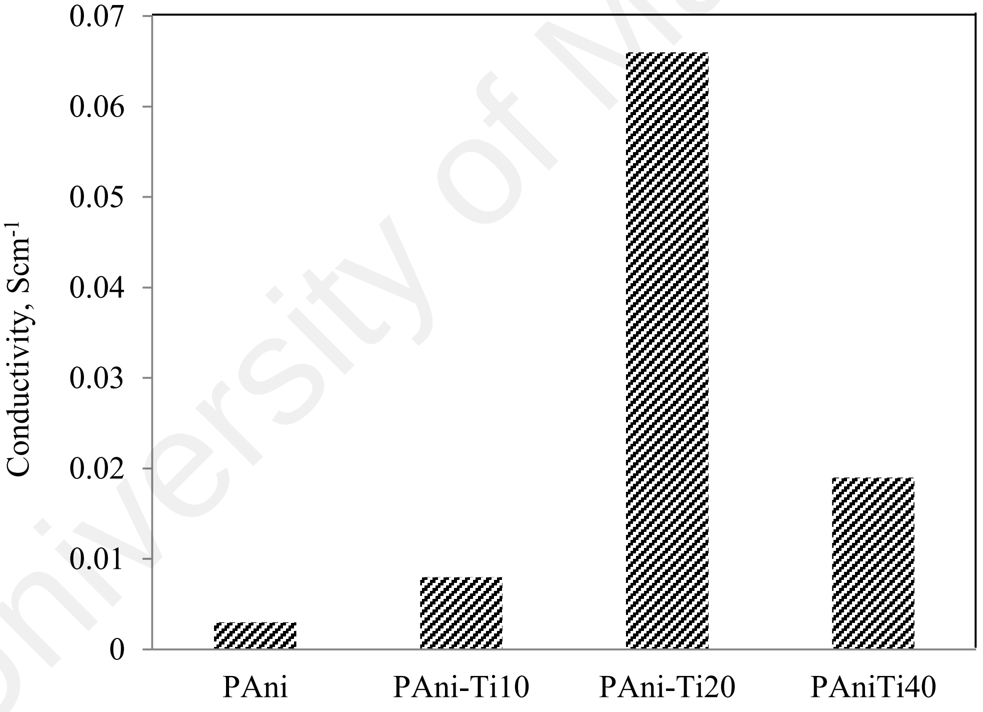

Figure 4.3: Conductivity of PAni and PAni-TiO_2 composites with different TiO_2 content.

4.1.4 Adhesion Property

Table 4.3 shows the adhesion property of PAni and PAni-TiO_2 (10%, 20% and 40%) on FTO glass substrate based on the grade of adhesion test from 0B to 5B. Pristine PAni exhibited very poor adhesion performance of 0B because it can be categorized as a high surface energy material. Therefore, when pristine PAni is coated onto FTO substrate, it will exhibits higher surface energy than the attractive forces toward the FTO surface, which results in lower bond strength (Callow et al., 2005).

On the other hand, it can be observed that all PAni-TiO_2 composites possessed better adhesion grade compare to pristine PAni. The adhesion of PAni-Ti10 and PAni-Ti20 has improved to 3B while the adhesion of PAni-Ti40 has attained 2B. PAni-TiO_2 composites showed better adhesion towards the FTO substrate due to the possibility of hydrogen bonding between NH•••O−Ti of PAni-TiO_2 with O−H of the FTO glass (Biggs et al., 2015).

An excessive amount of TiO_2 (40%) might act as a barrier that block the linkage between PAni-TiO_2 and FTO substrate which reduce its adhesion property. This is because excess TiO_2 probably agglomerates on the surface outside the nanorod/nanotube of PAni-$TiO_{2.}$ The same phenomenon was reported by Jumat and co-workers (Jumat et al., 2017; Shahabuddin et al., 2016; Phang & Kuramoto, 2010). TiO_2 nanoparticles become irregularly distribute in the matrix and interacts less with PAni. This has caused low possibility of hydrogen bonding between PAni-TiO_2 (40%) with FTO glass, resulting in poor adhesion property (Nihmath & Ramesan, 2017).

Table 4.3: Adhesion test for PAni and PAni-TiO$_2$ composites with different TiO$_2$ content.

Films	Test Grade (ASTM D3359)
PAni	0B
PAni-Ti10	3B
PAni-Ti20	3B
PAni-Ti40	2B

4.2 Characterizations of POB Alkyd with different Acid Number (AN)

4.2.1 FTIR Analysis

As for the synthesis of POB alkyd, the final samples were collected with desired AN during esterification reaction. Among all samples, POB alkyd with lower AN were expected to have more C=O and C=C that will resulted excellent adhesion performance on the substrate. In this study, POB alkyd with AN of 5.66, 14.74 and 17.60 mgKOH/g were taken out at the end of synthesis reactions. All of these AN of POB alkyd showed FTIR spectra with similar pattern. FTIR spectrum of the POB alkyd with AN of 5.66 mgKOH/g is as shown in Figure 4.5 whereas FTIR spectra for AN of 14.74 and 17.60 mgKOH/g are attached in **Appendix A**. The peaks present in the FTIR spectra were summarized in **Table 4.4**.

From the spectrum, a strong peak at 1733– 1734 cm^{-1} can be attributed to the stretching of carbonyl group in ester linkages as a result of esterification reaction between monoglycerides and diacids (PA and FA) during alkyd synthesis. Besides, small peaks at 1582 – 1583 cm^{-1} and 1602 cm^{-1} arising from C=C of the aromatic rings in PA. Another important peak of POB alkyd is associated with the broad band of hydroxyl groups (-OH) present at 3490 – 3491 cm^{-1} (Ataei et al., 2011; Shahabudin et al., 2016). FTIR spectrum as shown in **Figure 4.4** confirmed that the functional groups of POB alkyd compound.

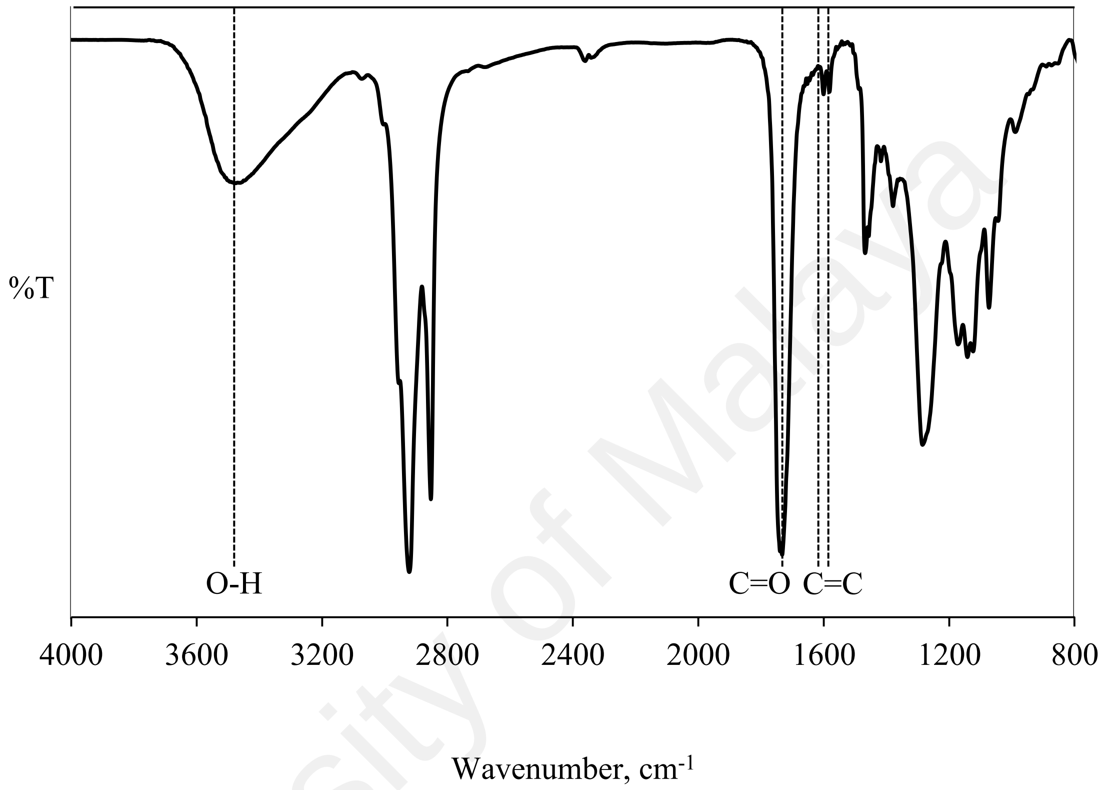

Figure 4.4: FTIR spectrum of POB Alkyd.

Table 4.4: Peak assignments for FTIR spectra of POB Alkyd.

Functional groups	Wavenumber (cm^{-1})
C-O stretch of 1° alcohol	1074 − 1075
C-O stetch of ester	1286 − 1288
-CH_3 bend	1380 − 1381
-CH_2 bend	1468 − 1469
aromatic C=C stretch	1582 − 1583and 1602
C=O stretch of ester	1733 – 1734
sp^3 C-H stretch	2853, 2923
aromatic C-H stretch	3080 − 3086
OH stretch	3490 − 3491

4.2.2 ^{1}H NMR Analysis

Figure 4.5 shows the ^{1}H NMR spectrum of POB alkyd and the peaks observed in the spectrum were summarized in **Table 4.5**. The proton for terminal methyl groups ($-CH_3$) of fatty acids can be depicted by the peak at around 0.87 ppm while peak at 1.23 ppm, attributed to the protons of $-CH_2$ present in the alkyd chain. The peak appeared at 5.32 ppm are due to the protons attached to unsaturated carbon (R−CH=CH−R) and peak at 6.90 ppm corresponds to the −OOC−CH=CH−COO− which confirmed that fumaric acid has been introduced into the alkyd chain. The proton for the aromatic ring was confirmed by the peak at around 7.54 ppm and 7.74 ppm, attributed to the incorporated of PA in the alkyd chain (Ataei et al., 2011; Shahabudin et al., 2016). Thus, a plausible structure of POB alkyd compound is shown in **Figure 4.6**.

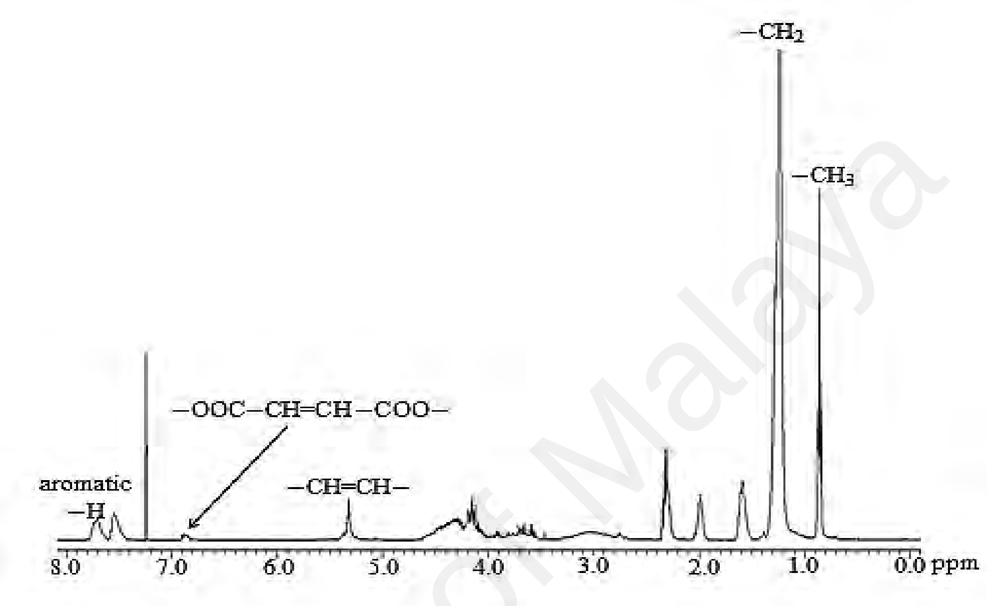

Figure 4.5: ^{1}H NMR spectrum of POB alkyd.

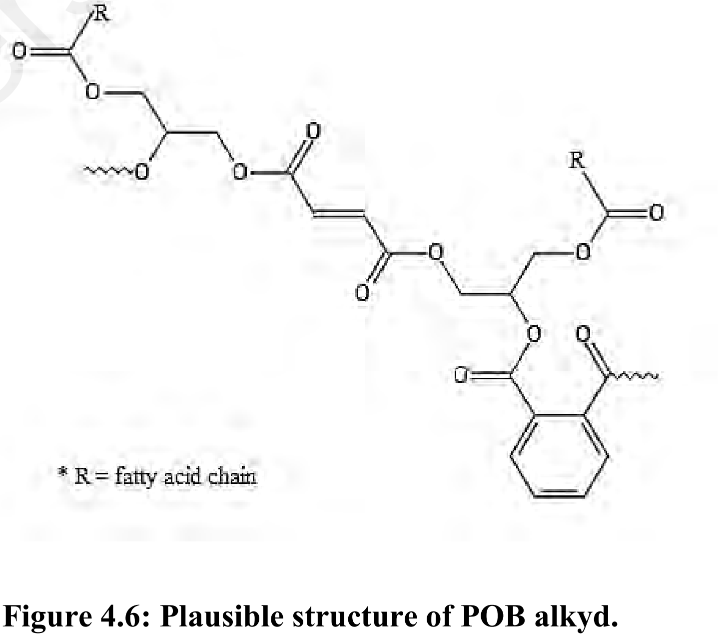

Figure 4.6: Plausible structure of POB alkyd.

Table 4.5: Peak assignments for ^1H NMR spectra of POB alkyd.

Chemical shifts (ppm)	Protons
0.87	-R-C$\boldsymbol{H_3}$
1.23	-R-C$\boldsymbol{H_2}$-R
2.30	-OOC-C$\boldsymbol{H_2}$-
5.32	-$\boldsymbol{H}$C=C$\boldsymbol{H}$-
6.90	-OOC-C$\boldsymbol{H}$=C$\boldsymbol{H}$-COO-
7.54, 7.74	aromatic -C$\boldsymbol{H}$=C$\boldsymbol{H}$-

4.2.3 Adhesion Property

Table 4.6 shows the result of adhesion test for POB alkyd with different AN. All films showed excellent adhesion property on FTO glass with 5B grade as there was no any detached flakes of the films observed after performing adhesion test. The films were strongly adhere to the FTO glass due to the possibility of hydrogen bonding between C=O group of the POB alkyd with −OH of the FTO glass (Biggs et al., 2015; Dutta et al., 2006).

Table 4.6: Adhesion test of POB Alkyd with different AN.

POB Alkyd with different AN (mg KOH/g)	Test Grade (ASTM D3359)
5.66	5B
14.74	5B
17.60	5B

4.3 Characterizations of PAni/Alkyd and PAni-TiO_2/Alkyd

4.3.1 PAni/Alkyd with different AN of POB Alkyd

4.3.1.1 FTIR Analysis

In this study, the preparation of PAni modified with POB alkyd (PAni/Alkyd) films were investigated by different ratios (PAni:Alkyd = 1:0.5, 1:0.75 and 1:1) and different AN of POB alkyd (5.66, 14.74 and 17.60 mgKOH/g). FTIR spectra of PAni/Alkyd prepared using ratio 1:0.5 and with different AN of POB alkyd are shown in **Figure 4.7**. The peaks present in the FTIR spectra were summarized in **Table 4.7**. The peaks at 1466 – 1468 cm^{-1} , 1601 – 1627 cm^{-1} can be attributed to the benzenoid and quinoid of PAni while peaks at 1723 – 1728 cm^{-1} corresponded to the C=O stretch from POB alkyd. Two peaks at 2855 cm^{-1} and 2930 cm^{-1} are assigned to the sp^3 C-H stretching of POB alkyd. FTIR spectra as shown in **Figure 4.7** confirmed the chemical structures of PAni/Alkyd with different AN.

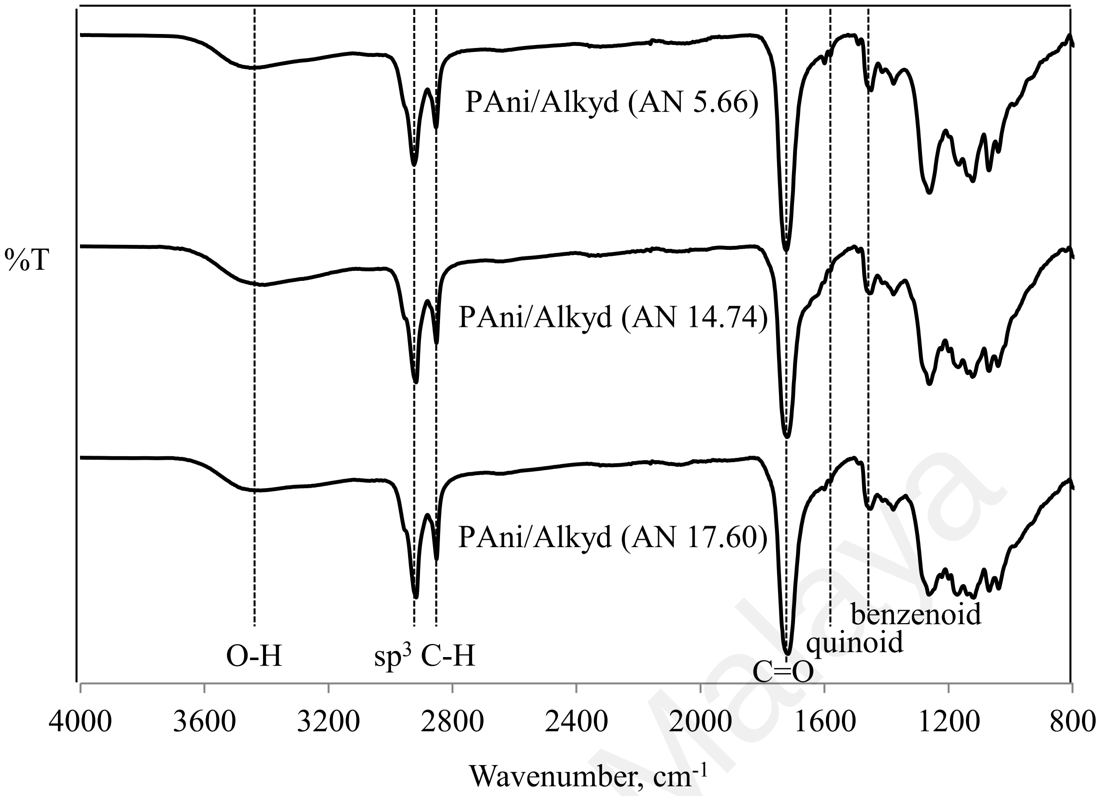

Figure 4.7: FTIR spectra of PAni/Alkyd films with different AN of POB alkyd.

Table 4.7: Peak assignments for FTIR spectra of PAni/Alkyd films with different AN of POB alkyd.

Functional groups	Wavenumber (cm^{-1})
Benzenoid (PAni)	1466 – 1468
Quinoid (PAni)	1602 – 1627
C=O stretch of ester (POB alkyd)	1723 – 1728
OH stretch (POB alkyd)	3474 – 3481

4.3.1.2 UV-Vis Analysis

The UV-Vis absorption spectra for PAni and PAni/Alkyd films using ratio 1:0.5 with different AN of POB alkyd are shown in **Figure 4.8**. Meanwhile, **Table 4.8** shows the characteristic peaks that were observed from PAni/Alkyd films. From the UV-Vis spectra, it can be observed that there is a red shift from 750 nm to 815 nm from pristine PAni to PAni/Alkyd significantly proved that the delocalization of polaron is higher after addition of POB alkyd. It is because addition of POB alkyd will make the structure of pristine PAni changed from coil-like to expanded coil-like structure. This expanded coil like structure will lower the stearic hindrance during the crosslink between PAni and POB alkyd. Thus, it is expected to improve the adhesion on substrate later on (Xua et al., 2005).

Besides, PAni/Alkyd films prepared using ratio 1:0.75 and 1:1 also showed similar pattern as this PAni/Alkyd spectra that were attached in **Appendix B**. UV-Vis spectra as shown in **Figure 4.8** confirmed that PAni/Alkyd with different AN were in the conducting state.

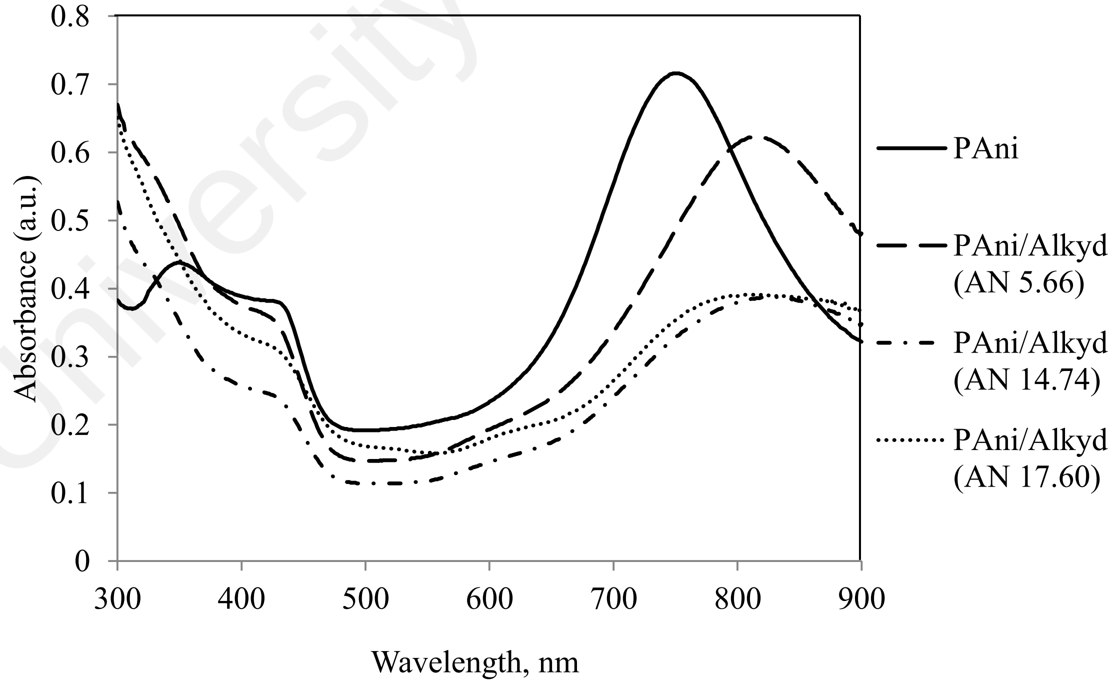

Figure 4.8: UV-Vis spectra of PAni and PAni/Alkyd films with different AN of POB alkyd.

Table 4.8: Peak assignments for UV-Vis spectra of PAni/Alkyd films with different AN of POB alkyd.

Transitions	Wavelength (nm)
polaron–π^*	418 − 435
π–polaron	781 − 815

4.3.1.3 Conductivity Property

As mention earlier, PAni/Alkyd were prepared using different AN of POB alkyd with several ratio (1:0.5, 1:0.75 and 1:1) in order to obtain PAni/Alkyd films that possessed low curing time, high electrical conductivity and best adhesion of 5B grade. **Figure 4.9** shows the curing time of PAni/Alkyd films with different ratio and AN of POB alkyd. It can be observed that PAni/Alkyd with ratio 1:0.5 and AN of 5.66 mgKOH/g have the shortest curing time (10 min). This is due to the conversion of acid groups during the esterification reaction of POB alkyd. This conversion is very important because the carboxyl functionality (F-COO) of PA and FA will delay the drying rate and POB alkyd with lowest AN value will have the highest conversion of acid groups (Menkiti & Onukwuli, 2011).

The conductivity of PAni film on FTO substrate was measured using four point probe method and its conductivity is 1.31×10^{3} Scm^{-1}. By comparing the results in **Table 4.9**, the incorporation of POB alkyd into PAni film showed decreasing in conductivity of the films. Besides, it can be observed that different AN of POB alkyd could affect the conductivity of PAni/Alkyd films but there is no constant pattern of their conductivity recorded in this study.

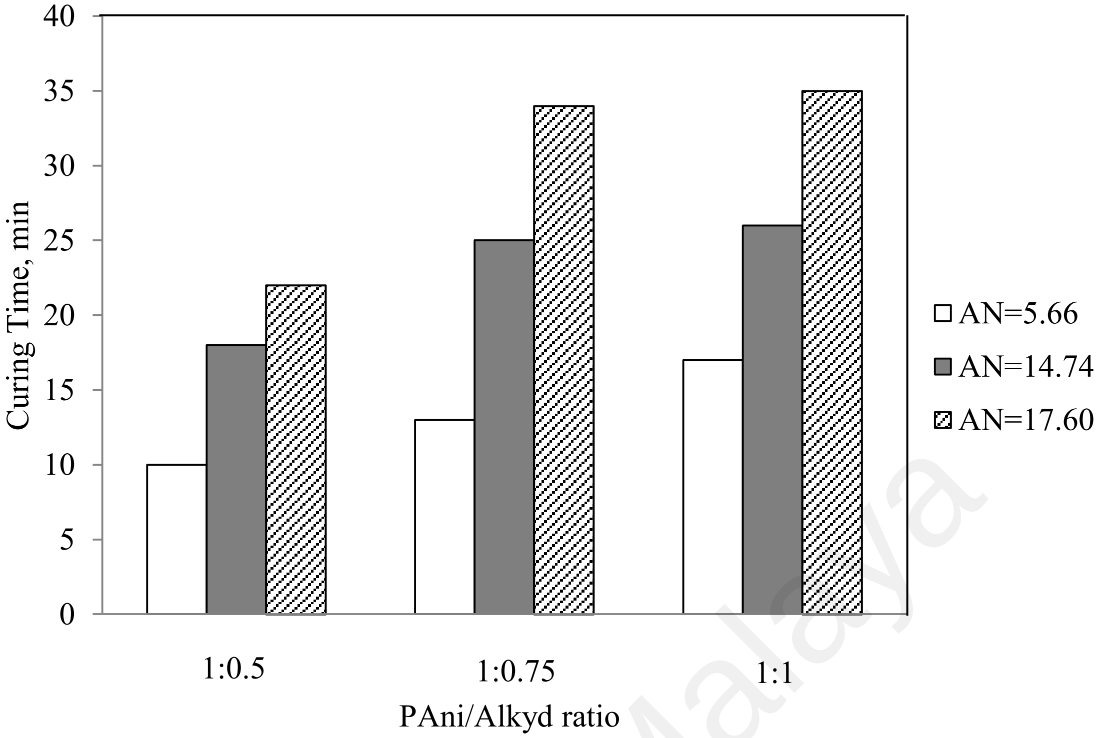

Figure 4.9: Curing time of PAni/Alkyd films with different ratio and AN of POB alkyd.

Table 4.9: Conductivity of PAni/Alkyd films with different ratio and AN of POB alkyd.

PAni/Alkyd with different AN (mg KOH/g alkyd)	Conductivity (Scm^{-1})		
	1:0.5 (PAni:Alkyd)	1:0.75 (PAni:Alkyd)	1:1 (PAni:Alkyd)
5.66	2.56×10^{2}	2.54×10^{2}	2.52×10^{2}
14.74	2.44×10^{2}	2.59×10^{2}	2.45×10^{2}
17.60	2.52×10^{2}	2.60×10^{2}	2.36×10^{2}

4.3.1.4 Adhesion Property

Adhesion test of PAni film coated on FTO substrate was carried out and the result obtained as 0B which indicated poor adhesion performance. However, it was observed that all PAni/Alkyd films achieved good adhesion on FTO glass with 5B grade as shown in **Table 4.10**. This indicates that PAni/Alkyd films using selected AN of POB alkyd were able to impart good adhesive property to improve the adhesion of PAni on the substrate. This is due to the presence of reactive C=C group in the POB alkyd that could undergo crosslinking with the quinoid of PAni during UV irradiation, thus has enhanced film's adhesion on FTO substrate (Kawata et al., 2013; Ramlan et al., 2017).

Best result was observed for PAni/Alkyd at a ratio 1:0.5 with the POB alkyd having AN of 5.56 mgKOH/g due to its shortest curing time (10 min), high conductivity (2.56×10^{2} Scm^{-1}) and good adhesion (5B) that can offers an excellent potential application as counter electrode (CE) material for dye-sensitized solar cell (DSSC). However, the final curing time of the films that obtained under UV curing system still can be improved for the cost effective reason. Thus, this study was further continued with addition of reactive diluents into the coating mixture of PAni/Alkyd in order to achieve lower curing time.

Table 4.10: Adhesion test of PAni/Alkyd films with different ratio and AN of POB alkyd.

PAni/Alkyd with different AN (mg KOH/g)	Test Grade (ASTM D3359) 1:0.5 (PAni:Alkyd)	1:0.75 (PAni:Alkyd)	1:1 (PAni:Alkyd)
5.66	5B	5B	5B
14.74	5B	5B	5B
17.60	5B	5B	5B

4.3.2 PAni/Alkyd with different types of Reactive Diluents

4.3.2.1 FTIR Analysis

Based on the previous discussion, the optimum ratio used for the preparation of PAni/Alkyd films is 1:0.5 with AN of 5.66 mgKOH/g. This study was continued with the addition of reactive diluents into PAni/Alkyd coating mixture in order to reduce the curing time of the films and at the same time exhibits 5B grade of adhesion test. **Figure 4.10** shows the chemical structures of the selected reactive diluents for improving curing time purpose.

Besides, FTIR spectra of PAni/Alkyd prepared using ratio 1:0.5 and with different types of reactive diluents are shown in **Figure 4.11**. The peaks present in the FTIR spectra were summarized in **Table 4.11**. In general, all PAni/Alkyd films showed similar pattern of FTIR spectra. Both peaks at 1450 − 1458 cm^{-1} and 1600 − 1602 cm^{-1} can be attributed to the benzenoid and quinoid of PAni, respectively. Meanwhile peaks at 1725 − 1727 cm^{-1} and 3473 − 3479 cm^{-1} corresponds to the C=O and -OH stretch from POB alkyd, respectively (Ang, 2015; Kawata et al., 2013).

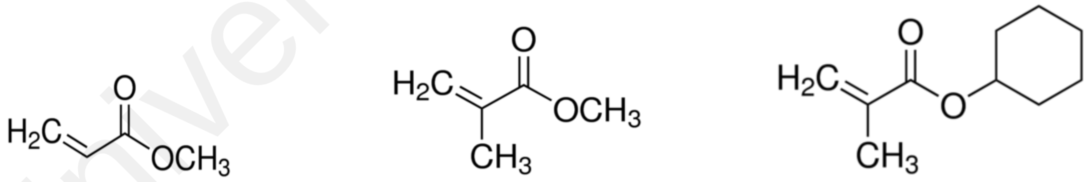

MA MMA CMA

Figure 4.10: Chemical structures of selected reactive diluents.

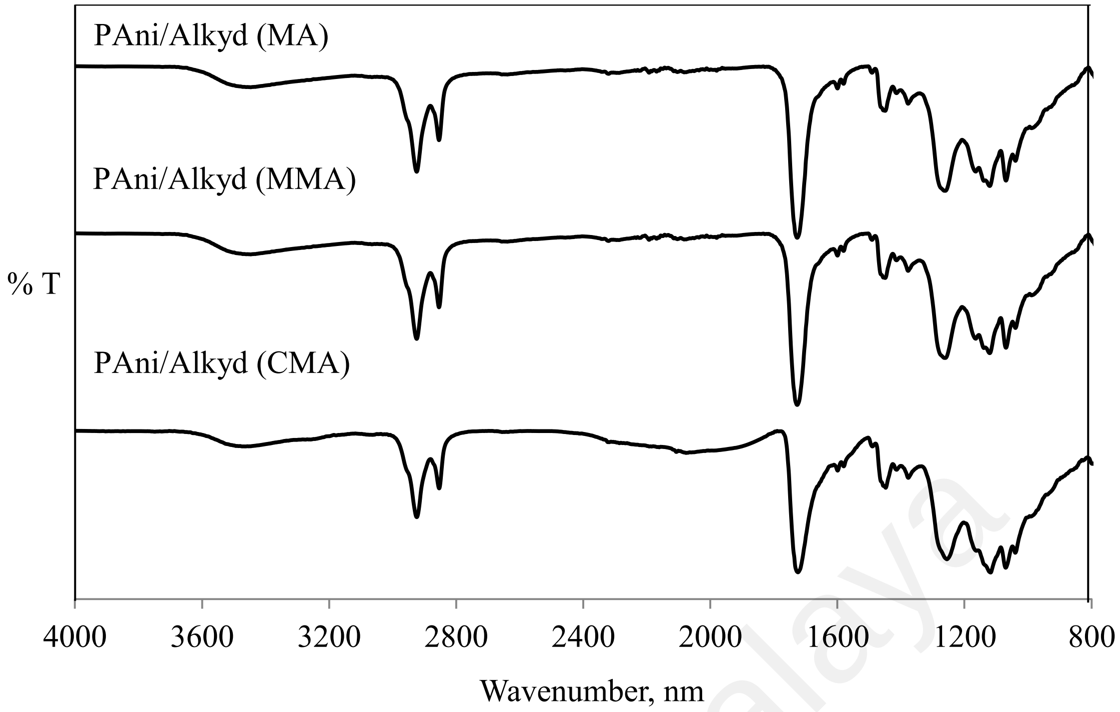

Figure 4.11: FTIR spectra of PAni/Alkyd films with different types of reactive diluents.

Table 4.11: Peak assignments for FTIR spectra of PAni/Alkyd films with different types of reactive diluents.

Functional groups	Wavenumber (cm^{-1})
Benzenoid (PAni)	1450 – 1458
Quinoid (PAni)	1600 – 1602
C=O stretch of ester (POB alkyd)	1725 – 1727
OH stretch (POB alkyd)	3473 – 3479

4.3.2.2 UV-Vis Analysis

The UV-Vis absorption spectra for PAni/Alkyd films using ratio 1:0.5 with different types of reactive diluents are shown in **Figure 4.12**. Meanwhile, **Table 4.12** shows the characteristic peaks that were observed from PAni/Alkyd films. All films possessed similar UV-Vis spectrum pattern. The absorption peaks at 315 − 334 nm were attributed to the π-π* transition while the peaks at 417 − 424 nm indicated to the polaron-π* transition and peaks at 734 − 780 nm represented the π-polaron transition. These peaks are characteristic peaks of the conducting forms of PAni.

From the UV-Vis spectra, it can be observed that the π–polaron peak of PAni/Alkyd (CMA) shift to the lowest wavelength from 780 nm (for MA diluent) to 742 nm (for CMA diluent). This significantly proved that the addition of CMA diluent possessed the highest delocalization of polaron compared to MMA and MA diluents. It is because addition of CMA diluent could expand the coil-like structure and reduce the stearic hindrance during the crosslinking between PAni and POBA alkyd (Aksimentyera et al., 2010; Yao et al., 2014).

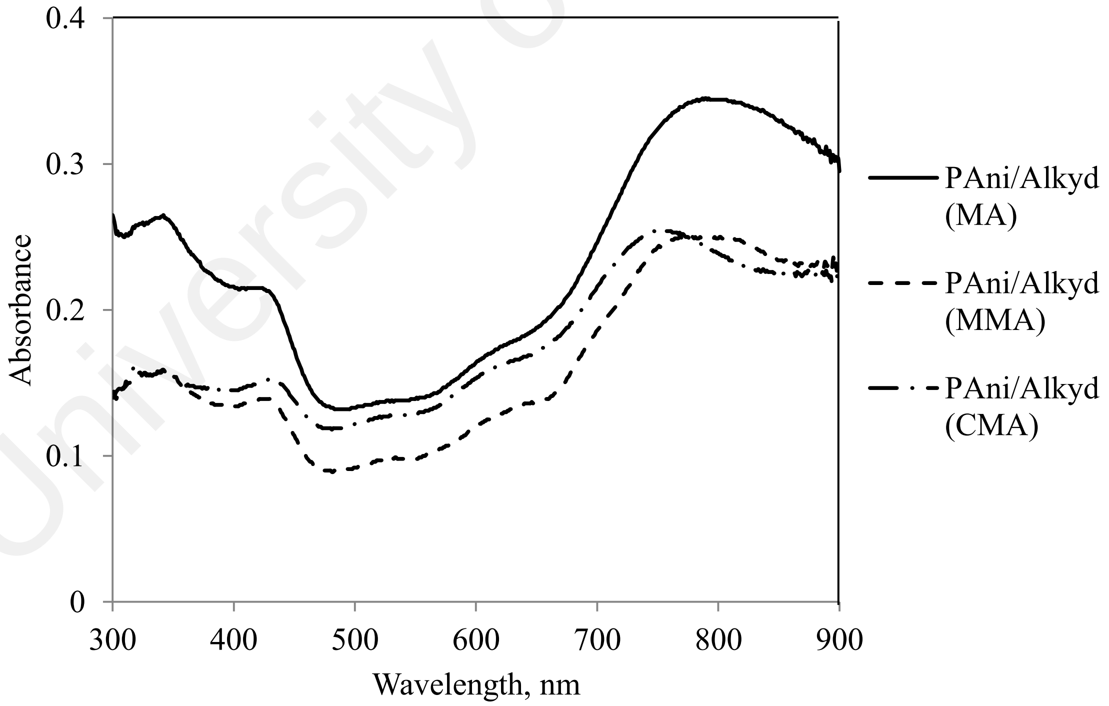

Figure 4.12: UV-Vis spectra of PAni/Alkyd films with different types of reactive diluents.

Table 4.12: Peak assignments for UV-Vis spectra of PAni/Alkyd films with different type of reactive diluents.

Transitions	Wavelength (nm)
polaron–π*	417 – 424
π–polaron	734 – 780

4.3.2.3 Conductivity Property

Principally, the purpose of adding reactive diluent into PAni/Alkyd coating mixture is to obtain films with lower curing time. Based on **Figure 4.13**, it can be observed that PAni/Alkyd (CMA) film exhibits lowest curing time, 5 min compare to the others films. (Aksimentyera et al., 2010; Yao et al., 2014). This result showed that the curing time of PAni/Alkyd film was successfully reduced from 10 min without reactive diluent to 5 min with incorporation of CMA as a reactive diluent.

Besides, the electrical conductivities of PAni/Alkyd with and without incorporation of reactive diluents are as shown in **Table 4.13**. It can be observed that PAni/Alkyd with reactive diluents possessed higher conductivity in the range of 6.24×10^{2} Scm^{-1} to 6.49×10^{2} Scm^{-1} compared to PAni/Alkyd without reactive diluent (2.56×10^{2} Scm^{-1}). PAni/Alkyd (CMA) film recorded the highest conductivity compared to other reactive diluents. As discussed earlier, addition of CMA diluent will change the coil-like structure of PAni to more expanded coil-like structure, thus eventually enhanced the electrical conductivity of PAni/Alkyd film. Moreover, CMA reactive diluent presumably reduce viscosity and enhance overall mobility of the current carrying electrons in the backbone of PAni/Alkyd, resulting in high electrical conductivity (Dai et al., 2014; Mendes-Felipe et al., 2019; Syu et al., 2019; Ugur et al., 2014).

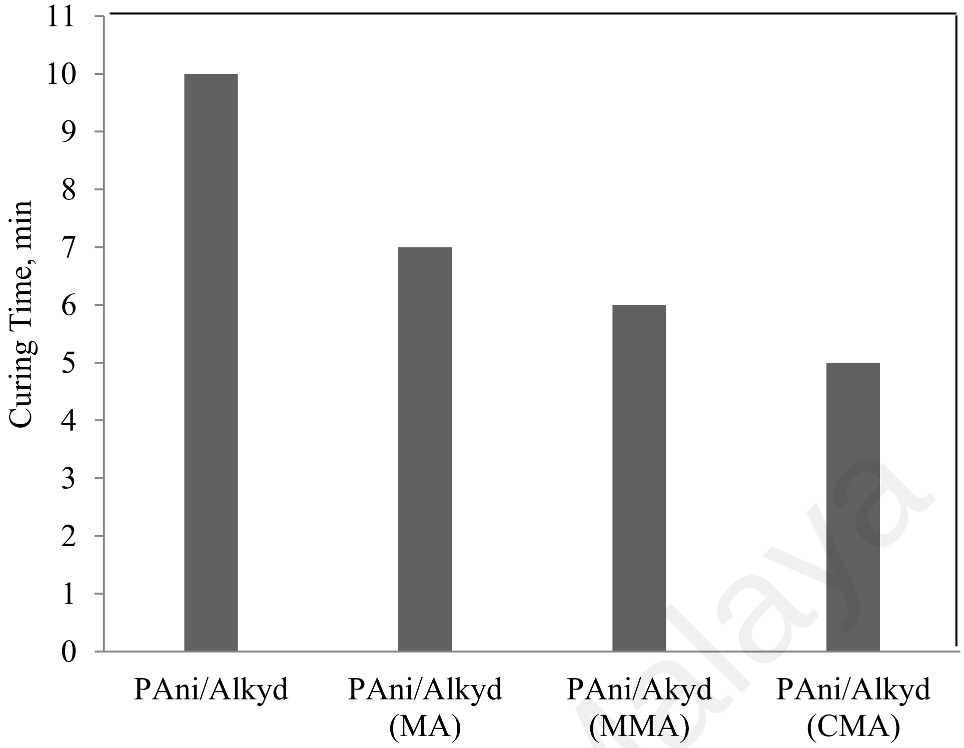

Figure 4.13: Curing time of the PAni/Alkyd films with and without reactive diluents.

Table 4.13: Conductivity of PAni/Alkyd films with and without reactive diluents.

Films	Conductivity (Scm^{-1})
PAni/Alkyd (without reactive diluent)	2.56×10^2
PAni/Alkyd (MA)	6.24×10^2
PAni/Alkyd (MMA)	6.37×10^2
PAni/Alkyd (CMA)	6.49×10^2

4.3.2.4 Adhesion Property

Incorporation of reactive diluents into the PAni/Alkyd coating not only can improve the curing process of films but also indirectly produces high-solid content in PAni/Alkyd formulation that contributed to better film forming on substrate under UV irradiation (Tiwari et al., 2016). As shown in **Table 4.14**, the adhesion property for all PAni/Alkyd films with different types of reactive diluents that coated on FTO substrate exhibited 5B grade. Therefore, it has significantly confirmed that PAni/Alkyd can adhere strongly on the FTO substrate with addition of reactive diluents. In this study, it can be observed that reactive diluent is potentially a good additive in PAni/Alkyd composite where it can reduces the curing time of the films as well as enhance the electrical conductivity without affect the adhesion performance on FTO substrate.

Table 4.14: Adhesion test of PAni/Alkyd films with and without reactive diluents.

Films	Test Grade (ASTM D3559)
PAni/Alkyd (without reactive diluent)	5B
PAni/Alkyd (MA)	5B
PAni/Alkyd (MMA)	5B
PAni/Alkyd (CMA)	5B

4.3.3 PAni-TiO_2/Alkyd with different TiO_2 content

4.3.3.1 FTIR Analysis

Figure 4.14 shows the overlay of FTIR spectra of PAni-TiO_2/Alkyd composites with different TiO_2 content and the peaks present in the spectra are summarized in **Table 4.15**. In general, PAni-Ti10/Alkyd, PAni-Ti20/Alkyd and PAni-Ti40/Alkyd showed similar patterns of FTIR spectra. It can be observed that PAni-TiO_2/Alkyd composites showed a weak peak at 1100 – 1120 cm^{-1} that corresponds to the Ti−O−C stretching due to the interaction between PAni and TiO_2 nanoparticles (Sambasevam et al., 2015).

Small peaks at ~1580 cm^{-1} and ~1602 cm^{-1} are associated to the C=C of aromatic rings of PA in the POB alkyd. Besides, addition of POB alkyd into PAni-TiO$_2$ composites has led to the appearance of strong peak at 1725 – 1730 cm^{-1} owing to the ester linkages and a broad peak of -OH at ~3400 cm^{-1} (Cai et al., 2014; Hübert et al., 2011). The resulted FTIR spectra in this study confirmed the chemical structures of PAni-TiO$_2$/Alkyd with different TiO$_2$ content.

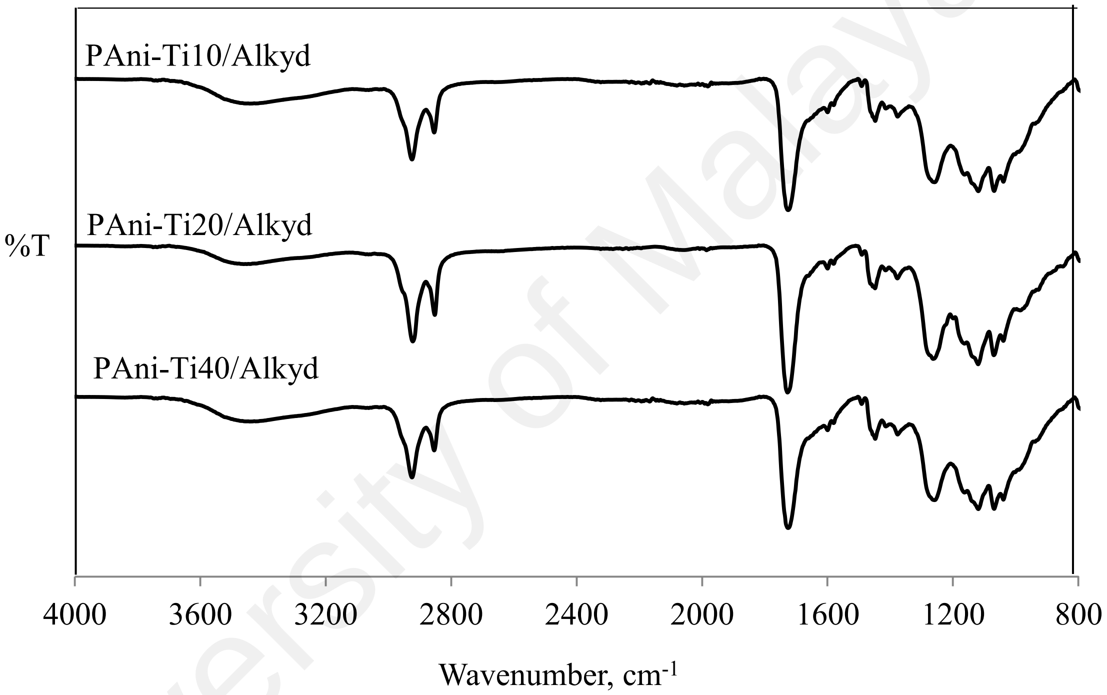

Figure 4.14: FTIR spectra of PAni-TiO$_2$/Alkyd with different TiO$_2$ content.

Table 4.15: Peak assignments for FTIR spectra of PAni-TiO_2/Alkyd composites.

Functional groups	Wavenumber (cm^{-1})
Ti-O-C stretch (PAni-TiO_2)	1100 – 1120
aromatic C=C stretch (POB alkyd)	1580 and 1602
C=O of ester (POB alkyd)	1725 – 1730
-OH stretch (POB alkyd)	~3400

4.3.3.2 UV-Vis Analysis

UV-Vis spectra of pristine PAni and PAni-TiO_2/Alkyd composites with different TiO_2 content are as shown in **Figure 4.15** whereas the peaks present from UV-Vis spectra are assigned in **Table 4.16**. PAni-TiO_2/Alkyd with different TiO_2 content (10%, 20% and 40%) had similar patterns as the spectrum of pristine PAni. The three characteristic peaks of typical conducting forms are observed at 345 – 352 nm , 430 – 440 nm and 750 – 785 nm, attributed to the π–π*, polaron–π* and π–polaron transitions, respectively.

From the UV-Vis spectra, addition of both TiO_2 and POB alkyd into pristine PAni has caused the wavelength shifts of π–polaron peaks from lower wavelength of 750 nm (PAni) to higher wavelength of 776 – 785 nm (PAni-TiO_2/Alkyd). This condition is referred to the solvatochromic shift which can be either red or blue shift. Red shift occurs when there is a movement of the polaron peak to higher wavelength while blue shift involving movement of the polaron peak to lower wavelength (Budzak et al., 2016). Thus, the interaction between PAni with both TiO_2 and POB alkyd with different TiO_2 content initiated a red shift as shown in **Figure 4.15**.

Apart from that, PAni-Ti20/Alkyd film shows the highest absorbance capacity that appears at 785 nm compare to PAni-Ti40/Alkyd and PAni-Ti10/Alkyd. Thus, 20% of TiO_2 content added is the optimum value that could have initiated the strongest intermolecular interaction within PAni and TiO_2 presumably attributed from the hydrogen bonding between N–H proton of PAni with the oxygen atom of TiO_2 nanoparticles (Abaci et al., 2014; Katoch et al., 2012).

The resulted UV-Vis spectra in this study confirmed that pristine PAni and PAni-TiO_2/Alkyd in the conducting emeraldine salt (ES) state. Besides, the proposed reaction mechanisms of PAni-TiO_2 with POB alkyd were shown in **Figure 4.16** (Kawata et al., 2013; Zhao et al., 2014).

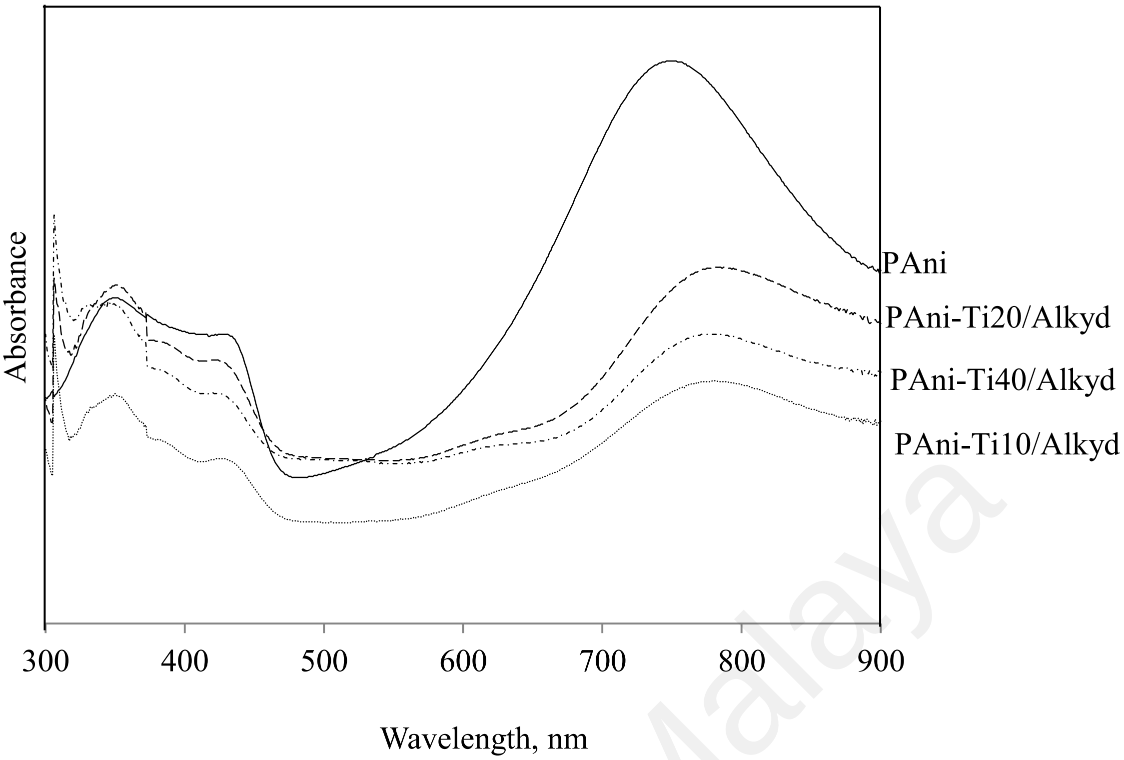

Figure 4.15: UV-Vis spectra of PAni and PAni-TiO$_2$/Alkyd with different TiO$_2$ content.

Table 4.16: Peak assignments for UV-Vis spectra of PAni and PAni-TiO$_2$/Alkyd with different TiO$_2$ content.

Polymer	π–π* (nm)	polaron–π* (nm)	π–polaron (nm)
PAni	352	440	750
PAni-Ti10/Alkyd	348	433	779
PAni-Ti20/Alkyd	350	430	785
PAni-Ti40/Alkyd	345	435	775

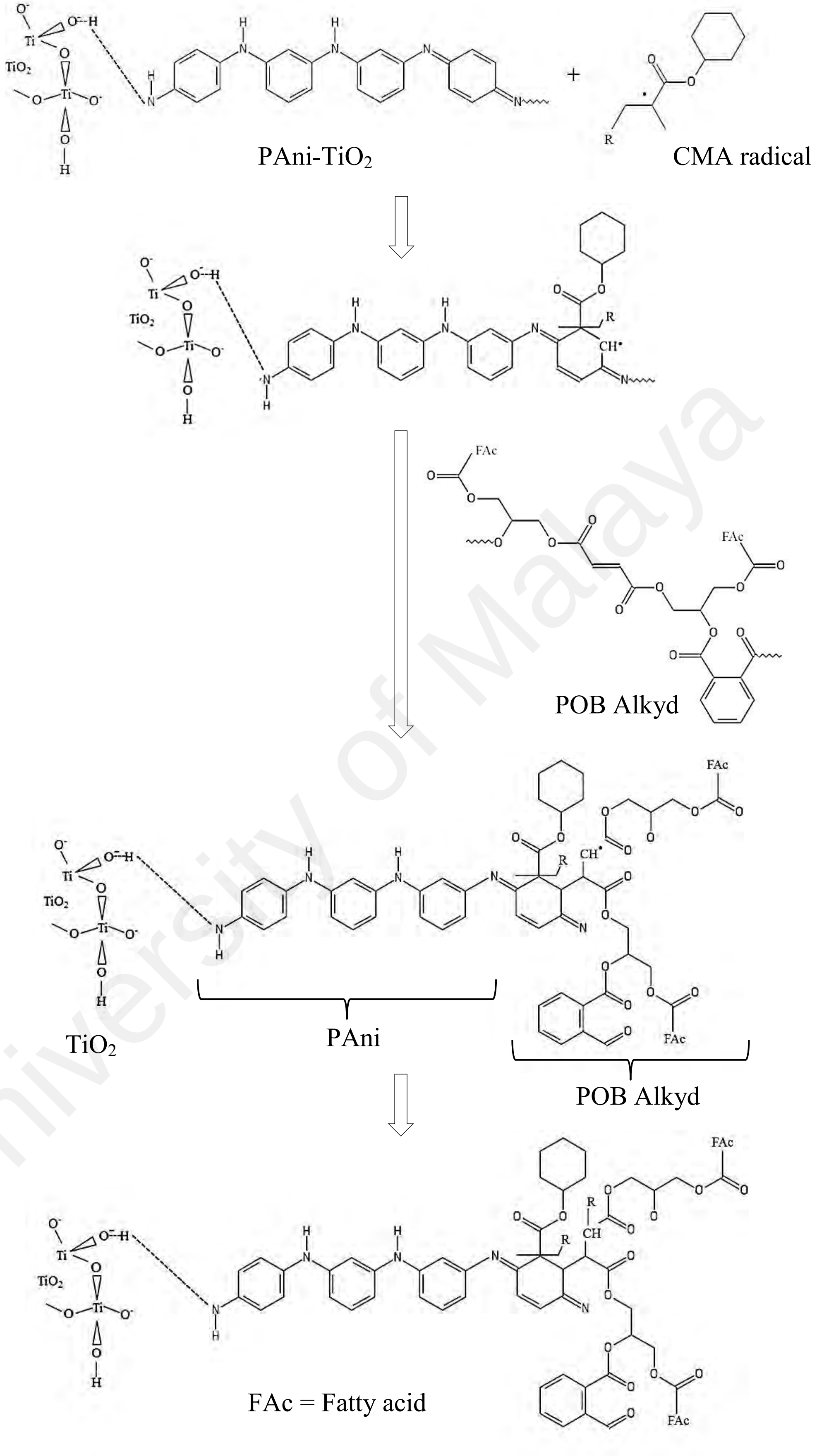

Figure 4.16: Plausible reaction mechanisms between PAni-TiO$_2$ and Alkyd under UV irradiation.

4.3.3.3 XRD Analysis

Figure 4.17 shows the X-ray diffractograms of PAni-TiO_2/Alkyd with different TiO_2 content. It can be noted that all PAni-TiO_2/Alkyd exhibited a sharp and distinct peaks at 33.6°, 37.7°, 51.5° and 61.5° indicating the presence of TiO_2 nanoparticles (Kotresh et al., 2016; Nayak et al., 2018).

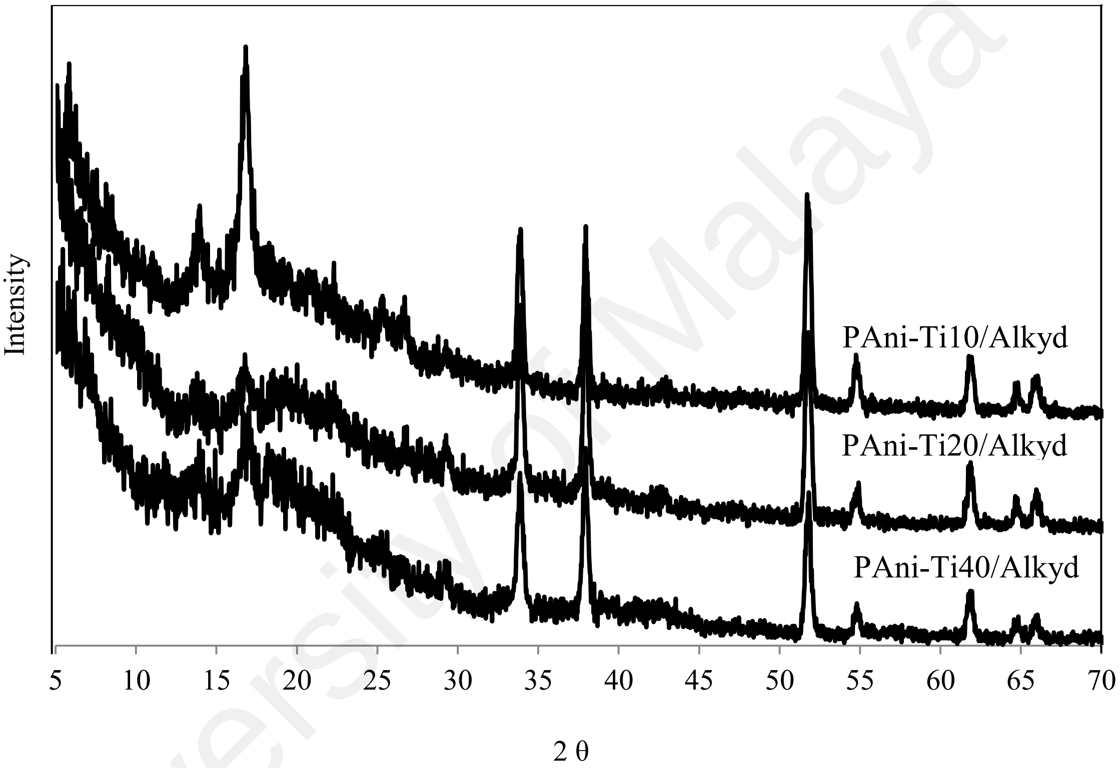

Figure 4.17: X-ray diffractogram of PAni-TiO_2/Alkyd with different TiO_2 content.

4.3.3.4 Conductivity Property

Figure 4.18 shows the conductivity of pristine PAni and PAni-TiO_2 with different TiO_2 content (10%, 20% and 40%) after addition of POB alkyd on FTO glasses prior to its application as CE in DSSC which used a conductive substrate. Application of PAni/TiO_2 on FTO glass significantly increases the conductivity from 6.59×10^{-2} Scm^{-1} (ordinary glass slide) to $6.11-6.32\times10^{2}$ Scm^{-1} (FTO substrate). This phenomenon happened because fluorine dopant from FTO substrate act as electron donor that can provide free electron along the PAni/TiO_2 backbone, hence increased the electrical conductivity of PAni/TiO_2 on FTO substrate (Banyamin et al., 2014 and Molapo et al., 2012)

Besides, it can be observed that the conductivity of PAni-TiO_2/Alkyd with different TiO_2 content were decreased in the range of 6.11×10^2 Scm^{-1} to 6.24×10^2 Scm^{-1} after addition of POB alkyd compare to pristine PAni (1.31×10^3 Scm^{-1}). This is because POB alkyd was slightly blocked the conductive pathway of PAni, thus lowering the conductivity (Kawata et al., 2013 and Li et al., 2009). Among PAni-TiO_2/Alkyd films, PAni-Ti20/Alkyd shows the highest conductivity of 6.32×10^2 Scm^{-1} due to its highest interfacial polarization between PAni and TiO_2 nanoparticles and the uniform dispersion of TiO_2 in the PAni matrix (Ramesan et al., 2014; Sampreeth et al., 2017).

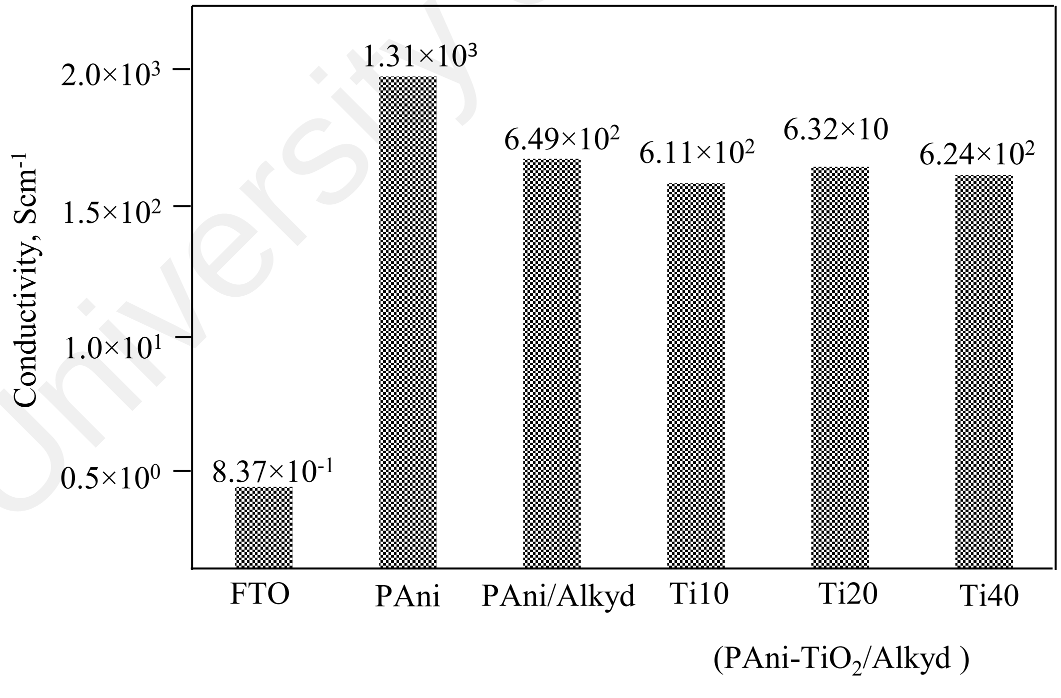

Figure 4.18: Conductivity of FTO, pristine PAni, PAni/Alkyd and PAni-TiO_2/Alkyd films with different TiO_2 content.

4.3.3.5 Adhesion Property

Table 4.17 shows the adhesion property of the pristine PAni and PAni-TiO_2 (10%, 20% and 40%) with and without addition of POB alkyd based on the grade of adhesion test from 0B to 5B. As mentioned at the early stage of study, PAni exhibits very poor adhesion performance on FTO substrate with 0B grade. However, with the addition of POB alkyd into PAni-TiO_2 composites, the adhesion of PAni and PAni-TiO_2 films improved significantly to 5B except for PAni-Ti40/Alkyd which only attained 3B. This indicated that POB alkyd is able to improve the adhesion of the films. However, an excessive amount of TiO_2 might act as a barrier that block the linkage between PAni-TiO_2/Alkyd and FTO glass which affect the adhesion to the FTO substrate (Alam et al., 2013; Issam and Cheun., 2009; Uzoh et al., 2013). Thus, similar condition also happened towards the adhesion of PAni-TiO_2 and PAni-TiO_2/Alkyd composites on normal glass slides.

A plausible mechanism for interaction between PAni-TiO_2/Alkyd was shown in **Figure 4.19**. It can be observed that, PAni-TiO_2/Alkyd composite could strongly adhere to the FTO substrate due to the possibility of hydrogen bonding between C=O of alkyd with -OH of the FTO glass (Biggs et al., 2015; Dutta et al., 2006).

Table 4.17: Adhesion test for pristine PAni, PAni-TiO_2 and PAni-TiO_2/Alkyd with different TiO_2 content.

Films	Adhesion Test (ASTM D3359)			
	PAni	PAni-Ti10	PAni-Ti20	PAni-Ti40
Without Alkyd	0B	3B	3B	2B
With Alkyd	5B	5B	5B	3B

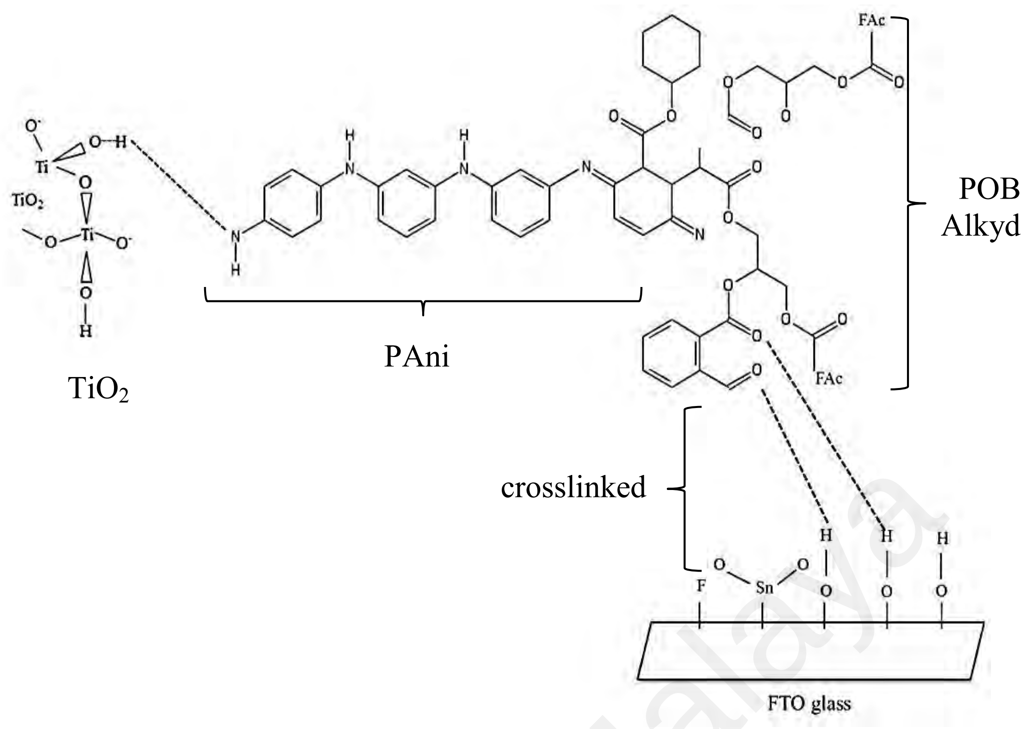

Figure 4.19: Plausible mechanism for interaction between PAni-TiO_2/Alkyd with FTO.

Recently, Kawata et al. reported on the application of PAni-TiO_2 alkyd in DSSC but the films preparation involving the addition of m-Cresol which is classified as a toxic substance. The toxicity of m-Cresol deserved great attention as there are many potential health effects upon by exposure to m-Cresol which can cause nose and throat irritation. Moreover, ingestion or dermal contact with this chemical can lead to serious gastrointestinal damage, severe skin damage and even death. Hence, it is very important to minimize and cut down the usage of hazardous chemicals for the benefits of human health and environment (Kamijo et al., 2003; Paiva et al., 2016).

Table 4.18 shows the comparison between PAni-TiO_2/Alkyd films prepared by Kawata et al. (with m-Cresol) with the films that were obtained in this study. It can be observed that both films attained good adhesion (5B). The conductivity of PAni-TiO_2/Alkyd films without m-Cresol (6.11×10^{2} Scm^{-1} to 6.32×10^{2} Scm^{-1}) was higher than PAni/m-Cresol/TiO_2/Alkyd (9.03×10^{0} Scm^{-1} to 7.29×10^{1} Scm^{-1}). Besides, based on previous research studies from 2013 to 2019, the conductivity value of PAni that potentially could serve as a good CE in DSSC is in the range of 1.15×10^{-4} Scm^{-1} to 7.74×10^{2} Scm^{-1} with PCE range of 0.42% to 12.30%. So, the conductivity value achieved in this study, in the range of 6.11×10^{2} Scm^{-1} to 6.32×10^{2} Scm^{-1}, was sufficient to enhance its efficiency as CE in DSSC device (Hassan et al., 2013; Lee et al., 2015; Saad et al., 2014; Tas et al., 2017).

More environmental friendly and lower cost materials of CE component in DSSC are the foci in this study. Thus, the preparation of PAni-TiO_2/Alkyd films with good adhesion and conductivity behaviour can be potentially applied as CE in DSSC devices. As for the application part of study, the films that possessed adhesion property with 5B grade which are PAni/Alkyd, PAni-Ti10/Alkyd and PAni-Ti20/Alkyd were chosen as CE material for DSSC device for further study.

Table 4.18: Film's properties for PAni-TiO_2/Alkyd with and without the addition of m-Cresol.

Research	Films	Conductivity (Scm^{-1})	Test Grade (ASTM D3359)
Current Research	PAni/Alkyd	6.49×10^{2}	5B
	PAni-TiO_2/Alkyd	$6.11 – 6.32\times10^{2}$	5B
Kawata et al., (2013)	PAni/m-Cresol/TiO_2/ Alkyd	$9.03\times10^{0} – 7.29\times10^{1}$	5B

4.4 Application of PAni, PAni/Alkyd and PAni-TiO_2/Alkyd in DSSC

As discussed earlier, PAni/Alkyd, PAni-Ti10/Alkyd and PAni-Ti20/Alkyd films were the best candidates as CE materials for DSSC application due to its high conductivity (6.11×10^2 Scm^{-1} to 6.32×10^2 Scm^{-1}) and good adhesion of 5B on FTO substrate. Therefore, the PCE of these films in DSSC device were investigated for the final part of this research study. Pristine PAni as CE was applied as a control for comparison. **Figure 4.20** shows the current-voltage (I-V) curve of DSSC with different type of CE films. The derived photovoltaic parameters such as open-circuit voltage (Voc), short-circuit current density (Jsc), fill factor (*ff*) and overall power conversion efficiency (PCE), η are tabulated in **Table 4.19**.

Principally, PCE value of DSSC is mainly depends on the photovoltaic parameters obtained such as Voc, Jsc and *ff* values. *ff* value is calculated based on **Equation 3.4** as well as PCE is calculated based on **Equation 3.5**. Refer to the overall results of photovoltaic parameters, the PCE of pristine PAni as CE film (3.70%) is higher compare to PAni/Alkyd (0.60%), PAni-Ti10/Alkyd (0.20%) and PAni-Ti20/Alkyd CE films (0.30%) as shown in **Table 4.20**. Pristine PAni as CE film exhibits the highest PCE up to 3.70% with the highest Voc, Jsc and *ff* of 0.61 V, 12.20 $mAcm^{-2}$ and 49.79%, respectively.

Pristine PAni possessed the highest Jsc value of 12.20 $mAcm^{-2}$ compare to PAni/Alkyd and PAni-TiO_2/Alkyd CE with Jsc value of 2.70 – 6.50 $mAcm^{-2}$ due to the highest electrocatalytic activity of the pristine PAni. In general, high electrocatalytic activity of the CE film is the vital factor that may produces the best performance for PCE of the system during DSSC measurement. It is because pristine PAni with high electrocatalytic activity not only can increases the electron transfer at the interface of electrolyte and CE but also promotes the reduction of I_3^- ions at the CE. Finally, it is significantly to enhance the PCE of the system during DSSC measurement (Cho et al., 2012; He et al., 2004; Xu et al., 2019).

Apart from that, the lower Jsc of PAni/Alkyd, PAni-Ti10/Alkyd and PAni-Ti20/Alkyd (2.70 – 6.50 mAcm^{-2}) is caused by the incorporation of TiO_2 and POB alkyd that block the electron transfer between electrolyte and CE. This phenomena eventually lower down the collection of the charge carrier at CE film, thus reduce the PCE of the system during DSSC measurement. Based on **Table 4.20**, the dramatic decrease of Jsc values from 12.20 mAcm^{-2} (pristine PAni) to 6.50 – 2.70 mAcm^{-2} (PAni/Alkyd and PAni-TiO_2/Alkyd) is caused by the decreasing of electrical conductivity for PAni/Alkyd and PAni-TiO_2/Alkyd (6.11×10^{2} Scm^{-1} to 6.49×10^{2} Scm^{-1}) compare to pristine PAni (1.31×10^{3} Scm^{-1}) (Benlin He et al., 2013).

Therefore, it is foreseen that, the high electrical conductivity for the CE film of pristine PAni is a crucial factor that may affected the Jsc value as well as the electrocatalytic activity of CE, thus contribute to the performance for PCE of the system during DSSC measurement. Among all CE films with the incorporation of POB alkyd, PAni/Alkyd recorded the highest PCE of 0.60% due to its high electrical conductivity. In this research study, the main role of POB alkyd is to improve the adhesion of PAni on FTO substrate by the reactive C=C of the POB alkyd that undergo crosslinking in the PAni/Alkyd coating.

However, the POB alkyd is a nonconductive binder that may block the conductive pathway of PAni. Adaptation of the conductive binder as a future plan may not only increase the adhesion towards the substrate but also increase the performance for PCE of the system.

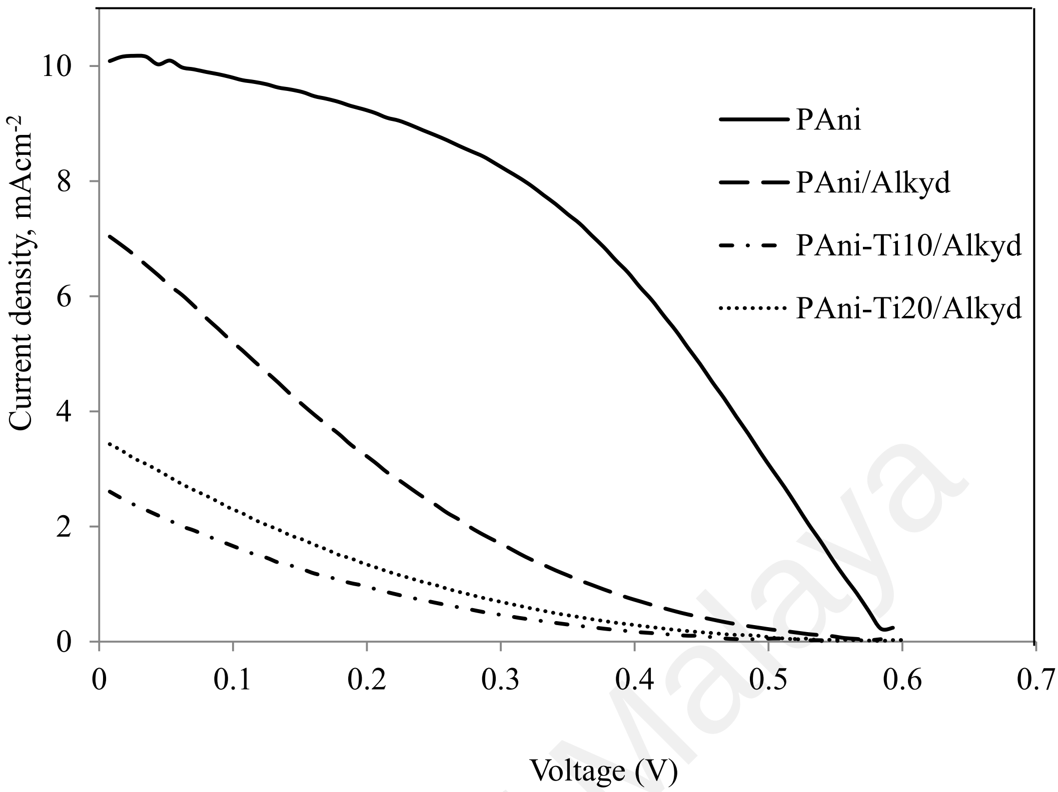

Figure 4.20: I-V curve of DSSC with various types of PAni as CE films.

Table 4.19: Photovoltaic parameters of DSSC with various types of PAni as CE films.

CE Films	Voc (V)	Jsc (mAcm $^{-2}$)	*ff* (%)	PCE, η (%)
PAni	0.61	12.20	49.79	3.70
PAni/Alkyd	0.60	6.50	15.89	0.60
PAni-Ti10/Alkyd	0.56	2.70	12.68	0.20
PAni-Ti20/Alkyd	0.56	3.30	14.13	0.30

Table 4.20 shows the comparison between the prepared film's properties that were used as CE in DSSC with the previous research study by Kawata and co-workers. It can

be observed that the PCE of PAni/m-Cresol/TiO_2/Alkyd was higher (3.00%) compare to this study (0.20% – 0.60%). This is due to the present of m-Cresol which can act as a secondary dopant that might extended the coil-like structure of PAni and facilitate electron movement along PAni chain in both interchain and intrachain. Besides, m-Cresol also functions as a solvent that will dissolve the TiO_2 paste, thus it will reduce the blockage of TiO_2 along PAni chain. Thus, PAni/m-Cresol/TiO_2/Alkyd composite will exhibits high electrical conductivity and high PCE in DSSC device (Lee et al., 2009; Niu et al., 2011)

However, the presence of toxic substance like m-Cresol produced non-environmental friendly material as CE for DSSC. The toxicity of m-Cresol deserved great attention as there are many potential health effects upon by exposure to m-Cresol which can cause nose and throat irritation. Moreover, ingestion or dermal contact with this chemical can lead to serious gastrointestinal damage, severe skin damage and even death. Hence, it is very important to minimize the usage of hazardous chemicals especially for the benefits of human health (Agency for Toxic Substances and Disease Registry, ATSDR, 2008).

Initially, this research study was conducted in order to produce an environmentally PAni/Alkyd and PAni-TiO_2/Alkyd as CE in DSSC device without using any toxic secondary dopant like m-Cresol. In addition, TiO_2 particle was introduced to replace TiO_2 paste used by previous research study as it will reduce the preparation cost for the CE films of DSSC. As a results, PAni/Alkyd and PAni-TiO_2/Alkyd as CE films with good adhesion (5B), high electrical conductivity (6.11×10^{2} Scm^{-1} to 6.49×10^{2} Scm^{-1}) and moderate PCE (0.20% – 0.60%) in DSSC were successfully obtained.

Table 4.20: Comparison of the film's properties with the previous research study.

Research	Films	PCE of DSSC (%)	Advantage	Disadvantage
This research study	PAni/Alkyd PAni-Ti10/Alkyd PAni-Ti20/Alkyd	0.60 0.20 0.30	Environmental friendly, good adhesion and low cost (using TiO_2 particles)	Low PCE
Kawata et al., (2015)	PAni/m-Cresol/ TiO_2/Alkyd	3.00	High PCE and good adhesion	Non-environmental friendly (m-Cresol, toxic) and high cost (using TiO_2 paste)

This initial research results also confirmed that PAni and PAni-TiO_2 modified with POB alkyd can be potentially applied as a cost-effective and environmental friendly materials used for DSSC study. Besides, this research study opens new perspectives for the use of PAni composite as a conducting material together with an incorporation of alkyd as a non-conductive binder without any toxic substances in solar panel application.

CHAPTER 5: CONCLUSION

5.1 Conclusion

This study applied PAni as CE material with incorporation of TiO_2 and POB alkyd for DSSC application. A series of PAni and PAni-TiO_2 with different TiO_2 content (10%, 20% and 40%) in ES state (1.31×10^3 Scm^{-1}) were successfully synthesized through chemical oxidation method at 0°C. POB alkyd were synthesized via alcoholysis and polycondensation reactions with different AN of 5.66, 14.74 and 17.60 mg KOH/g alkyd. FTIR, UV-Vis, XRD and ^{1}H NMR spectra have confirmed the chemical structures of PAni, PAni-TiO_2 and POB alkyd.

Among all PAni/Alkyd films, PAni/Alkyd using ratio 1:0.5 with AN of 5.66 mg KOH/g alkyd and CMA as diluent is the optimum parameters to exhibit the lowest curing time of 5 min under UV irradiation and adhesion of 5B on FTO substrate. Conductivity and adhesion are two main factors that contribute high PCE in DSSC device. Based on previous research studies from 2013 to 2017, PAni with conductivity range of 1.15×10^{-4} Scm^{-1} to 7.74×10^2 Scm^{-1} is potentially behave as a good CE in DSSC.

In this study, the conductivity of PAni/Alkyd and PAni-TiO_2/Alkyd with different TiO_2 content were decreased from 1.31×10^3 Scm^{-1} (pristine PAni) to 6.11×10^2 Scm^{-1} after addition of POB alkyd. This is because POB alkyd was slightly blocked the conductive pathway of PAni, thus lowering the conductivity. However, the adhesion of PAni has improved significantly from 0B to 5B. This indicated that POB alkyd is able to improve the adhesion of the films and the resulted conductivity is potentially applied in DSSC application.

The PAni/Alkyd and PAni-TiO_2/Alkyd films that used for DSSC application as CE in this study showed film's thickness of ~0.02 μm, conductivity range of 6.11×10^2 Scm^{-1} to 6.49×10^2 Scm^{-1} and good adhesion of 5B. PAni/Alkyd as CE showed the highest PCE of 0.60% compared to PAni-Ti10/Alkyd (0.20%) and PAni-Ti20/Alkyd (0.30%) due to its higher electrical conductivity.

Previous study on the application of PAni/m-Cresol/TiO_2/Alkyd exhibited good PCE of 3.00% in DSSC device but required high cost and produced non-environmental friendly CE material with the presence of toxic m-Cresol. Although the PAni/Alkyd that prepared in this study showed moderate PCE of 0.60%, this PAni/Alkyd film can be potentially applied as a cost-effective and environmental friendly materials with moderate electrical conductivity (6.49×10^2 Scm^{-1}) and best adhesion of 5B.

5.2 Suggestion for Future Research

As discussed earlier, electrical conductivity and adhesion are two major factors that play an important role for high performance of DSSC device. PAni as CE material that is applied to induce high conductivity property can be further modified using other synthesis parameters for example different types of oxidant, different type of dopant and different oxidant to dopant ratio. The conductivity of PAni also can be improved through others synthesis conditions such as different polymerization temperature, different polymerization reaction times, etc.

On the other hand, POB alkyd plays an important role in improving the adhesion property of PAni on FTO substrate. The introduction of POB alkyd as adhesive binder in PAni composite is crucial in producing and maintaining an excellent performance of CE in DSSC device. In future, it would be more interestingly to modified alkyd resins by combining palm oil with other vegetables oil such as soybean, castor and linseed oil to increase the unsaturation sites in alkyd chain, thus lowering the curing time of alkyd films (Sharmin et al., 2015).

By the way, POB alkyd that used as binding in this study is an insulating material that will reduce the conductivity of the film. Thus, an introduction of conductive binder such as metal filler particles including Ni, Cu, carbon and graphite into alkyd resin could be explored to produce an electrically conductive adhesive material (Sancaktar and Bai., 2011). As for the DSSC application, chemical characterizations such as cyclic voltammetry and electrochemical impedance spectroscopic analyses could be investigated for detail understanding on the fundamental of reduction, charge transfer and transport processes during DSSC measurement.

REFERENCES

AbdulAlmohsin, A. S., Li, Z., Mohammed, M., Wu, K.., & Cui, J. (2012). Electrodeposited polyaniline/multi-walled carbon nanotube composites for solar cell applications. *Synthetic Metals, 162*, 931-935.

Afzal, A. B., Akhtar, M. J., Nadeem, M., & Hassan, M. M. (2009). Investigation of structural and electrical properties of polyaniline/gold nanocomposites. *Journal of Physical Chemistry C, 113*, 17560-17565.

Agency for Toxic Substances and Disease Registry (ATSDR). (2008). Toxicological profile for Cresols. Atlanta, GA: U.S. Department of Health and Human Services, Public Health Service.

Ahad, I. Z. M., Harun, S. W., Gan, S. N., & Phang, S. W. (2017). Application of fiber bragg grating sensor coated with polyaniline as an optical sensor for chloroform detection. *Polymers & Polymer Composites, 25*(7), 555-562.

Al-Daghman, A. N. J., Ibrahim, K., Ahmed, N. M., & Abdullah, A. M. (2016). Effect of doping by stronger ions salt on the microstructure of conductive polyaniline-ES: structure and properties. *Journal of Optoelectronics and Biomedical Materials, 8*(4), 175-183.

Alam, M., Akram, D., Sharmin, E., Zafar, F., & Ahmad, S. (2013). Vegetable oil based eco-friendly coating materials: a review article. *Arabian Journal of Chemistry, 7*, 469-479.

Ali, M. A., Saion, E., Yahya, N., Kassim, A., Dahlan, K. M., & Hashim, S. (2007). Synthesis of conducting polyaniline nanocomposites by radiation doping. *Journal of Engineering Science and Technology, 2*(1), 111-118.

Amalina, A., Suendo, V., Reza, M., Milana, P., Sunarya, R. R., Adhika, D. R., & Tanuwijaya, V. V. (2019). Preparation of polyaniline emeraldine salt for conducting-polymer-activated counter electrode in dye sensitized solar cell (DSSC) using rapid-mixing polymerization at various temperature. *Bulletin of Chemical Reaction Engineering & Catalysis,* 14(3), 521-528.

An, G. H., Lee, E. H., & Ahn, H. J. (2016). Ruthenium and ruthenium oxide nanofiber supports for enhanced activity of platinum electrocatalysts in the methanol oxidation reaction. *Physical Chemistry Chemical Physics, 18*(22), 14859-14866.

Ang, D. T. C. (2015). Effect of reactive diluent on physicochemical and thermal properties of UV-curable alkyd coatings. *Journal of Coatings Technology and Research,* 1-8.

Ang, D. T. C., & Gan, S.N. (2012). Novel approach to convert non-self drying palm stearin alkyds into environmental friendly UV curable resins. *Progress in Organic Coatings, 73*, 409-414.

Asim, N., Sopian, K., Ahmadi, S., Saeedfar, K., Alghoul, M.A., Saadatian, O., & Zaidi, S.H. (2012). A review on the role of materials science in solar cells. *Renewable and Sustainable Energy Reviews, 16*, 5834-5847.

Ataei, S., Yahya, R., & Gan, S.N. (2011). Effect of methyl methacrylate content on coatings' properties of palm oleic acid-based macromer. *Journal of Coatings Technology and Research, 8*(6), 719–725.

Bagher, A. M., Vahid, M. M. A., & Mohsen, M. (2015). Types of solar cell application. *American Journal of Optics and Photonics, 3*(5), 94-113.

Bahrami, M., & Abbaszadeh, P. (2013). An overview of renewable energies in Iran. *Renewable and Sustainable Energy Reviews, 24*, 198-208.

Bai, H., & Shi, G. (2007). Gas sensors based on conducting polymers. *Sensors, 7*, 267-307.

Baldan, A., (2012). Adhesion phenomena in bonded joints. *International Journal of Adhesion and Adhesives*, *38*, 95-116.

Balint, R., Cassidy, N. J., & Cartmell, S. H. (2014). Conductive polymers: Towards a smart biomaterial for tissue engineering. *Acta Biomaterialia*, *10*, 2341-2353.

Banyamin, Z. Y., Kelly, P. J., West, G., & Boardman, J. (2014). Electrical and optical properties of fluorine doped tin oxide thin films prepared by magnetron sputtering. *Coating, 4*, 732-746.

Bella, F., Gerbaldi, C., Barolo, C., & Grätzel, M. (2015). Aqueous dye-sensitized solar cells. *Chemical Society Reviews, 44*(11), 3431-3473.

Biggs, C. I., Edmondsonb, S., & Gibson, M. I. (2015). Thiol–ene immobilisation of carbohydrates onto glass slides as a simple alternative to gold–thiol monolayers, amines or lipid binding. *Biomaterial Science*, *3*, 175-181.

Boddula, R., & Srinivasan, P. (2014). Emeraldine base form of polyaniline nanofibers as new, economical, green, and efficient catalyst for synthesis of Z-Aldoximes. *Journal of Catalysts, 2014*, 1-6.

Bora, A., Mohan, K., Phukan, P., & Dolui, S. K. (2017). A low cost carbon black/ polyaniline nanotube composite as efficient electro-catalyst for triiodide reduction in dye sensitized solar cells. *Electrochimica Acta,259*, 233-244.

Bhadraa, S., Khastgir, D., Singhaa, N. K., & Leeb, J. H. (2009). Progress in preparation, processing and applications of polyaniline. *Progress in Polymer Science*, *34*, 783–810.

Budzak, S., Laurent, A. D., Laurence, C., Medved, M., & Jacquemin, D. (2016). Solvatochromic shifts in UV−vis absorption spectra: the challenging case of 4-Nitropyridine N-Oxide. *Journal of Chemical Theory and Computation, 12*, 1919-1929.

Cai, H., Tang, Q., He, B., Wang, W., Yuan, S., & Chen, H. (2014). Self-assembly of graphene oxide/polyaniline multilayer counter electrodes for efficient dye-sensitized solar cells. *Electrochimica Acta, 121*, 136-142.

Callow, J. A., Callow, M. A., Ista, L. K., Lopez, G., & Chaudhury, M. K. (2005). The influence of surface energy on the wetting behaviour of the spore adhesive of the marine alga ulva linza (synonym enteromorpha linza). *Journal of the Royal Society Interface, 2*, 319-325.

Chapin, D. M., Fuller, C. S., & Pearson, G. L. (1954). A new silicon *p-n* junction photocell for converting solar radiation into electrical power. *Journal of Applied Physics, 25*(5), 676-677.

Chehimi, M. M., Abel, M. L., Perruchot, C., Delamar, M., Lascelles, S. F., & Armes, S. P. (1999). The determination of the surface energy of conducting polymers by inverse gas chromatography at infinite dilution. *Synthetic Metals*, *104*, 51-59.

Chen, J., Li, B., Zheng, J., Zhao, J., Jing, H., & Zhenping, Z. (2011). Polyaniline nanofiber/carbon film as flexible counter electrodes in platinum-free dye-sensitized solar cells. *Electrochimica Acta, 56*, 4624-4630.

Chen, X., Tang, Q., He, B., Lin, L., & Yu, L. (2014). Platinum-free binary Co-Ni alloy counter electrodes for efficient dye-sensitized solar cells. *Angewandte Chemie International Edition, 53*(40), 10799-10803.

Chittavanich, P., Miller, K., & Soucek, M. D. (2012). A photo-curing study of a pigmented UV-curable alkyd. *Progress in Organic Coatings*, *73*, 392-400.

Cho, S., Hwang, S. H., Kim, C., & Jang, J. (2012). Polyaniline porous counter-electrodes for high performance dye-sensitized solar cells. *Journal of Materials Chemistry, 22*(24), 12164.

Chung, I., Lee, B., He, J., Chang, R. P. H., & Kanatzidis, M. G. (2012). All-solid state dye-sensitized solar cells with high efficiency. *Nature, 485*, 486-489.

Cusano, D. A. (1963). CdTe solar cells and photovoltaic heterojunctions in II-VI compounds. *Solid State Electronics, 6*(3), 217-218.

Dao, V., & Choi, H. (2013). An optimum morphology of platinum nanoparticles with excellent electrocatalytic activity for a highly efficient dye-sensitized solar cell. *Electrochimica Acta, 93*, 287-292.

Deivanayaki, S., Ponnuswamy, V., Ashokan, S., Jayamurugan, P., & Mariappan, R. (2013). Synthesis and characterization of polypyrrole/TiO_2 composites by chemical oxidative method. *International Journal for Light and Electron Optics, 124*(12), 1089-1091.

Dhoke, S. K., Sinha, T. J. M., & Khanna, A. S. (2009). Effect of nano-Al_2O_3 particles on the corrosion behavior of alkyd based waterborne coatings. *Journal of Coatings Technology and Research*, *6*(3), 353-368.

Díaz, G. C., Tapanes, N. de la C. O., Câmara, L. D. T., & Aranda, D. A. G. (2014). Glycerol conversion in the experimental study of catalytic hydrolysis of triglycerides for fatty acids production using Ni or Pd on Al_2O_3 or SiO_2. *Renewable Energy, 64*, 113-122.

Dinte, E., & Sylvester, B. (2017). Adhesives: applications and recent advances. *Applied Adhesive Bonding in Science and Technology*: Halil Özer, IntechOpen.

Duan, Y., Chen, Y., Tang, Q., Zhao, Z., Hou, M., Li, R., & Zhang, Z. (2015). A dye-sensitized solar cell having polyaniline species in each component with 3.1%-efficiency. *Journal of Power Sources, 284,* 178-185.

Duong, T., Tuan, T. Q., Dung, D. V. A., Quy, N. V., Vu, D., Nam, M. H., Chien, N. D., Yoon, S., & Le, A. (2014). Application of polyaniline nanowires electrodeposited on the FTO glass substrate as a counter electrode for low-cost dye-sensitized solar cells. *Current Applied Physics*, *14*, 1607-1611.

Dutta, N., Karak N., & Dolui S. K. (2006). Alkyd–epoxy blends as multipurpose coatings. *Journal of Applied Polymer Science, 100*, 516-521.

Elba, M. E., Rehim, E. M. A., & Ashery, R. E. (2018). Progress in organic coating: synthesis and characterization alkyd resin based on soya bean oil and glycerin using zirconium octoate as catalyst. *Chemical Technology: An Indian Journal, 13*(1), 118.

Eslah, S., & Nouri, M. (2019). Synthesis and characterization of tungsten trioxide/polyaniline/polyacrylonitrile composite nanofibers for application as a counter electrode of DSSCs. *Russian Journal of Electrochemistry, 55*(4), 291-304.

Fang, X., Ma, T., Guan, G., Akiyama, M., Kida, T., & Abe, E. (2004). Effect of the thickness of the Pt film coated on a counter electrode on the performance of a dye-sensitized solar cell. *Journal of Electroanalytical Chemistry, 570*(2), 257-263.

Güner, F. S., Yăgcı, Y., & Erciyesa, A. T. (2006). Polymers from triglyceride oils. *Progress in Polymer Science*, *31*, 633-670.

Han, G., Kusunose, T., & Sekino, T. (2008). The preparation and characterization of organic solvent dispersible polyaniline coated titania hybrid nanocomposites. *Materials Science Forum, 569*, 161-164.

Han, Y., Chang, M., Ho, K., Hsieh, T., Tsai, J., & Huang, P. (2014). Electrochemically deposited nano polyaniline films as hole transporting layers in organic solar cells. *Solar Energy Materials & Solar Cells, 128*, 198–203.

Hassan, E., Khattab, N., Rehim, M. A., Salam, H., Ismail, L. F. M., & Turky, G. (2013). Performance of dye sensitized solar cell based on polyaniline composites. *Research and Reviews in Materials Science and Chemistry, 2*(2), 71-98.

He, B., Tang, Q., Wang, M., Chen, H., & Yuan, S. (2014). Robust polyaniline–graphene complex counter electrodes for efficient dye-sensitized solar cells. *ACS Applied Materials & Interfaces, 6*(11), 8230-8236.

Hlaing, N. N., & Oo, M. M. (2008). Manufacture of alkyd resin from castor oil. *World Academy of Science, Engineering and Technology, 48*, 155-161.

Hübert, T., Boon-Brett, L., Black, G., & Banach, U. (2011). Hydrogen sensors – A review. *Sensors and Actuators, B157*, 329-352.

Hussein, A. K. (2015). Applications of nanotechnology in renewable energies—A comprehensive overview and understanding. *Renewable and Sustainable Energy Reviews, 42*, 460–476.

Islam, M. K., Hosen, Beg M. D., & Jamari, S. S. (2014). Alkyd based resin from non-drying oil. *Procedia Engineering, 90*, 78–88.

Issam, A. M., & Cheun C.Y. (2009). A study of the effect of palm oil on the properties of a new alkyd resin. *Malaysian Polymer Journal, 4*(2), 42-49.

Jangid, N. K., Chauhan, N. P. S., Meghwal, K., Ameta, R., & Punjabi, P. B. (2014). A Review: conducting polymers and their applications. *Research Journal of Pharmaceutical, Biological and Chemical Sciences, 5*(3), 383-412.

Jeon, J., Ma, Y., Mike, J. F., Shao, L., Balbuena, P. B., & Lutkenhaus, J. L. (2013). Oxidatively stable polyaniline:polyacid electrodes for electrochemical energy storage. *Physical Chemistry Chemical Physics, 15*, 9654-9662.

Jeong, H., Pak, Y., Hwang, Y., Song, H., Lee, K. H., Ko, H. C., & Jung, G. Y. (2012). Enhancing the charge transfer of the counter electrode in dye-sensitized solar cells using periodically aligned platinum nanocups. *Small, 8*(24), 3757-3761.

Jumat, N. A., Phang, S. W., Ching, J. J., & Basirun, W. J. (2017). Synthesis of polyaniline-TiO_2 nanocomposites and their application in photocatalytic degradation. *Polymers & Polymer Composites, 25*(7), 507-514.

Kalendová, A., Veselý, D., & Stejskal, J. (2008). Organic coatings containing polyaniline and inorganic pigments as corrosion inhibitors. Progress in Organic Coatings, *62*, 105-116.

Kamijo, Y., Soma, K., Kokuto, M., Ohbu, M., Fuke, C., & Ohwada, T. (2003). Hepatocellular injury with hyperaminotransferasemia after cresol ingestion. *Archives of Pathology & Laboratory Medicine*, *127*, 364-366.

Karaoglan, N., & Bindal, C. (2020). Synthesis and optical characterization of benzene sulfonic acid doped polyaniline. *Engineering Science and Technology, an International Journal, 21*, 1152-1158.

Kawata, K., Gan, S. N., Ang, D. T., Sambasevam, K. P., Phang S. W., & Kuramoto, N. (2013). Preparation of polyaniline/TiO_2 nanocomposite film with good adhesion behavior for dye-sensitized solar cell application. *Polymer Composites, 34*, 1884-1891.

Koh, Y. N., Sambasevam, K. P., Yahya, R., & Phang, S. W. (2013). Improvement of microwave absorption for PAni/HA/TiO_2/Fe_3O_4 nanocomposite after chemical treatment. *Polymer Composites, 34*(7), 1186-1194.

Kotresh, S., Ravikiran, Y. T., Prakash, H. G. R., & Kumari, S. C. V. (2016). Polyaniline-titanium dioxide composite as humidity sensor at room temperature. *Nanosystems: Physics, Chemistry, Mathematics, 7*(4), 732-739.

Kouhnavard, M., Ikeda, S., Ludin, N. A., Khairudin, N. B. A., Ghaffari, B. V., Mat-Teridi, M. A., Ibrahim, M. A., Sepeai, S., & Sopian, K. (2014). A review of semiconductor materials as sensitizers for quantum dot-sensitized solar cells. *Renewable and Sustainable Energy Reviews, 37*, 397-407.

Lee, K., Cho, S., Kim, M., Kim, J., Ryu, J., Shin, K.-Y., & Jang, J. (2015). Highly porous nanostructured polyaniline/carbon nanodots as efficient counter electrodes for Pt-free dye-sensitized solar cells. *Journal of Materials Chemistry A, 3*(37), 19018-19026.

Lee, K. H., Park, B. J., Song, D. H., Chin, I. J., & Choi, H. J. (2009). The role of acidic m-cresol in polyaniline doped by camphorsulfonic acid. *Polymer, 50*(18), 4372-4377.

León-Silva, U., Nichoa, M. E., Hu, H., & Cruz-Silva, R. (2007). Effect of modified ITO substrate on electrochromic properties of polyaniline films. *Solar Energy Materials & Solar Cells, 91*, 1444-1448.

Li, D., Huang, J., & Kaner, R. B. (2009). Polyaniline nanofibers: a unique polymer nanostructure for versatile applications. *Accounts of Chemical Research, 42*(1), 135-145.

Li, Q., Wu, J., Tang, Q., Lan, Z., Li, P., Lin, J., & Fan, L. (2008). Application of microporous polyaniline counter electrode for dye-sensitized solar cells. *Electrochemistry Communications, 10*, 1299-1302.

Li, X., Wang, G., Li, X., & Lu, D. (2004). Surface properties of polyaniline/nano-TiO_2 composites. *Applied Surface Science, 229*(1-4), 395-401.

Li, Y., Lu, D., & Wong, C. P. (2009). Intrinsically conducting polymers (ICPs). *Electrical Conductive Adhesives with Nanotechnologies* (pp. 361-424): Springer, Boston, MA Publishers.

Li, Z., Ye, B., Hu, X., Ma, X., Zhang, X., & Deng, Y. (2009). Facile electropolymerized-PANI as counter electrode for low cost dye-sensitized solar cell. *Electrochemistry Communications*, *11*, 1768-1771.

Lia, X., Wang, G., Li, X., & Lu D. (2004). Surface properties of polyaniline/nano-TiO2 composites. *Applied Surface Science, 229*, 395-401.

Liang, L., Liu, C., Xiao, X., Chen, S., Hu, A., & Feng, J. (2014). Optimized synthesis and properties of surfactant-free water-reducible acrylate-alkyd resin emulsion. *Progress in Organic Coatings, 77*, 1715-1723.

Manikandan, V. S., Kumar, S., Palai, A. K., Mohanty, S., & Nayak, S. K. (2019). Ternary composite based on $NiCo_2O_4$/rGO/PANI as an efficient Pt free tri-iodide reducing agent for dye-sensitized solar cell application. *Journal of Photochemistry and Photobiology A: Chemistry 382, 111939*, 1-7.

Menkiti, M. C., & Onukwuli, O. D. (2011). Utilization potentials of rubber seed oil for the production of alkyd resin using variable base oil lengths. *New York Science Journal, 4*(2), 51-59.

Miodek, A., Mejri, N., Gomgnimbou, M., Sola, C., & Korri-Youssoufi, H. (2015). E-DNA sensor of *mycobacterium tuberculosis* based on electrochemical assembly of nanomaterials (MWCNTs/PPy/PAMAM). *Analytical Chemistry, 87*(18), 9257-9264.

Mishra, A. K. (2018). Conducting polymers: concepts and applications. *Journal of Atomic, Molecular, Condensate & Nano Physics, 5*(2), 159-193.

Mokhtar, N., Chye, D. A. T., & Phang, S. W. (2017). Morphology, conductivity and microwave absorption behavior of polyaniline nanocomposites after chemical treatment. *Polymers & Polymer Composites, 25*(7), 545-554.

Mokurala, K., Kamble, A., Bhargava, P., & Mallick, S. (2015). RF sputtered iridium (Ir) film as a counter electrode for dye-sensitized solar cells. *Journal of Electronic Materials, 44*(11), 4400-4404.

Molapo, K. M., Ndangili, P. M., Ajayi, R. F., Mbambisa, G., Mailu, S. M., Njomo, N., Masikini, M., Baker, P., & Iwuoha, E. I. (2012). Electronics of conjugated polymers (I): polyaniline. *International Journal of Electrochemical Science, 7*, 11859-11875.

Mustafa, S. M. F., Gan, S. N., & Yahya, R. (2013). Synthesis and characterization of novel alkyds derived from palm oil based polyester resin. *Asian Journal of Chemistry, 25*(15), 8737-8740.

Nanvaee, A. A., Yahya, R., & Gan, S. N. (2013). Cleaner production through using by-product palm stearin to synthesis alkyd resin for coating applications. *Journal of Cleaner Production, 54*, 307–314.

Nasirian, S., & Moghaddam, H. M. (2014). Hydrogen gas sensing based on polyaniline/anatase titania nanocomposite. *International Journal of Hydrogen Energy, 39*, 630-642.

Nath, B. C., Gogoi, B., Boruah, M., Sharma. S, Khannam, M., Ahmed, G. A. & Dolui, S. K. (2014). High performance polyvinyl alcohol/multi walled carbon nanotube/polyaniline hydrogel (PVA/MWCNT/PAni) based dye sensitized solar cells. *Electrochimica Acta 146*, 106-111.

Nayak, S. M., Husain, J., Kalyane, S., & Prasad, M. V. N. A. (2018). Synthesis, characterization and DC conductivity of polyaniline/titanium dioxide composites. *International Journal of Advanced Research in Engineering and Technology, 9*(4), 6-13.

Nazeeruddin, M. K., Kay, A., Rodicio, I., Humphry-Baker, R., Mueller, E., Liska, P., Vlachopoulos, N., & Graetzel, M. (1993). Conversion of light to electricity by cis-X2bis(2,2'-bipyridyl-4,4'-dicarboxylate) ruthenium (II) charge-transfer sensitizers (X = Cl-, Br-, I-, CN-, and SCN-) on nanocrystalline titanium dioxide electrodes. *Journal of the American Chemical Society, 115*(14), 6382-6390.

Niu, H., Luo, J., Wu, W., Mu, J., Wang, C., Bai, X., & Wang, W. (2011). Linear and star branched perylene-containing polyimides: Synthesis, characterization, and photovoltaic properties of novel donor-acceptor dyes used in solar cell. *Journal of Applied Polymer Science, 125*(1), 200-211.

Noh, Y., & Song, O. (2013). Property of palladium counter electrode for dye sensitized solar cells. *Journal of the Korean Institute of Metals and Materials 51*(1), 71-76.

Noh, Y., & Song, O. (2014). Properties of a Ru/Ti bilayered counter electrode in dye sensitized solar cells. *Electronic Materials Letters, 10*(1), 271–273.

Oladipo, G. O., Eromosele, I. C., & Folarin, O. M. (2013). Formation and characterization of paint based on alkyd resin derivative of ximenia americana (wild olive) seed oil. *Environment and Natural Resources Research, 3*(3), 52-62.

Onukwuli, O. D., & Mbonu, O. F. (2016). Kinetic model of the polyesterification reaction of the investigative study of the optimum unsaturated fatty acid content for auto-oxidative drying of palm-stearin-based alkyd resin. *International Journal of Novel Research in Engineering and Science, 3*(1), 30-42.

O' Regan, B., & Grätzel, M. (1991). A low-cost, high-efficiency solar cell based on dye-sensitized colloidal TiO_2 films. *Nature, 353* (6346), 737-740.

Paiva, T. O., Bastos, A. E. P., Marques, J. T., Viana, A. S., Lima, P. A., & Almeida, R. F. (2016). m-Cresol affects the lipid bilayer in membrane models and living neurons. *The Royal Society of Chemistry, 6*, 105699-105712.

Palaniappan, S., & John, A. (2008). Polyaniline materials by emulsion polymerization pathway. *Progress in Polymer Science, 33*, 732-758.

Park, K. H., Kim S. J., Gomes R., & Bhaumik, A. (2015). High performance dye-sensitized solar cell by using porous polyaniline nanotubes as counter electrode. *Chemical Engineering Journal, 260*, 393-398.

Park, K., Kim, S.J., Gomes, R., & Bhaumik, A. (2015). High performance dye-sensitized solar cell by using porous polyaniline nanotubes as counter electrode. *Chemical Engineering Journal, 260*, 393-398.

Patil, B. H., Jagadale, A. D., & Lokhande, C. D. (2012). Synthesis of polythiophene thin films by simple successive ionic layer adsorption and reaction (SILAR) method for supercapacitor application. *Synthetic Metals, 162*, 1400-1405.

Phang, S. W., & Kuramoto, N. (2010). Microwave absorption property of polyaniline nanocomposites containing TiO_2 and Fe_3O_4 nanoparticles after $FeCl_36H_2O$ treatment. *Polymer Composites, 31*(3), 516-523.

Phang, S. W., Tadokoro, M., Watanabe J., & Kuramoto, N. (2008). Synthesis, characterization and microwave absorption property of doped polyaniline nanocomposites containing TiO_2 nanoparticles and carbon nanotubes. *Synthetic Metals*, *158*, 251-258.

Qiu, Y., Lu, S., Wang, S., Zhang, X., He, S., & He, T. (2014). High-performance polyaniline counter electrode electropolymerized in presence of sodium dodecyl sulfate for dye-sensitized solar cells. *Journal of Power Sources, 253*, 300-304.

Ramlan, S. N. A., Basirun, W. J., Phang, S. W., & Ang, D. T. C. (2017). Electrically conductive palm oil-based coating with UV curing ability. *Progress in Organic Coatings, 112*, 9-17.

Ramli, M. F., Gan, S. N., Lim, W. H., & Phang, S. W. (2017). Application of a palm oil-based alkyd for the improvement of polyaniline properties. *Polymers & Polymer Composites, 25*(7), 537-544.

Saad, L., Feteha, M. Y., Ebrahim, S., Soliman, M., & Abdel-Fattah, T. M. (2014). Dye sensitized solar cell based on polyaniline-carbon nanotubes/graphite composite. *ECS Journal of Solid State Science and Technology, 3*(10), M55-M60.

Saleh, H. H., Sokary, R., & Ali, Z. I. (2019). Radiation – induced preparation of polyaniline/poly vinyl alcohol nanocomposites and their properties. *Radiochimica Acta, 107*, 725-735.

Sancaktar, E., & Liu, C. (2003). Use of polymeric emeraldine salt for conductive adhesive applications. *Journal of Adhesion Science and Technology, 17*(9), 1265-1282.

Sambasevam, K. P., Mohamad, S., & Phang, S. W. (2015). Effect of dopant concentrationon polyaniline for hydrazine detection. *Materials Science in Semiconductor Processing, 33*, 24-31.

Saranya, K., Rameez, Md., & Subramania, A. (2015). Developments in conducting polymer based counter electrodes for dye-sensitized solar cells – An overview. *European Polymer Journal, 66*, 207-227.

Shahabudin, N., Yahya, R., & Gan, S. N. (2016). Microcapsules filled with a palm oil-based alkyd as healing agent for epoxy matrix. *Polymers 2016, 8*(4), 125.

Sharmin, E., Zafar, F., Akram, D., Alam, M., & Ahmad, S. (2015). Recent advances in vegetable oils based environment friendly coatings: A review. *Industrial Crops and Products, 76,* 215-229.

Shirakawa, H., Louis, E. J., Macdiarmid, A. G., Chiang, C. K., & Heeger, A. J. (1977). Synthesis of electrically conducting organic polymers: halogen derivatives of polyacetylene, $(CH)_x$. *Journal of the Chemical Society, Chemical Communications,16*, 578-580.

Snaith, H. J., Moule, A. J., Klein, C., Meerholz, K., Friend, R. H., & Grätzel, M. (2007). Efficiency enhancements in solid-state hybrid solar cells via reduced charge recombination and increased light capture. *Nano Letters, 7*(11), 3372-3376.

Stejskal, J., Sapurina, I., & Trchová, M. (2010). Polyaniline nanostructures and the role of aniline oligomers in their formation. *Progress in Polymer Science, 35*, 1420-1481.

Su, N. (2015). Polyaniline-doped spherical polyelectrolyte brush nanocomposites with enhanced electrical conductivity, thermal stability, and solubility property. *Polymers, 7*, 1599-1616.

Su'ait, M. S., Rahman, M. Y. A., & Ahmad, A. (2015). Review on polymer electrolyte in dye-sensitized solar cells (DSSCs). *Solar Energy, 115*, 452-470.

Sun, J., Tang, C., Xu, J., Yin, X., Nie, S., Wang, H., Sun, K., Cho, S. J., & Gong, H. (2015). Au coated amorphous indium zinc oxide (a-IZO) bilayer and its application as counter electrode for dye-sensitized solar cell. *International Journal of Hydrogen Energy, 40*, 10194-10199.

Tas, R., Can, M., & Sonmezoglu, S. (2017). Exploring on photovoltaic performance of dye-sensitized solar cells using polyaniline as a counter electrode: role of aluminum-solvent interactions. *IEEE Journal of Photovoltaics, 7*(3), 792-801.

Tas, R., Gulen, M., Can, M., & Sonmezoglu, S. (2016). Effect of solvent and copper-doping on polyaniline conducting and its application as a counter electrode for efficient and cost-effective dye-sensitized solar cell. *Synthetic Metals, 212*, 75-83.

Theerthagiri, J., Senthil, A. R., Madhavan, J., & Maiyalagan, T. (2014). Recent progress in non-platinum counter electrode materials for dye-sensitized solar cells. *ChemElectroChem, 2*(7), 928-945.

Uzoh, C. F., Onukwuli, O. D., Odera, R. S., & Ofochebe, S. (2013). Optimization of polyesterification process for production of palm oil modified alkyd resin using response surface methodology. *Journal of Environmental Chemical Engineering, 1*, 777-785.

Wan, L., Wang, B., Wang, S., Wang, X., Guo, Z., Xiong, H., & Zhou, W. (2014). Water-soluble polyaniline/graphene prepared by in situ polymerization in graphene dispersions and use as counter-electrode materials for dye-sensitized solar cells. *Reactive and Functional Polymers, 79*, 47-53.

Wang, N., Li, J., Lv, W., Feng, J., & Yan W. (2015). Synthesis of polyaniline/TiO_2 composite with excellent adsorption performance on acid red G. *The Royal Society of Chemistry, 5*, 21132-21141.

Wu, C. G., DeGroot, D. C., Marcy, H. O., Schindler, J. L., Kannewurf, C. R., Liu, W. J., Hirpo, W., & Kanatzidis, M. G. (1996). Redox intercalative polymerization of aniline in V2O5 xerogel. The postintercalative intralamellar polymer growth in Polyaniline/Metal oxide nanocomposites is facilitated by molecular oxygen. *Chemistry of Materials, 8*, 1992-2004.

Wu, J., Lan, Z., Lin, J., Huang, M., Huang, Y., Fan, L., Luo, G., Lin, Y., Xie, Y., & Wei, Y. (2017). Counter electrodes in dye-sensitized solar cells. *Royal Society of Chemistry, 46*, 5975-6023.

Wu, J., Li, Y., Tang, Q., Yue, G., Lin, J., Huang, M., & Meng, L. (2014). Bifacial dye-sensitized solar cells: A strategy to enhance overall efficiency based on transparent polyaniline electrode. *Scientific Reports, 4*, 1-7.

Wu, J., Tang, Z., Huang, Y., Huang, M., Yu, H., & Lin, J. (2014). A dye-sensitized solar cell based on platinum nanotube counter electrode with efficiency of 9.05%. *Journal of Power Sources, 257*, 84-89.

Xu, M., Wang, W., Zhong, Y., Xu, X., Wang, J., Zhou, W., & Shao, Z. (2019). Enhancing the triiodide reduction activity of a perovskite-based electrocatalyst for dye-sensitized solar cells through exsolved silver nanoparticles. *Journal of Materials Chemistry A.7*(29), 17489-17497.

Xua J., Liu W., & Lia H. (2005). Titanium dioxide doped polyaniline. *Materials Science and Engineering C, 25*, 444–447.

Yang, B., Zuo, X., Chen, P., Zhou, L., Yang, X., Zhang, H., Li, G., Wu, M., Ma, Y., Jin, S., & Chen, X. (2014). Nanocomposite of tin sulfide nanoparticles with reduced graphene oxide in high-efficiency dye-sensitized solar cells. *ACS Applied Materials & Interfaces, 7*, 137-143.

Yang, P., & Tang, Q. (2016). A branching NiCuPt alloy counter electrode for high-efficiency dye-sensitized solar cell. *Applied Surface Science, 362*, 28-34.

Yang, P., Duan, J., & Tang, Q. (2015). Cobalt sulphide decorated polyaniline complex counter electrodes for efficient dye-sensitized solar cell. *Electrochimica Acta, 184*, 64-69.

Yavuz, A. G., & Gök, A. Preparation of TiO_2/PANI composites in the presence of surfactants and investigation of electrical properties. *Synthetic Metals, 157*,235-242.

Yu, Y., Tang, Q., He, B., Chen, H., Zhang, Z., & Yu, L. (2016). Platinum alloy decorated polyaniline counter electrodes for dye-sensitized solar cells. *Electrochimica Acta 190*, 76-84.

Yue, G., Tan, F., Li, F., Chen, C., Zhang, W., Wu, J., & Li, Q. (2014). Enhanced performance of flexible dye-Sensitized solar cell based on nickel sulfide/polyaniline/titanium counter electrode. *Electrochimica Acta, 149*, 117-125.

Zhang, H., He, B., Tang, Q., & Yu, L. (2015). Bifacial dye-sensitized solar cells from covalent-bonded polyaniline–multiwalled carbon nanotube complex counter electrodes. *Journal of Power Sources, 275*, 489-497.

Zhao, X., Li, M., Song, D., Cui, P., Zhang, Z., Zhao, Y., Shen, C., & Zhang, Z. (2014). A novel hierarchical Pt- and FTO-free counter electrode for dye-sensitized solar cell. *Nanoscale Research Letter, 9*, 202.

Zheng, X. Q., Yang, L. T., & Wang, K. P. (2011). Synthesis and characterization of alkyd resin based on soybean oil polyols. *Advanced Materials Research,* Vols. *239-242*, 1721-1724.

Zoshki, A., Rahmani, M. B., Masdarolomoor, F., & Pilehrood, S. H. (2017). Room temperature gas sensing properties of polyaniline/ZnO nanocomposite thin films. *Journal of Nanoelectronics and Optoelectronics, 12,* 465-471.

LIST OF PUBLICATIONS AND PAPERS PRESENTED

List of publications

1. Phang, S. W., **Ramli, M. F.,** Khong, C. H., Lim, W. H., and Gan, S. N. (2018). Effect of titanium dioxide on adhesion and conductivity behaviour of polyaniline composite for solar cell application. *Macromolecular Symposia, 382*(1), 180010, 1-7.

2. **Ramli, M. F.,** Gan, S. N., Lim, W. H., and Phang, S. W. (2017). Application of a palm oil-based alkyd for the improvement of polyaniline properties. *Polymers & Polymer Composites, 25*(7), 537-544.

Conference and presentations

1. Application of a Palm Oil-Based Alkyd for the Improvement of Polyaniline Properties, 10th International Materials Technology Conference & Exhibition, International Symposium on Coatings and Corrosion (ISCC 2016), 16-19th May 2016, Putra World Trade Centre, Kuala Lumpur.

2. The Effect of Curing Method to Improve the Adhesion Property of Polyaniline/Alkyd Film, 10th International Materials Technology Conference & Exhibition, International Symposium on Coatings and Corrosion (ISCC 2016), 16-19th May 2016, Putra World Trade Centre, Kuala Lumpur.

3. Application of Palm Oil-Based Alkyd in Conducting Polymer, Oils and Fats International Congress 2016, 19th-21st October 2016, Hotel Istana, Kuala Lumpur.

4. Effect of Titanium Dioxide on Adhesion and Conductivity Behaviour of Polyaniline Composite for Solar Cell Application, 25th POLYCHAR 2017 World Forum on Advanced Materials, 9-13th October 2017, Putra World Trade Centre, Kuala Lumpur.

5. Preparation of Natural Dye and Polyaniline/Alkyd Counter Electrode for Dye-Sensitized Solar Cell, International Palm Oil Congress (PIPOC) 2017, 14-16th November 2017, Kuala Lumpur Convention Centre, Kuala Lumpur.